Universidad de Navarra

Facultad de Ciencias

Multiomics characterization of immune cells for improved monitoring of response and resistance to immunotherapy in multiple myeloma

Tesis Doctoral

Cristina Pérez Ruiz

Universidad de Navarra

Facultad de Ciencias

Multiomics characterization of immune cells for improved monitoring of response and resistance to immunotherapy in multiple myeloma

Memoria presentada por Dª Cristina Pérez Ruiz para aspirar al Grado de Doctor por la Universidad de Navarra en el Programa de Doctorado de Medicina Aplicada y Biomedicina.

Firma del doctorando

El presente trabajo ha sido realizado bajo la Dirección de los Doctores Bruno David Lourenço Paiva y Juana Merino Roncal en el Departamento de Oncohematología y autorizan su presentación ante el Tribunal que lo ha de juzgar.

Pamplona, 27 de abril de 2022

Dr. Bruno David Lourenço Paiva

Dra. Juana Merino Roncal

A ti, papá.

Porque desde la estrella que más brilla en el cielo

sé que me acompañas en cada paso que doy.

Acknowledgements

Si hay algo que me han enseñado estos años de tesis es que la vida es mejor cuando se está bien acompañado. Por suerte, he tenido conmigo a los mejores y no puedo estar más orgullosa de ello. La verdad, no se me da bien lo de abrirme en canal y mostrar lo que siento, pero la ocasión lo merece.

Nunca me imaginé escribir los agradecimientos de mi tesis entre lágrimas e intentando no romperme en cada palabra, pero tengo que empezar agradeciendo a la persona que me lo dio todo. A ti, papá. Gracias. Gracias por no dudar de mí ni un momento en los 27 años que hemos pasado juntos. No tengo palabras que puedan expresar lo que se siente cuando pierdes a tu persona favorita. Tu "princesita" ha tenido que crecer de golpe este último año y no está siendo fácil. Aprendí de ti a trabajar por lo que se quiere, a ser fuerte, constante, a querer bien y a entender que todo es mejor con una sonrisa en la cara. Así es como te recuerdo siempre en mi cabeza, sonriendo. Sé que hoy lo estarías haciendo y que, una vez más, estarías orgulloso de la persona en la que me estoy convirtiendo. Sé que siempre vas a seguir a mi lado. Te quiero.

Gracias a ti, mamá. Tú más que nadie sabe lo que me ha costado llegar hasta aquí y si no hubiese sido por tus pequeños empujones no lo habría conseguido. Has aguantado mi mal genio, mis enfados y todas las veces que he querido dejarlo y ahora, con tu fuerza y la de papá, fíjate dónde estamos. Eres la persona más luchadora que conozco y ahora no estás sola. Juntas vamos a poder con todo siempre, te lo prometo.

Gracias a mi tía Hermi. Si mis padres han sido estos años los que me aguantaban, tú has sido la que entendía cada cosa que me pasaba. A veces no hacen falta palabras para saber que alguien está ahí y que te quiere. Gracias por acompañarme día a día, darme mi espacio y creer que soy capaz de todo.

Ahora a la familia que se elige. Gracias a mis amigos. Siempre se ha dicho que es preferible calidad antes que cantidad, ¡y vaya si tienen razón!

Empiezo con los que me han acompañado casi desde el día que nací, mis amigos de Quintanarraya, Peñalba y Bilbao. Gracias a mi Karina. Si hay alguien que sabe lo que he sentido en estos años de tesis eres tú, mi científica favorita. Eres casi más que una hermana

para mí. No eres tú, ni yo, somos juntas. Eres mi Pepito Grillo, pero también mi parte de locura. Si hay algo que me guste de esta vida es saber, al 100%, que vamos a pasarla juntas. Gracias a mi Aitor. Mi otro yo. Ojalá pudieran encontrar una amistad tan pura y bonita como la que tenemos nosotros. Eres todo lo bueno que puede existir en el mundo. A mi Carla. Gracias por creer en mí siempre y estar cuando te he necesitado sin yo ni siquiera pedirlo. Llevamos 27 años haciendo maldades ¡y todavía nos quedan muchos más! A toda mi gente de la Favela, a mis Radicales y demás. Me dais vida. Sois como un chute de aire fresco cuando estoy perdida y quiero agradeceros todo lo bueno que me pase porque, en gran parte, es por vosotros.

A Andrea, María, Idoia, Patricia y Jessica, mis Influensix. Gracias por enseñarme que las amistades que se cuidan duran para siempre y que estamos juntas tanto para celebrar lo bueno como para acompañarnos en nuestros peores momentos. Nos quedan muchas alegrías por vivir. Os quiero infinito.

A Marta. A ti ya no sé cómo agradecerte todo lo que hemos vivido. Me hace muy feliz saber que desde los 3 añitos estamos juntas, las Pérez. Si hay algo que se nos da bien en esta vida es disfrutarla y ten por seguro que así seguirá siendo. Me encanta vernos crecer en todos los sentidos y, la nueva etapa que empieza ahora la viviremos juntas.

A Álex, César y Jorge, mis amiwitos. Yo no sé qué haría sin vosotros (¡ni con vosotros!). De verdad que llevo tiempo intentado inspirarme para escribir algo bonito y todo lo que me viene a la cabeza con vosotros son risas, alegría y locura. Creo que no hay nada más bonito que eso. Nos hemos juntado lo mejor de cada casa y hemos creado nuestra familia particular. Gracias por dejarme ser parte de esto.

Y ahora gracias a todos mis compañeros que me han enseñado tanto durante estos años de tesis. Poco a poco hemos creado una familia y no puedo estar más agradecida de haber aterrizado aquí ya por 2016. Empiezo con mis chicas del Despacho Sin Ventana, Sara y Rosalinda. Si el primer día que estuvimos juntas me dicen que llegaríamos a estar así, no me lo habría creído. Entre remodelaciones del despacho, fotos para colgar en el corcho, cotilleos e interminables visitas a Skyscanner nos hemos convertido en más que compañeras de despacho. Gracias por escucharme cuando he necesitado desahogarme y

por brindar conmigo celebrando la vida. Ha sido un enorme placer poder compartir este viaje con vosotras.

A Laura, mi oasis de paz en toda esta locura. Has sido mi descubrimiento y, quizás, la que más me ha entendido aquí. Gracias por hacerme esta etapa mucho más llevadera y, si con esto no nos va bien… ¡siempre nos quedará montar nuestros negocios gastronómicos! A Catarina, Catia, Camila, Espe, Juanjo e Ibai. Gracias por todas las risas, por los momentos de desconexión y por ayudarme siempre que lo he necesitado. Aprender de vosotros ha sido todo un lujo, tanto dentro del laboratorio como fuera de él. Sois geniales y me siento muy afortunada de poder contar con vosotros. A Aintzane. Gracias por ser la primera en dedicarle su tiempo en enseñar a una jovenzuela inexperta en el laboratorio. Creo que no podría haber aprendido tanto de nadie más cuando puse un pie en este mundillo. A Idoia, Sonia, Aitziber y Diego. Sois mi team favorito. Gracias por recibirme siempre con una sonrisa, incluso cuando he llegado con mis experimentos locos a haceros el día un poco más “divertido”. Sin duda, esto no habría sido posible sin vosotros. A Goretti, Leire, Marta e Irene. Gracias por aportar alegría y cariño y demostrar que este laboratorio es una familia. A Andrea, Astrid, Judith, Jaione y Laura. Gracias por vuestra ayuda y vuestra paciencia. Sois increíbles. A mi equipazo del 1.04, Sarai y Amaia. Millones de gracias por enseñarme tanto y darme la confianza para ser una más del súper equipo de genómica. Sois una parte imprescindible de todo esto.

A Ciro. Si hay alguien de quien he aprendido durante estos años esa persona eres tú. Tus locas ideas, tu ambición, la confianza que has depositado en mí desde el día que te encontré en mi despacho con tu cuaderno contándome no sé qué locura de unos linfocitos T… ¡y fíjate a lo que hemos llegado! Todo eso me ha hecho convertirme en la investigadora que soy ahora. ¡Y que se prepare el mundo que todavía nos quedan muchas cosas por contar!

A Juana y Jesús San Miguel. Gracias por darme la oportunidad de que esto haya sido posible. De poder formarme como investigadora de la manera que siempre lo quise hacer. Siempre es fundamental contar con grandes mentores para crecer.

A la Asociación Española Contra el Cáncer. Durante todos estos años he tenido muchas ocasiones para agradeceros la ayuda y la confianza depositada en mí. Ha sido un verdadero

sueño contar con el apoyo de una organización tan prestigiosa y, conocer de cerca la gran labor que lleva a cabo es impresionante. Millones de gracias por todo, estoy segura de que seguiremos en contacto.

Y, por último, a Bruno. Se quedan cortas todas las palabras de agradecimiento. Le diste la oportunidad de trabajar en su vocación a esa chica que apareció aquí en 2016 y que no había oído nunca la palabra citometría. Me has enseñado a retarme a mí misma, a tener un espíritu crítico, a querer siempre más y a creer que soy capaz de todo. Volvería a decir mil veces sí a todas las ideas locas que hemos sacado adelante durante todos estos años. Gracias por ayudarme a que esta tesis haya sido posible y confiar siempre en mí.

Gracias infinitas a todos por acompañarme en esta aventura.

Index

1. Glossary

A

ACE: abundance-based coverage estimator

ATAC-seq: assay for transposase accessible chromatin with high-throughput sequencing

AUC: area under curve

B

BM: bone marrow

C

CAR: chimeric antigen receptor

CDR3: complementarity-determining region 3

CI: confidence interval

CITE-seq: cellular indexing of transcriptomes and epitopes by sequencing

CM: central memory

CyTOF: cytometry by time of flight

D

DNA: deoxyribonucleic acid

DNN: deep neural network

E

EM: effector memory

ERGO: pEptide tcR matchinG predictiOn

E:T: effector-to-target

F

FACS: fluorescence-activated cell sorting

G

G-MDSCs: granulocytic myeloid-derived suppressor cells

GFP: green fluorescent protein

GZMB: granzyme B

GZMH: granzyme H

GZMK: granzyme K

H

HA: healthy adults

HR: hazard ratio

I

ICB: immune checkpoint blockade

IFIT: interferon-induced proteins with tetratricopeptide repeats

IMIDs: immunomodulatory drugs

IMWG: International myeloma working group

ISS: International staging system

L

LAMP1: lysosomal-associated membrane protein 1

LDH: lactate dehydrogenase

M

M-MDSCs: monocytic myeloid-derived suppressor cells

MAIT: mucosal-associated invariant T

MFC: multidimensional flow cytometry

MGUS: monoclonal gammopathy undetermined significance

MM: multiple myeloma

MRD: measurable residual disease

MRI: magnetic resonance imaging

MSC: mesenchymal stromal cells

N

NRBCs: nucleated red blood cells

NK: natural killer

O

OS: overall survival

P

PB: peripheral blood

PCA: principal component analysis

PCs: plasma cells

PFS: progression-free survival

R

R-ISS: revised-International staging system

RNA: ribonucleic acid

ROC: receiving operator curve

RT: retrotranscriptase

S

scATAC-seq: single-cell assay for transposase accessible chromatin with high-throughput sequencing

scDNA-seq: single-cell DNA sequencing

SCM: stem cell memory

scRNA-seq: single-cell RNA sequencing

scTCR/BCR-seq: single-cell TCR/BCR sequencing

SEM: standard error of the mean

sFLC: serum free light chains

SMM: smoldering multiple myeloma

SOM: self-organizing map

T

TCR: T cell receptor

TGF-β: transforming growth factor β

TILs: tumor infiltrating lymphocytes

Treg: T regulatory cells

TSS: transcription start sites

U

UMAP: uniform manifold approximation and projection

V

VISTA: V-Set Immunoregulatory Receptor

VPD: violet proliferation dye

W

WES: whole exome sequencing

Y

YFP: yellow fluorescent protein

2. Introduction

2.1. MULTIPLE MYELOMA

Multiple myeloma (MM) is the second most frequent hematological neoplasm and is characterized by the clonal expansion and accumulation of terminally differentiated plasma cells (PCs) in the bone marrow (BM), as well as in peripheral blood (PB) and extramedullary sites as the disease progresses.[1,2] It represents 1.8% of all new cancer patients, being more frequent in males than in females (8.8 vs 5.7 new cases per 100.000 individuals). The median age at the onset of MM is 69 years.[3] It remains a largely incurable disease, being the median age at death 75 years and the 5-year relative survival 55.6%.[4]

MM is characterized by the secretion of a monoclonal immunoglobulin (M protein) by clonal PCs and it can be detected in serum and/or urine. The most typical symptoms of MM are included under the CRAB nomenclature, namely hypercalcaemia, renal insufficiency, anemia and bone disease with lytic lesions. Diagnosis of MM is based on more than 30 g/L of M protein in serum/urine, more than 10% BM PCs or a biopsy-proven plasmocytoma, a serum free light-chain (sFLC) ratio greater than 100, the identification of focal lesions by magnetic resonance imaging (MRI) and/or the presence of CRAB symptoms.[5] MM is usually preceded by asymptomatic states named monoclonal gammopathy of undetermined significance (MGUS) and smoldering MM (SMM). Patients with MGUS are characterized by less than 30 g/L of M protein in serum/urine and less than 10% BM PCs. The diagnosis of SMM is based on more than 30 g/L of M protein in serum/urine and/or in between 10% to 60% PCs in BM (Table 1). Only a small proportion of patients with MGUS progress to active MM. However, the annual risk of progression from smoldering to active MM is 10% per year.[6]

Disorder	Disease definition
MGUS	All 3 criteria must be met: • Serum monoclonal protein < 3 g/dL • Clonal BM PCs < 10% • Absence of end-organ damage such as CRAB symptoms
SMM	Both criteria must be met: • Serum monoclonal protein ≥ 3 g/dL, or urinary monoclonal protein ≥ 500 mg/24h and/or clonal BM PCs 10-60% • Absence of myeloma defining events or amyloidosis
MM	Both criteria must be met: • Clonal BM PCs ≥ 10% or biopsy-proven bony or extramedullary plasmacytoma • Any one or more of the following myeloma defining events: - Evidence of end-organ damage attributed to CRAB symptoms - Clonal BM PCs ≥ 60% - sFLC ratio ≥ 100 - > 1 focal lesions on MRI studies

Table 1. International Myeloma Working Group Diagnostic Criteria for MM and Related Plasma Cell Disorders. Adapted from *Rajkumar, S. V.* Multiple myeloma: Every year a new standard? *Hematol. Oncol*. **37**, 62–65 (2019).

One of the most consolidated models for risk-stratification of patients with active MM is the International Staging System (ISS). It proposes a risk value depending on the serum levels of β2-microglobulin and albumin.[7] The International Myeloma Working Group (IMWG) revised the ISS (R-ISS) with the incorporation of cytogenetic abnormalities and the serum levels of lactate dehydrogenase (LDH).[8] Cytogenetic abnormalities associated with high-risk MM are del(17p), amp(1q), del(1p), t(4;14), t(14;16) and t(14;20). Among these, del(17p), t(4;14) and t(14;16) are included in the R-ISS. Other tumor features such as gene expression profiling[9,10] and somatic mutations[11–13] are prognostic but not routinely performed in laboratory diagnostics. There is growing interest in patients' immune status to predict disease progression, but there are no robust biomarkers for clinical implementation.[14]

2.2. TREATMENT OF MULTIPLE MYELOMA

Even though MM remains largely incurable, survival and quality of life have improved significantly in the last 15 years. The principal aims of MM treatment are to eliminate tumor cells and to resolve disease-related symptoms. Treatment strategies have changed

dramatically in the last two decades with the incorporation of drugs that are effective and present low toxicity when administrated for a long time. New combination therapies aim at increasing response rates and at inducing deep, durable responses, which correlates with longer progression-free (PFS) and overall survival (OS).[15]

In transplant-eligible patients, the standard of care includes induction with a three or four drug combination (commonly a proteasome inhibitor plus an immunomodulatory drug [IMID] and dexamethasone, with or without a monoclonal antibody), followed by high-dose therapy and autologous stem cell transplantation with lenalidomide maintenance, until progression. Consolidation before maintenance is optional and may be useful in some patients (e.g. those with high-risk MM and/or persistent disease after intensification).[16,17] In elderly patients that are not deemed fit for autologous stem cell transplantation, treatment (until progression) was developed around proteasome inhibitors and IMID combinations, with or without a monoclonal antibody (Figure 1).[17,18]

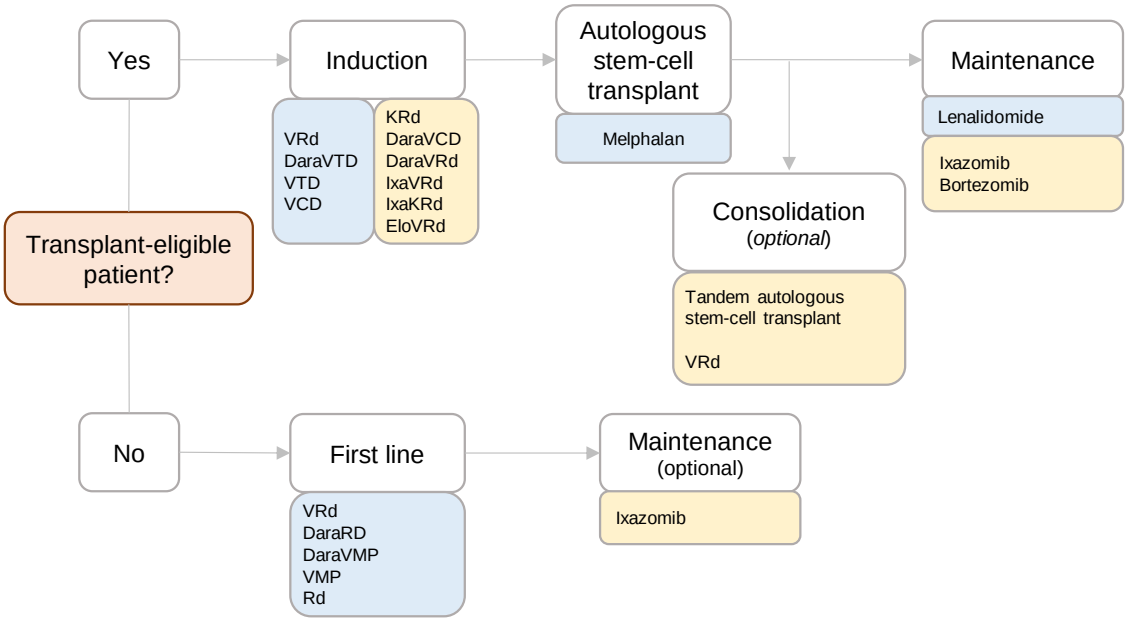

Figure 1. Scheme of the treatment strategy of newly diagnosed MM patients according to EHA-ESMO guidelines.[17] Blue and yellow boxes correspond to approved treatment approaches or to those being investigated in clinical trials, respectively. C: cyclophosphamide; D/d: dexamethasone; Dara: daratumumab; Elo: elotuzumab; Ixa: ixazomib; K: carfilzomib; M: melphalan; P: prednisone; R: lenalidomide; T: thalidomide; V: bortezomib.

Treatments that are currently approved or under investigation for MM are summarized in Figure 2 and include:

- Proteasome inhibitors (e.g. bortezomib, carfilzomib or ixazomib).[16,19–21]
- DNA destabilizing agents (e.g. melphalan or cyclophosphamide).[22,23]
- Epigenetic drugs (e.g. panobinostat).[24]
- Inhibitors of the nuclear export (e.g., selinexor).[25]
- Immune-based therapies:
    - IMIDs[26] (e.g. thalidomide, lenalidomide, pomalidomide or iberdomide).[16,18,27–29]
    - Monoclonal antibodies:
        - Targeting CD38. CD38 is expressed on MM cells, endothelial cells, activated immune cells, hematopoietic progenitors, T cells, B cells, monocytes and NK cells.[30] Compared to normal cells, malignant PCs have higher expression of CD38.[31] Treatments for MM include daratumumab (approved by FDA in 2015),[32] isatuximab (approved by FDA in 2020),[33] mezagitamab (phase I)[34] or SAR442085 (phase I).[35]
        - Targeting CD47. CD47 is a transmembrane protein that is upregulated in MM cells and plays a crucial role in preventing phagocytosis.[36] Treatments for MM include AO-176 (phase I/II)[37] or TTI-622 (phase I).[38]
        - Targeting SLAMF7. SLAMF7 is widely expressed by cells from the immune system (macrophages, NK cells, T cells and B cells). Interaction with it initiates a cascade of events culminating in the cytolytic activity of NK cells. Normal cells exhibit limited SLAMF7 expression whereas 97% of MM cells express it.[39] The FDA first approved the use of elotuzumab in 2015.[40]
        - Targeting TIGIT. TIGIT is involved in T cell regulation and is located on NK and T cells. Preclinical data have shown greater TIGIT expression on MM cells.[41] Treatments for MM include COM902 (phase I)[42] or tiragolumab (phase I).[43]
    - Bispecific antibodies:
        - BCMA/CD3. There are multiple molecules under clinical development. REGN5458,[44] TNB-383B,[45] elranatamab,[46] AMG701,[47] CC-93269 are in phase I,[48] REGN5459 is in phase I/II[49] and teclistamab is in phase II.[50]
        - FcRH5/CD3. FcRH5 is B-cell surface marker, most expressed on MM PCs. Cevostamab is being investigated in phase I clinical trials.[51]

- GPRC5D/CD3. GPRC5D is highly expressed on PCs. One such molecule under clinical research is talquetamab (phase I).[52]

Most probably, bispecific antibodies targeting BCMA[53] or GPRC5D[54] may be approved soon for the treatment of relapsed/refractory patients.

- Trispecific antibodies: there are two novel trispecific antibodies under investigation in phase I trials: HPN217 (BCMA/CD3/albumin)[55] and SAR442257 (CD38/CD28/CD3).[56]
- Antibody drug-conjugates:
  - Targeting BCMA. BCMA is preferentially expressed by mature B lymphocytes and is the target most commonly used in MM immunotherapy.[57] Belantamab mafodotin received FDA approval in 2020[58] and AMG224 and MEDI2228 are both being investigated in phase I trials.[59,60]
  - Targeting CD38. There are two anti-MM treatments under clinical investigation in phase I trials (TAK-169 and TAK-573).[61,62]
  - Targeting CD74. CD74 is highly expressed in MM cells and STRO-001 one anti-MM treatment that is in phase I research.[63]
- Chimeric antigen receptor (CAR) T cells targeting BCMA (e.g. ide-cel and cilta-cel).[64] Both have been approved recently by the FDA.

Increased knowledge of MM biology and its immune dysregulation, together with the development of several immune-based therapies, have led to a renewed interest in immunotherapy for the treatment of this disease. Currently, there are many immunotherapeutic strategies in development for MM,[65] such as agents that reverse tumor-mediated immune paralysis (e.g., CELMoDs and immune checkpoint inhibitors), agents that selectively target the malignant clone in the form of monoclonal and bispecific antibodies (e.g. targeting FcRH5 [BFCR4350A])[66,67] and agents that activate immune cells to target the tumor (CAR T and CAR NK cells [e.g. NKG2D-based CAR][68], and MM vaccines [e.g. vaccines with previously stimulated dendritic cells with MM antigens, vaccines with genetically modified MM PCs to express GM-CSF and activate antigen presenting cells, and vaccines with MM-derived peptides as MAGE-A3]).[69–72]

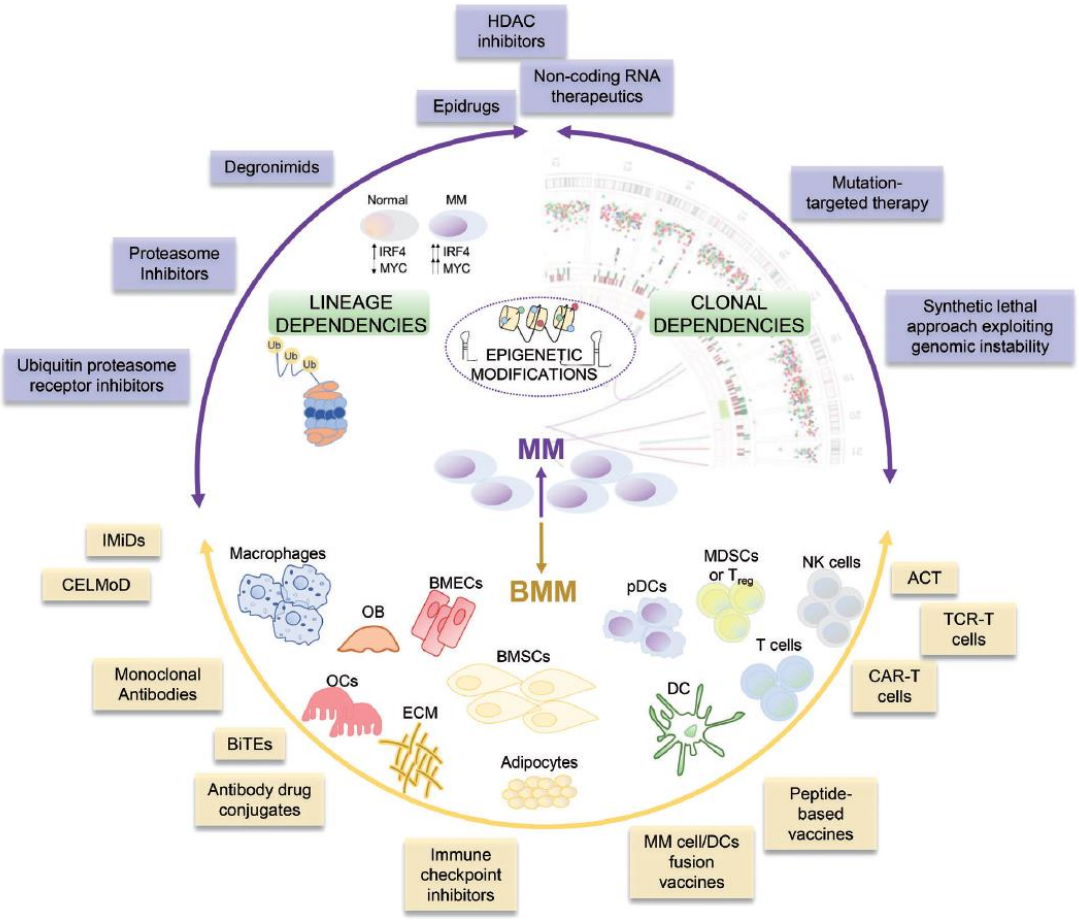

Figure 2. Overview of different anti-MM strategies. Purple: strategies designed to directly target MM cell vulnerabilities; Yellow: strategies aiming to disrupt MM BM microenvironment (BMM). OB: osteoblast; OC: osteoclasts; BMEC: bone marrow endothelial cells; ECM: extracellular matrix; BMSC: bone marrow stromal cells; DC: dendritic cell; pDC: plasmacytoid DC; MDSC: myeloid derived suppressor cells; Treg: regulatory T cell. From *Annamaria Gulla & Kenneth C. Anderson*. Multiple myeloma: the (r)evolution of current therapy and a glance into future. *Haematologica* **105**, 2358–2367 (2020).

2.3. PATHOGENESIS OF MULTIPLE MYELOMA

2.3.1. Genetic drivers

The entire process of myelomagenesis is not fully understood. However, there is sufficient evidence that genetic abnormalities play an important role in disease progression. Translocations involving the immunoglobulin heavy chain (IgH) gene locus or chromosomal duplications (hyperdiploidy, commonly of odd chromosomes) are among the primary genetic

events that possibly drive myelomagenesis. These are followed by secondary genetic events including additional copy number abnormalities, DNA hypomethylation and somatic mutations (Figure 3).[73]

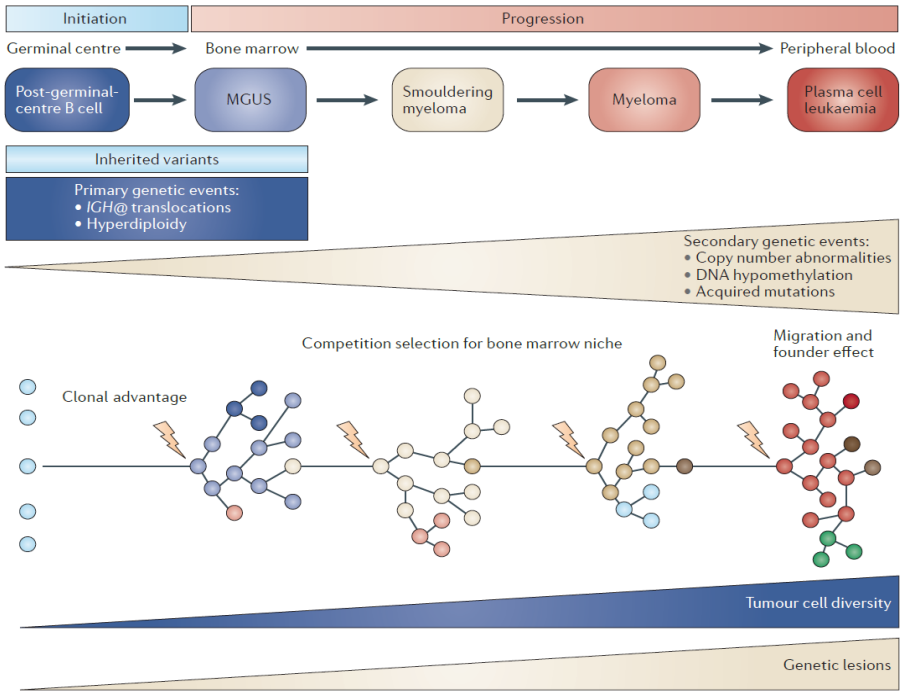

Figure 3. Initiation and progression of myeloma. The development of MM starts with pre-malignant stages of the disease, MGUS and SMM; by contrast, MM presents several clinical features (CRAB), which provide an indication that treatment is required. Later in the disease progression, PCs are no longer restrained to growth within the BM and can be found at extramedullary sites. Transition through these different states requires the acquisition of genetic abnormalities. From *Morgan, G. J., Walker, B. A. & Davies, F. E*. The genetic architecture of multiple myeloma. *Nat. Rev. Cancer* **12**, 335–348 (2012).

Despite the lack of unifying genetic events driving the progression of benign monoclonal gammopathies to full-blown MM, patients displaying certain alterations are at greater risk of malignant transformation.[74,75] While MM presents a variable mutational landscape, there are genes that are frequently mutated (e.g. *KRAS*, *NRAS*, *FAM46C*, *DIS3* and *TP53*).[76] The sum of translocations, copy number alterations and recurrent somatic mutations affects signaling pathways associated with nuclear factor-κB, mitogen-activated protein kinases, MYC, proliferation, migration, DNA-damage repair and apoptosis.[73] These pathways are the basis of new drug research.[77]

2.3.2. Immune deregulation

MM is a singular type of cancer because tumor PCs are in direct contact with immune cells that are present in the BM, and the interaction between these is another determinant of disease progression and treatment resistance.[78] In recent years, this interaction has gained importance to better understand mechanisms of immune escape.[79] During tumor progression, the immune system evolves into a more immunosuppressive state characterized by the expansion of regulatory immune cells (T regulatory cells [Tregs] and myeloid-derived suppressor cells [MDSCs]), inhibition of effector cells (T and NK cells),[80,81] production of pro-inflammatory cytokines that suppress dendritic cells, and disruption of the antigen presentation machinery through downregulation of co-stimulatory molecules (Figure 4).[82]

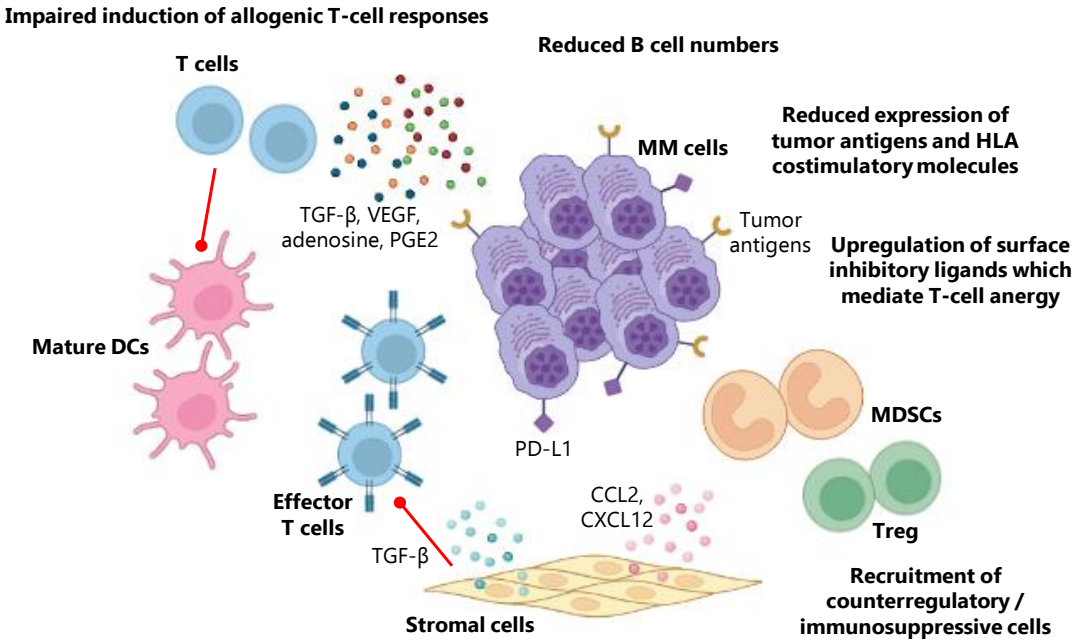

Figure 4. MM is one example of disrupted immunosurveillance and immune evasion. Some evidence underscoring the disturbed immune system in MM are impaired induction of allogeneic T-cell responses, reduction in the B-cell compartment with altered B-cell differentiation and antibody response, decrease in the expression of tumor antigens and HLA costimulatory molecules, upregulation of inhibitory ligands such as PD-L1 and recruitment of immunosuppressive cell populations like MDSCs or Tregs. VEGF: vascular endothelial growth factor; PGE2: prostaglandin E2; HLA: human leucocyte antigen; PD-L1: programmed death-ligand 1; Tregs: regulatory T cells; MDSCs: myeloid-derived suppressor cells; DC: dendritic cell; CCL2: C-C motif chemokine ligand 2; CXCL12: C-X-C motif chemokine ligand 12. Adapted from *Rodríguez-Otero, P., Paiva, B., Engelhardt, M., Prósper, F. & San Miguel, J. F*. Is immunotherapy here to stay in multiple myeloma? *Haematologica* **102**, 423–432 (2017).

There are numerous studies that show increased frequency of Tregs in the PB of MM patients compared to healthy adults (HA).[83–85] In fact, MM patients with abundance of Tregs in PB showed inferior PFS and OS.[86,87] Importantly, IMIDs are reported to inhibit expansion and function of Tregs by decreasing *FOXP3* mRNA expression.[88] MDSCs also accumulate in the tumor microenvironment due to the release of soluble factors by tumor cells.[89] Indeed, it has been suggested that MM PCs induce MDSCs development and survival, whereas MDSCs promote tumor growth and induce immunosuppression. These are able to influence innate and adaptive immune responses through depletion of L-arginine, generation of oxidative stress, induction of cytotoxic T-cell apoptosis, and activation of Tregs.[90–92] Patients with increased numbers of MDSCs have worse prognosis.[93] In addition, MDSCs from MM patients are able to attract more Tregs than those from HA, leading to a more suppressive immune microenvironment.[94] Moreover, therapies such as dexamethasone, melphalan, cyclophosphamide or even IMIDs could expand and potentiate MDSCs immunosuppressive effects, most likely due to counter regulatory mechanisms. Therefore, new strategies to target these cells are needed to augment the efficacy of MM directed therapies.[95] However, MDSCs have been extensively studied in mice and less frequently in humans. Whereas in mice they are identified based on expression of Gr-1 and CD11b, the immunophenotype of their human counterpart remains unclear.[96] Commonly, they are defined as a $CD11b^{+}CD33^{+}HLADR^{-/lo}$ subset among mononucleated cells isolated after density gradient.[92,97] MDSCs suppression could become an important strategy for increasing and prolonging the efficacy of novel immunotherapies (e.g. chimeric antigen receptor T cells or T-cell engager bispecific antibodies), but for this to happen, precise knowledge about the phenotype of MDSCs would be required for its clinical monitoring in the MM tumor microenvironment.

When it comes to effector cells, tumor-infiltrating lymphocytes (TILs) are central players in the tumor microenvironment, shaping fundamental clinical properties such as progression from benign to malignant states and response to immunotherapies.[98,99] Indeed, re-activation and clonal expansion of tumor-reactive T cells are critical to the success of immune checkpoint blockade (ICB), adoptive transfer of TILs and IMIDs.[100] Boosting immunity of tumor-reactive T cells by immunotherapy drugs requires the interaction of unique T-cell receptors (TCR) with cognate peptide-MHC.[101] Increasing evidence indicate that only a proportion of TILs are able to recognize tumor antigens.[102] Thus, the lack of intrinsic tumor

reactivity in a large fraction of intratumoral T cells implies that studies examining T cell differentiation and exhaustion states in the tumor microenvironment will essentially be assessing the phenotypic state of a large number of bystander T cells that are irrelevant to tumor control.[103] However, the single-cell landscape of TILs in MM patients lags behind what has been accomplished in solid tumors. Thus, while MM treatment is being redefined by immunotherapies,[104] single-cell studies of TILs remain scarce[105] and the phenotype of tumor-reactive T cells mainly unknown. For example, IMIDs are a backbone of MM treatment but there are no markers to monitor tumor-specific T cell reactivity and predict clinical benefit.

Other mechanisms by which malignant PCs escape from immune surveillance include decreased B cell precursors in the BM of MM patients, leading to an abnormal antibody production. MM patients also show disruption in antigen presentation, displaying defects in PB dendritic cells (reduced number of plasmacytoid dendritic cells (pDCs), myeloid DCs (mDCs) or PB monocytes).[82] All of these mechanisms lead to continuous expansion of malignant PCs, which will further modify the BM microenvironment through cytokine production and bidirectional interactions with other cell types (Figure 5).[106]

While MM patients exhibit the most depressed humoral immunity, individuals with MGUS may present significantly decreased antibody levels.[107] In fact, there could be a disease-related immunodeficiency that is independent of anti-MM treatment, and may involve B-cell dysfunction resulting in hypogammaglobulinemia, as well as T-cell, dendritic cells and natural killer (NK) cell abnormalities.[108] Accordingly, there is considerable interest in using immunotherapy to harness the immune system and help preventing disease progression. For example, the use of lenalidomide in patients with high-risk SMM led to significantly prolonged time-to progression when compared to observartion[109,110], in part because of enhanced immune surveillance.[111] Since these observations, numerous clinical trials have been initiated in high-risk SMM, and the positive results of the QuiReDex study have been recently reproduced.[110] The prospect of early detection and intervention with immunotherapy urges the identification of novel immune biomarkers to improve patient stratification.

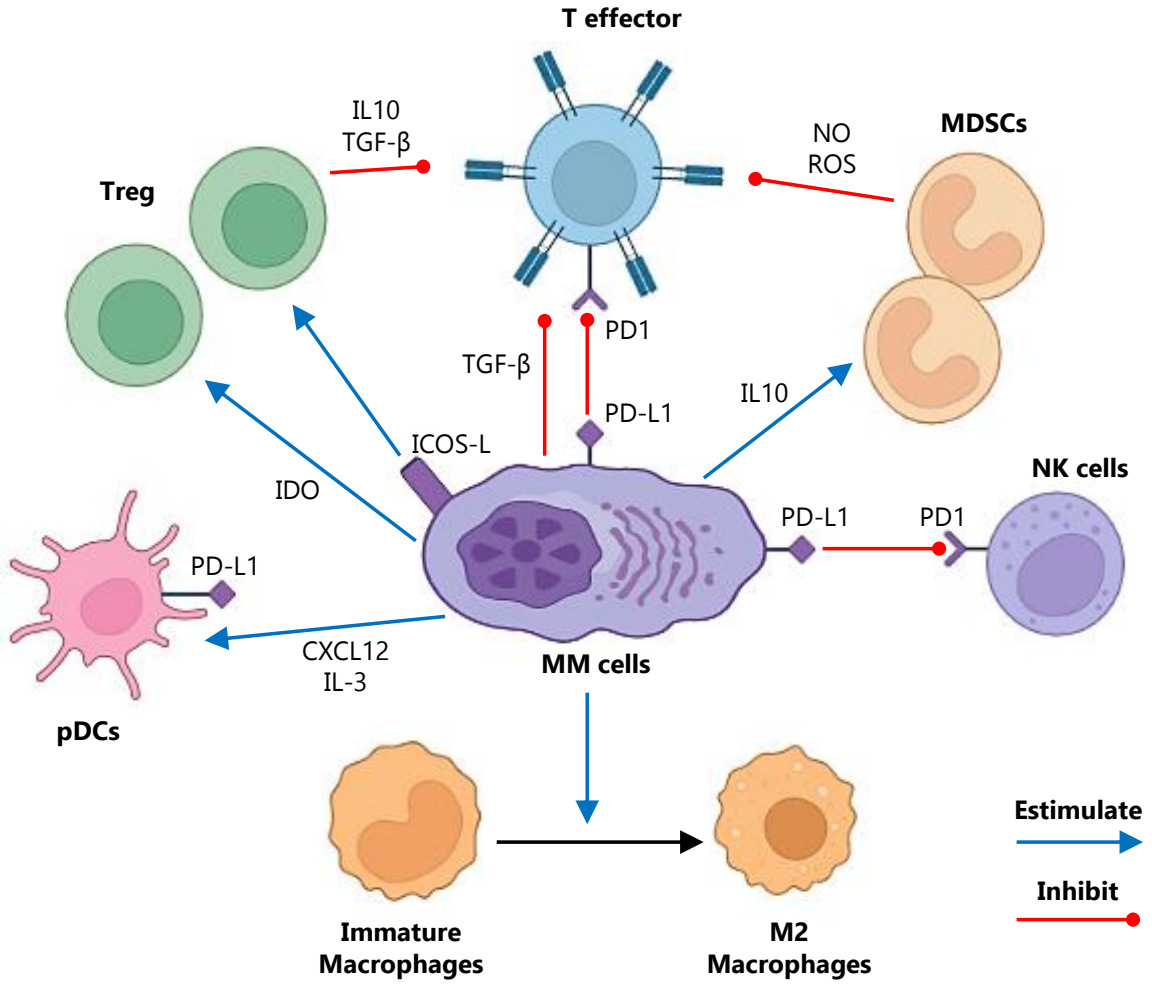

Figure 5. Possible interactions in the MM immune microenvironment. MDSCs: myeloid derived suppressor cells, MM: multiple myeloma cells, NK cells: natural killer cells, pDCs: plasmacytoid dendritic cells, Treg: regulatory T cells, ICOS-L: inducible T-cell co-stimulator ligand, IDO: indoleamine 2,3-dioxygenase, NO: nitric oxide, PD1: programmed cell death -1, PD-L1: programmed death-ligand 1, ROS: reactive oxygen species, TGF-β: transforming growth factor β. Adapted from *Kawano, Y., Roccaro, A., Azzi, J. & Ghobrial, I.* Multiple Myeloma and the immune microenvironment. *Curr. Cancer Drug Targets* **17**, 1–1 (2017).

Despite the increasing knowledge about the tumor microenvironment in MM and its precursor states, the precise phenotype of clinically relevant immunosuppressive and effector cells remains unknown. However, the growing availability of multiomics single-cell technologies investigated in large data sets could help defining the immunological and molecular characteristics of these cells towards next-generation immune monitoring.

2.4. HIGH-THROUGHPUT SINGLE-CELL TECHNIQUES FOR IMMUNE PROFILING

Numerous high-throughput single-cell techniques have been used to study the immune status of patients with MM. An oversimplified view of these techniques allows their classification in two main groups: flow cytometry and genomics.

2.4.1. Flow Cytometry

Flow cytometry is commonly used for immune monitoring due to its ability to rapidly measure multiple parameters with high accuracy and single-cell resolution, low operating costs and wide availability. Furthermore, technological advances in flow cytometry led into an increasing number of parameters being measured simultaneously in millions of single-cells.[112] However, fast-growing high-dimensional data continues to be manually analyzed through traditional inspection of two-dimensional biaxial plots and the sequential application of Boolean gates, which are hand-drawn based on marker intensity distribution of individual cells.[113] In theory, this may lead to low-reproducible, subjective and potentially biased results; in practice, such time/labor-consuming analyses are almost unfeasible in large datasets. Thus, there is an unmet need of novel computational tools.

2.4.1.1. Conventional flow cytometry

A few decades ago, antibody panels were limited to 3-4 markers that required multiple combinations (tubes) in each experiment. This proved to be problematic when analyzing small sample volumes and/or limited cell numbers. In the last 15 years, newer instruments were developed allowing the analysis of more than 8-10 markers simultaneously, which provided a more detailed analysis of immune cells in single aliquots.[114] The availability of high-throughput fluorescence-activated cell sorting (FACS) was paramount to detect and physically isolate multiple cell types with high purity for subsequent genomic and/or functional studies.[115] Multidimensional flow cytometry (MFC) immunophenotyping of BM and PB PCs affords cost-effective assessment of clonality, and provides prognostic information on the risk of progression in SMM, and the identification of MM patients with dismal outcome (e.g., high numbers of circulating tumor cells) or long-term survival despite suboptimal responses through the characterization of MGUS-like phenotypes.[116] Recent technical progress led to the development of next-generation flow cytometry that represents a validated, highly sensitive, cost-effective and widely available technique for standardized

measurable residual disease (MRD) evaluation, which also could be used for the detection of circulating tumor cells.[117] MFC enables deep characterization of immune cell types and the develop of immune signatures predictive of outcome in SMM[118] and active MM.[118,119] However, precise knowledge about the phenotype of key immune cell types predicting disease progression and response to immunotherapy, remains limited.

2.4.1.2. Acoustic flow cytometry

Acoustic positioning of cells has the advantage of concentrating particles in a precise position without the concurrent acceleration imparted by hydrodynamic focusing in conventional flow cytometry. It does not require a sheath flow and therefore fluid consumption and waste output is minimized. The acoustic technology generates ultrasonic waves that transport particles to the center of the sample stream (acoustic focusing), which increases the probability that cells may flow through the optical system.[120] This technology has not been used routinely in MM.

2.4.1.3. Spectral flow cytometry

Conventional flow cytometry detects signals from specific fluorophores over defined wavelengths. However, spectral flow cytometry collects the entire profile of excited fluorophores in every detector (spectral signature). It enables the individual resolution of fluorophores with similar emission spectra so the number of markers in a multicolor panel can be expanded to more than 40 (theoretical limit is of approximately 60). This ability to add more markers allows the identification of rare cell subsets, which is very useful for immunophenotypic studies.[121,122] Because of the recent availability of this technology, there are no large series studies reported thus far in MM.

2.4.1.4. Mass cytometry

Mass cytometry by time of flight (CyTOF) detects metal intensities from antibodies conjugated with isotopically enriched heavy-metal reporter ions, giving the possibility of analyzing more than 50 markers simultaneously.[123] CyTOF has been sporadically used in MM to characterize the immune status of small series of patients.[124,125] Its high cost and low sample turnover have limited its use worldwide and narrowed the application of mass cytometry to specific experiments where, for example, the detection of underrepresented cell types is not an objective.

2.4.1.5. Computational flow cytometry

Standard flow cytometry has been frequently used for immune monitoring[126] and newer instruments measuring 30 or more parameters will undoubtedly enhance its ability to profile patients with cancer. However, data interpretation based on multiple biaxial plots that increase quadratically with the number of parameters being analyzed is a "dimensionality explosion" that cannot be prolonged[126]. Thus, the analysis of high-dimensional single-cell flow cytometry should rely on computational methods that leverage the multi-parametric nature of this technology. Computational flow cytometry is a data-driven approach to analyze, visualize and interpret data in a more automated, reproducible and unbiased way when compared to manual analysis.[112,113,127] A few software tools were developed in recent years to perform quality control, visualize or analyze high-dimensional large flow cytometry datasets.[128–134] Computational flow cytometry has been recently applied for the first time in MM to identify immune biomarkers of disease progression.[118]

2.4.2. Genomics

Novel single-cell sequencing technologies are emerging as powerful tools to characterize the immune system. They enable analyses of the chromatin, DNA, RNA and even protein expression.

2.4.2.1. Single-cell RNA sequencing (scRNA-seq)

scRNA-seq is a powerful approach for the detection and quantitative analysis of messenger RNA molecules in individual cells with high resolution and on a genomic scale. It allows the identification of differentially expressed genes and functional oncogenic and immunological pathways in small cell clusters, contributing to deep characterization of the tumor microenvironment.[135–137] It enables asking and answering questions that cannot be approached with bulk data,[138] and the technologies and tools needed for conducting scRNA-seq studies have become more accessible in recent years.[137] In the context of MM and its precursor states, scRNA-seq has been used to achieve a deeper characterization of the immune microenvironment in small series of patients,[105,139] to identify signatures of resistance and progression in MM patients,[140–142] or to uncover tumor heterogeneity.[143]

2.4.2.2. Single-cell TCR/BCR sequencing (scTCR/BCR-seq)

In combination with scRNA-seq, it is possible to perform single-cell sequencing of paired, full-length Ig sequence and T-cell receptor α/β (scTCR/BCR-seq).[144,145,146] TCR and BCR are composed of two chains, α and β, produced through combinations of variable (V), diversity (D) (for the β-chain only), joining (J) and constant (C) gene segments.[147] Because there is a very low probability of producing an exact V(D)J rearrangement twice in an individual,[148] the TCR and BCR sequence can be used as a identifier of T and B cell clones. This is useful for measuring antigen-driven clonal expansion and longitudinal clonal dynamics,[149] as well as the heterogeneity inside the T and B cell compartments.[150] These single cells phenotypes also provide information on T and B cell differentiation pathways. This is seminal for understanding the etiology and pathology of immune-mediated diseases and also in designing therapeutic strategies.[147] This approach has been used in MM to understand the transcriptomic profile of clonal PCs[151] and to identify unique T cell clonotypes that are enriched among BM infiltrating T cells.[152]

2.4.2.3. Single-cell DNA sequencing (scDNA-seq)

scDNA-seq has recently emerged as an efficient and scalable tool to study genetic heterogeneity. Bulk sequencing homogenizes the DNA content of thousands to millions of cells. However, genomic signals (variants, DNA modifications, or structural properties of DNA) that are present in only one or a small number of cells in a sample may be undetectable without interrogating single-cell genomes.[153] scDNA-seq is based on a microfluidic approach that barcodes amplified genomic DNA from thousands of individual cancer cells confined to droplets. The barcodes are then used to reassemble the genetic profiles of cells from next-generation sequencing data. scDNA-seq has been used to assess clonal evolution in acute myeloid leukemia[154] but, till this moment, there are only preliminary studies reporting the use of this technique in MM.[155]

2.4.2.4. Single-cell sequencing of surface antigens

The combination of the information obtained by scRNA-seq with that from the surface proteins of each individual cell provides a more detailed characterization of cellular phenotypes than transcriptome measurements alone. These methods are particularly useful to study cancer immunology and mainly include the cellular indexing of transcriptomes and

epitopes by sequencing (CITE-seq).[156] In MM, the CITE-seq approach has been used for study the T cell compartment in patients treated with CAR T cells.[157]

2.4.2.5. Assay for Transposase Accessible Chromatin with high-throughput sequencing (ATAC-seq) and single-cell ATACseq (scATAC-seq)

ATAC-seq is a method used for understanding the epigenetic structure of cells, providing information on transcription factor binding, the positions of modified and canonical nucleosomes, and chromatin accessibility at regulatory elements such as promoters, enhancers and insulators.[158] Recently, scATAC-seq has become a powerful tool for genomic studies, enabling the identification of cell type-specific regulatory elements and disease-associated regulatory networks at single-cell resolution. These techniques have helped discovering regulatory elements in immune cell subtypes,[159] and in MM they have been used to identify RNA regulatory elements that may predict clinical outcome.[160]

2.4.2.6. Spatial transcriptomics

Traditional RNA sequencing experiments provide quantitative information on expression levels but lose spatial information. The idea behind spatial transcriptomics was conceptually simple. The protocol begins with a tissue sectioned and immobilized on a chip prior to staining and imaging. The tissue is then permeabilized to release RNA, which is captured by poly-dT oligos immobilized on the array. Once bound to the chip, the RNA is reverse-transcribed and imaged or sequenced.[161] Spatial transcriptomics provides quantitative gene expression data and visualization of the distribution of mRNAs within tissue sections.[162] This novel approach has not yet been used in MM because the BM is a semisolid tissue, which is a technical barrier when compared to primary samples from solid tumors.

3. Hypothesis and Objectives

3.1. HYPOTHESIS

The role of immunotherapy in the treatment of MM has grown notoriously in recent years. That notwithstanding, not all patients respond to this type of drugs and the duration of response is variable. The unpredictable clinical benefit together with their excessive cost, urges the identification of new biomarkers for next-generation immune profiling that could facilitate the individualization of immunotherapy.

The hypothesis of the PhD thesis is that the simultaneous availability of advanced flow cytometry and (single-cell) sequencing will deliver unprecedented resolution in the characterization of immune cells. Exquisite knowledge on the molecular traits of immune response, as well as state-of-the-art experimental models and translational research in clinical trials, will contribute to the phenotypic identification of key immune cell types that determine response *vs* resistance to immunotherapies. Once identified, it would be possible to investigate the prognostic value of well-defined immune subsets according to previously unknown phenotypes, and propose new markers for next-generation immune profiling in MM.

3.2. OBJECTIVES

Never in the history of MM has immunotherapy been so important in the treatment of this disease, and therefore new biomarkers are needed to tailor immunotherapies according to patient's immune status. Because both suppressive and effector cells are possible determinants in the efficacy of immunotherapy, the objectives of this PhD thesis were the following:

1. To determine the phenotype and clinical significance of G-MDSCs in MM, and identify possible therapeutic strategies to reduce their immunosuppressive potential.
2. To identify MM-reactive T cells and unravel their phenotype for cost-effective immune profiling in patients treated with immunotherapies that rely on their presence.

4. Methods

4.1. Patients and treatment

A total of 1,269 BM samples from 51 HA, 111 MGUS, 214 SMM, 718 newly-diagnosed and 175 relapsed/refractory MM patients were analyzed (median ages of 64, 63, 63, 65 and 63 years, respectively). Only samples with > 90% viability (according to the percentage of debris identified by flow cytometry) were used for subsequent analysis. Of the 718 newly-diagnosed MM patients, 272 were enrolled in the PETHEMA/GEM2012MENOS65 clinical trial and 271 in the PETHEMA/GEMCLARIDEX clinical trial (registered at http://www.clinicaltrials.gov as #NCT01916252 and # NCT02575144, respectively). These cohorts were selected to determine the prognostic value of the distribution of various granulocytic subsets in the tumor microenvironment and to determine the prognostic value of the CD27 ratio measured in intratumoral T cells. Briefly, in the PETHEMA/GEM2012MENOS65 clinical trial, patients received six induction cycles of bortezomib, lenalidomide and dexamethasone, followed by autologous stem-cell transplantation conditioned with Bu-Mel or Mel-200 high dose therapy, and received two consolidation cycles of bortezomib, lenalidomide and dexamethasone.[16] Afterwards, patients were enrolled in the PETHEMA/GEM2014MAIN clinical trial (registered at www.clinicaltrials.gov as #NCT02406144), which randomized maintenance with lenalidomide plus dexamethasone or lenalidomide plus dexamethasone plus ixazomib for 2 years, after which patients continued with lenalidomide plus dexamethasone for 3 additional years if MRD positive or stopped therapy if MRD negative.[163] In the PETHEMA/GEMCLARIDEX clinical trial, patients received lenalidomide and low-dose dexamethasone plus/minus clarithromycin. The independent ethics committee at each study site approved the protocol and informed consent forms required before patient enrollment. The study was conducted per the ethical principles of the Declaration of Helsinki.

4.2. Multidimensional flow cytometry

MFC was used to evaluate the pre-established phenotype of G-MDSCs[91,92,164–169] in BM samples from HA (N = 7) and MM patients (N = 10), as well as to compare their phenotype in paired BM and PB samples from MM patients (N = 5). MFC was also used to analyze the phenotype of T cells in BM samples from HA (N = 26), MGUS (N = 108), SMM (N = 212), newly-diagnosed MM (N = 619) and relapsed/refractory MM patients (N = 175), and to evaluate the phenotype of T cells in paired PB samples of MM patients enrolled in the

PETHEMA/GEMCLARIDEX clinical trial (N = 54), at diagnosis and after three induction courses (C3). In all cases, samples were processed within 24 hours after collection, and stained following the EuroFlow lyse, wash, and stain standard sample preparation protocol adjusted to 10^6 nucleated cells. EDTA-anticoagulated human BM aspirates were stained with different combinations of monoclonal antibodies:

- HLADR-BV421, CD45-OC515, CD15-FITC, CD13-PE, CD33-PerCPCy5.5, CD16-PECy7, CD11b-APC, and CD14-APCH7, to identify $CD11b^{+}CD14^{-}$ $CD15^{+}CD33^{+}HLADR^{-}$ cells and compare their frequency in BM samples from HA vs MM patients.
- HLADR-PacB, CD45-OC515, CD36-FITC, CD13-PE, CD34-PerCPCy5.5, CD117-PECy7, CD11b-APC, and CD71-APCH7 for the screening of different granulocytic subsets in newly diagnosed patients enrolled in the PETHEMA/GEM2012MENOS65 study.
- CD138-BV421, CD27-BV510, CD38-FITC, CD56-PE, CD45-PerCPCy5.5, CD19-PECy7, CD117-APC and CD81-APCH7 to analyze all BM immune cell types.
- TIGIT-BV421, CD127-BV510, CD25-FITC, CD39-PE, CD8-PerCPCy5.5, PD-1-PeCy7, CD28-APC, CD4-APCH7 and CD27-BV421, CD45RA-BV510, CD62L-FITC, CXCR3-PE, CD8-PerCPCy5.5, CCR4-PeCy7, CCR6-APC, CD4-APCH7 to evaluate the expression of activation molecules, checkpoint inhibitors, and polarization of T cell subsets.
- CD4-BV421, PD1-BV510, CD45RA-FITC, CD127-PE, CD8-PerCPCy5.5, TCRgd-PECy7, CD25-APC and CCR7-APCH7 to evaluate T cell subsets in PB.
- HLA-DR-BV421, CD45-OC515, CD16-FITC, CD13-PE, CD34-PerCP-Cy5.5, CD117-PE-Cy7, CD11b-APC, and CD10-APCH7 in 3-dimensional cultures with daratumumab.
- CD138-BV421, CD3-BV510, CD38-FITC, CD4-PE, CD45-PerCP-Cy5.5, CD19-PE-Cy7, AnnexinV-APC and CD8-APCH7 in 3-dimensional cultures with lenalidomide.
- CD138-BV421, CD27-BV510, CD38-FITC, CD56-PE, CD45-PerCPCy5.5, CD19-PECy7, CD117-APC, and CD81-APCH7 to analyzed the percentage of various granulocytic subsets present in BM samples from 36 MM patients collected before and after treatment with daratumumab: immature neutrophils (CD38+, $CD45^{dim}$, $CD117^{+}$, SSC^{hi}), intermediate and mature neutrophils ($CD38^{-/lo}$, $CD45^{dim}$, $CD81^{-}$,

CD117^{-}, SSC^{hi}), basophils (CD38^{hi}, CD45^{dim}, CD81^{-}, CD117^{-}, SSC^{lo}), and eosinophils (CD38$^{-/lo}$, CD45^{bright}, CD81^{bright}, CD117^{-}, SSC^{hi}).

BM cells from mice were labelled with B220 (RA3-6B2), CD3 (17A2), NK-1.1 (PK136), CD11b (M1/70) and Gr-1 (RB6-8C5), all from Biolegend (San Diego, CA). Data acquisition of human and mice samples was performed in a FACSCanto II flow cytometer (Becton Dickinson/BD Biosciences, San Jose, CA) using FACSDiva 6.1 software (BD Biosciences). Flow cytometry data was analyzed using the Infinicyt software (Cytognos SL, Salamanca, Spain) and computational flow cytometry.

4.3. Computational flow cytometry

FCS files from 1,131 BM aspirates from 26 HA, 108 MGUS, 212 SMM, 619 newly diagnosed and 175 relapsed/refractory MM patients, and 108 PB samples from 54 newly diagnosed MM patients with paired samples at diagnosis and after three induction cycles, were analyzed using the semi-automated algorithm named "*FlowCT*".[118] This computational workspace is based on the analysis of multiple files by automated and unbiased cell clustering (Supplemental Figure 1). Briefly, FCS files were merged, underwent quality control, were normalized through batch removal steps and clustered using the algorithm *FlowSOM*.[128] It works following a four-step approach: 1) reading data; 2) building a self-organizing map (SOM) for clustering and dimensionality reduction; 3) building a minimum spanning tree connecting nodes according to their similarity; 4) computing an automated meta-clustering by grouping similar nodes. The meta-clustering step is critical for the definition of cell populations. In this phase, groups of similar nodes are "fused" to obtain more consistent populations following specific algorithms. The package *ConsensusClusterPlus,* separated from *FlowSOM*, was used to obtain better control of each function. At this stage, it is possible to decide the final number of clusters in which cells are being divided. After the computational clustering, the Infinicyt software (Cytognos SL, Salamanca, Spain) was used for the identification of each cluster.

4.4. 3-dimensional cultures

An organoid 3-dimensional model was developed to test the effect of daratumumab (10 mg/mL) on granulocytes from BM samples of MM patients (N = 3) and to test the effect of

lenalidomide (1 µM), alone or in combination with 10 µg/mL of an anti-HLA I (BioXCell, Lebanon, NH), on tumor plasma cell killing from BM aspirates of MM patients (N = 3). Cells were lysed with 1X BulkLysis buffer (Cytognos), and $1x10^6$ cells were embedded in 30 mL of Matrigel Matrix (Corning) and fibronectin (ratio of matrigel/fibronectin, 2:1). This mix was seeded per well in a 48-well plate (Cellstar) and left for 40 minutes in the incubator so that the Matrigel solidified. Afterward, 300 mL of RPMI 1640 medium (10% fetal bovine serum, 1% L-glutamine, 1% Penicillin-Streptomycin) supplemented with 10% of plasma from the same BM sample, 100 nM of interleukin-6 (IL-6), and 100 nM of insulin-like growth factor-1 per well, were added. Organoids were maintained in culture for 10 days at 37°C for the daratumumab experiment and daratumumab (10 mg/mL) was added to the medium on days 1 and 5 of culture. In the lenalidomide assay, organoids were maintained in culture for 5 days at 37ºC. Finally, organoids were desegregated with Cell Recovery Solution (Corning) and labelled with the combination of antibodies described above.

4.5. Fluorescence-activated cell sorting

Cells with the pre-established G-MDSC phenotype ($CD11b^+CD14^-CD15^+CD33^+HLADR^-$) and three maturation stages of the neutrophil lineage were sorted from HA (N = 15) and MM patients (N = 45) using a FACSAria II flow cytometer (BD Biosciences). Cells were stained with 7-AAD or Sytox Blue Dead to exclude dying events. Cells were stored in Lysis/Binding Buffer (Invitrogen, Carlsbad, CA) for RNA sequencing (RNA-seq) or in phosphate-buffered saline plus 0.005% bovine serum albumin until processing for ATAC-seq or used immediately for morphological assessment or functional assays.

T cells from the BM of HA (N = 3), MGUS/SMM (N = 5) and newly-diagnosed MM patients, as well as from the BM of control (N = 2), MGUS (N = 3) and MM (N = 3) mice were FACSorted in 100 µL of PBS+0.05% BSA for subsequent scRNA/TCR-seq.

4.6. Cytospin

A total of $1x10^6$ cells from various neutrophil subsets were FACSorted in PBS. Afterwards, cells were attached to slides by cytocentrifugation (Thermo Fisher Scientific, Waltham, MA). Slides were stained following the May-Grünwald/Giemsa method and evaluated in an optical microscope (CX-21; Olympus, Tokyo, Japan). Images are shown with a 400x magnification.

4.7. T cell proliferation

The impact in T cell proliferation of various neutrophil subsets was evaluated through FACSorting of each neutrophil subset and autologous T cells from BM samples of MM patients (N = 10) and HA (N = 4). T cells were labelled with Violet Proliferation Dye (VPD) 450 (BD Horizon™) according to the manufacturer's protocol. Afterwards, $0.4x10^5$ T cells were seeded per well in a 96-well U bottom plate previously coated with an anti-CD3 monoclonal antibody 2.5 µg/mL (overnight at 4ºC, eBioscienceTM San Diego, CA). This process was repeated for each neutrophil subsets, which were cultured with T cells in an E:T ratio of 1:1 in RPMI1640 medium (10% FBS, 1% L-Glu, 1% Penicillin-Streptomycin) and in presence of 1.2 µg/mL of an anti-CD28 monoclonal antibody (eBioscienceTM San Diego, CA, USA). After a 4-day incubation at 37ºC, cells were labelled with CD45-OC515, CD15-FITC, CD8-PE, 7AAD-PerCP-Cy5.5, CD4-PE-Cy7 and CD3-APCH7. Data acquisition was performed in a FACSCantoII flow cytometer and T cell proliferation was analyzed using the Infinicyt software, based on the diffusion of VPD to daughter cells.

4.8. T cell immunosuppression

Unique culture conditions were established to evaluate the immunosuppressive potential of various neutrophil subsets after depleting a single subset in each condition (N = 10). $0.25x10^6$ cells per condition were seeded in a 96-well plate and cultured in presence or absence of 30 nM of a BCMAxCD3 bispecific antibody in RPMI1640 medium (10% FBS, 1% L-Glu, 1% Penicillin-Streptomycin). After overnight incubation at 37ºC, cells were labelled with CD11b-BV421, CD45-KromeOrange, CD38-FITC, CD229-PE, CD16-PerCP-Cy5.5, CD56-PE-Cy7, Annexin-V-APC and CD138-APCH7. MM PCs death was determined according to the percentage of Annexin-V+ cells measured in a FACSCantoII flow cytometer. Data analysis was performed using the Infinicyt software.

4.9. RNA-seq

Various neutrophil subsets from HA (N = 8) and MM patients (N = 8), normal PCs from HA (N = 25) and tumor cells from MGUS (N = 12) and newly-diagnosed MM patients (N = 216) were isolated from total BM samples in a FACSAriaII and according to patient-specific aberrant phenotypes. RNA-seq data from mesenchymal stem cells (MSCs) isolated by

FACSorting from BM aspirates of age-matched HA (N = 8) and MM patients (N = 56)[170] was analyzed to compare the expression levels of genes coding for transforming growth factor β (TGF-β) and other soluble mediators potentially involved in the modulation of the BM tumor microenvironment. Bulk RNAseq was performed using a protocol adapted from single-cell massively parallel single-cell RNA-sequencing,[171] which enabled preparing libraries with as few as 20,000 cells as starting material. Briefly, RNA from each sample was barcoded in a retrotranscription (RT) reaction with AffinityScript Multiple Temperature Reverse Transcriptase (Agilent, Santa Clara, CA) and different RT primers. After qPCR, cDNA with similar Ct values were pooled together. cDNA was purified with SPRIselect 1.2X (Beckman Coulter –BC-, Brea, CA) and amplified using the T7 promotor as template previously introduced in the RT reaction. T7 polimerase (NEB) was added for 16 hours at 37ºC. RNA molecules were fragmented with 2 µL of 10X Zn^{2+} fragmentation buffer (Ambion™, ThermoFisher Scientific) for 1 minute at 70ºC and purified with SPRIselect 2X. Afterwards, a ssRNA adaptor (Illumina, San Diego, CA) was ligated to the 3'-end of the RNA fragments in presence of DMSO, 100 mM ATP, 50% PEG and T4 RNA ligase I (NEB) for 2 hours at 22ºC. A second RT reaction was performed with AffinityScript Multiple Temperature Reverse Transcriptase and resulting cDNA was purified with SPRIselect 1.5X. Finally, cDNA was amplified with 12.5 µL Kappa Hifi ready mix + 1 µL 25 µM primer mix per sample and purified with SPRIselect 0.7X. Qubit, TapeStation and qPCR analysis were done as quality controls and 4 nM of the final library were sequenced in a NextSeq 550 (Illumina).

Differential gene expression across all pairwise comparisons between groups was analyzed with *Deseq2* R package followed by k-means clustering of genes in R. A one-way ANOVA with multiple comparisons was used to determine the significance of differential gene expression across each neutrophil subset, between neutrophils derived from HA and MM patients, between neutrophils derived from PB or BM and before and after treatment with hypomethylating agents. Genes with a $P < 0.05$ were used for gene ontology analysis and gene set enrichment analysis using the *clusterprofiler* and *fgsea* R packages, respectively.

4.10. Treatment with TGF-β

Whole PB from HA (N = 3) was exposed to 1 ng/mL of TGF-β for 48 hours. After incubation at 37ºC, cells were labelled with SYTOX™ Blue (Thermo Fisher Scientific, MA, USA), CD15-

FITC, CD13-PE, CD45-PerCP-Cy5.5, CD16-PE-Cy7 and CD11b-APC and mature neutrophils were stored in Lysis/Binding Buffer (Invitrogen™, CA, USA) for RNAseq using the protocols described above.

4.11. ATAC-seq

Approximately 20,000 cells of various neutrophils subsets were FACSorted from total BM samples of HA (N = 3) or MM patients (N = 3), and placed in a PCR tube with 100 µL of PBS+BSA 0.05%. After centrifugation (500g, 4ºC, 10 min), the pellet was suspended in 25 µL of the transposase reaction mixture (15 µL of Buffer TD2x (Illumina), 1 µL of TDE1 enzyme (Illumina), 0.25 µL of 5% digitonin (Promega) and 8.75 µL of nuclease-free water). The resulting mix was incubated at 37ºC for 30 min at 450 rpm. Afterwards, the transposase reaction was stopped on ice and 5 µL of clean up buffer, 2 µL of 5% SDS and 2 µL of Proteinase K (New England Biolabs) were added to the previous mix and incubated for 30 min at 40ºC. Transposase-reaction products were cleaned up with AMPure magnetic beads 2X (BC). Finally, the DNA fragments were amplified with 22 µL Kappa Hifi ready mix + 4 µL of primer 1 i5 and 2 i7 mix per sample. Library was purified with AMPure magnetic beads 2X. Quality control was performed with Qubit and TapeStation, and 4 nM of the final library were sequenced in a NextSeq.

ATAC-seq reads were aligned to the hg19 genome build using bowtie2 with default parameters (except commands adapted for these specific data such as --very-sensitive and --non-deterministic options that improve accuracy and results when there are many identical reads) and filtered based on mapping score (MAPQ ≥ 30) by Samtools version 1.3.159. The MACS2 version 2.1.0 was used to identify peaks for each sample with default settings. *ChiPQC* package was used for quality control and blacklisted peaks removal. *ChipSeeker* was used to assess overlap of differential peaks and relate peaks to annotated transcription start sites using default options. DESeq2 was used to normalize and identify differential peaks across treatment conditions with p-value <0.05. *Clusterprofiler* R package was used to perform a gene ontology analysis.

4.12. Treatment with epigenetic drugs

Whole BM samples from MM patients (N = 3) was treated with a selective and reversible inhibitor of histone methyltransferase G9a and DNA-methyltransferase (CM-272),[172] testing two different drug concentrations (250 and 500 nM). Approximately $3x10^6$ cells were seeded per well in a 24-well plate and left in culture for 48 hours. Cells were treated at time 0 and +24 hours. After incubation at 37ºC, cells were labelled with SYTOX™ Blue (Thermo Fisher Scientific, MA, USA), CD15-FITC, CD13-PE, CD45-PerCP-Cy5.5, CD16-PE-Cy7 and CD11b-APC to evaluate the distribution of neutrophil subsets after drug exposure. A possible synergic effect between CM-272 and a BCMAxCD3 bispecific antibody was investigated in two functional assays. First, the immunosuppressive potential of various neutrophils subsets present in BM samples of MM patients (N = 5) was analyzed after depleting a single subset with FACS. A total of $0.25x10^6$ cells per condition were seeded in a 96-well plate and pre-incubated for 2-hours with CM-272 (10 nM) at 37ºC. After washing to remove the compound, $0.5x10^5$ H929 MM cells were added to the culture followed by incubation with a BCMAxCD3 bispecific antibody (30 nM) for 24-hours at 37ºC in RPMI1640 medium (10% FBS, 1% L-Glu, 1% Penicillin-Streptomycin). Secondly, the cytotoxic effect of T cells was analyzed in the presence of each neutrophil subset, sorted from BM samples of MM patients (N = 5). A total of $0.5x10^5$ cells were seeded in a 96-well plate. Neutrophils were pre-incubated for 2-hours with CM-272 (10 nM) at 37ºC. After washing to remove the compound, $0.5x10^5$ H929 MM cells and $0.5x10^5$ T cells were added to the culture and incubated with a BCMAxCD3 bispecific antibody (30 nM) for 24-hours at 37ºC in RPMI1640 medium. Cells were labelled with CD11b-BV421, CD45-KromeOrange, CD38-FITC, CD229-PE, CD16-PerCP-Cy5.5, CD56-PE-Cy7, Annexin-V-APC and CD138-APCH7. MM cell death was determined according to the percentage of Annexin-V+ H929 cells measured in a FACSCantoII flow cytometer. Data analysis was performed using the Infinicyt software.

4.13. Combined single-cell RNA and TCR sequencing in humans

scRNA-seq + scTCR-seq were performed in 17 BM aspirates from 3 HA, 3 MGUS, 2 SMM, 9 MM patients, as well as in 8 BM aspirates from 2 control ($Y_{cγ1}$), 3 MGUS ($BI_{cγ1}$) and 3 MM ($BI_{cγ1}$) bearing mice. Cells were FACS sorted (a mix of $0.8x10^5$ T cells + $0.8x10^5$ NK cells + $0.25x10^5$ monocytes + $0.15x10^5$ B cells) in 100 µL of PBS+0.05% BSA. Samples with at

least 90% viability were processed using the 10X Genomics (CA, USA) scRNA/TCRseq kit, following the manufacturer's instructions (Chromium Next GEM Single Cell V(D)J v1.1 protocol rev F for human samples and Chromium Next GEM Single Cell 5' v2 Dual Index protocol rev B for mice samples). Quality control was performed with Qubit Fluorometric Quantification (ThermoFisher Scientific, MA, USA) using the double-stranded DNA high-sensitivity assay kit, and with TapeStation (Agilent, Santa Clara, CA) using high-sensitivity screentapes. Libraries were sequenced on a NextSeq 550 (Illumina, San Diego, CA).

scRNA-seq and scTCR-seq data from humans and mice were analyzed separately. Sample demultiplexing, alignment to the hg38 human reference genome (or the respective mice genome) and single-cell gene count was performed using the Cell Ranger Single-Cell Software Suite v.2.0.1 (https://www.10xgenomics.com/). Expression matrixes were analyzed with the R package *seurat* 4.0 (https://satijalab.org/seurat/) and cells were filtered according to < 10% mitochondrial expression and at least 200 (but less than 2500) mRNA counts per cell. Once scaled and normalized, a genelist including the most variable genes was obtained by the FindVariableFeatures function. After removing genes belonging to the immunoglobulin families (which could work as a confounding factor during clustering), the genelist was used to derive the principal component analysis (PCA) vectors for each sample. The first 100 PCA were used to align samples (batch removal) using the R package *harmony*.[173] The new harmonized coordinates were used to develop UMAPs (dimensionality reduction). The shared nearest neighbor (SNN) algorithm based on 50 batch-corrected dimensions was used for clustering the cells into homogeneous groups that were manually identified according to the expression of canonical genes (see Supplemental Information) obtained from curated gene-sets. A sequential subclustering strategy (which consists basically in repeating the same steps as before on a specific subpopulation) to focus on clonotypic T cells was performed. Reconstruction of T cell trajectories was performed by ordering single cells in "pseudotime" according to their RNA expression through *Monocle 2* R package. This package accurately resolves biological processes (ordering cells) by learning an explicit principal graph from the single cell genomics data through Reverse Graph Embedding algorithm.[174]

TCR sequences defined by their CDR3 were obtained from Cell Ranger. T cells were considered as clonotypic if their frequency was >2/1000 cells and present in at least 3 cells, and this information was added to the Seurat object to analyze the transcriptome of these

cells. *scRepertoire* R package was used to assess clonotype distribution as well as to investigate clonal "diversity", characterized by clones frequency, repertoire richness and convergence.[146,175] Chao and abundance-based coverage estimator (ACE) indices were used to estimate clonal diversity and richness. These indices have been developed to deal with under sampling (i.e. 'unseen species'), and could therefore mitigate the fact that for technical reasons, only a fraction of repertoires is sequenced and analyzed.[146]

4.14. Whole exome sequencing (WES)

WES was performed in tumor cells from BM aspirates and PB T cells of MM patients (N = 23). Approximately 20,000 tumor cells were sorted in 100 µL of Lysis/Binding Buffer (ThermoFisher Scientific, MA, USA), using the same strategy described above for bulk RNA-seq. The quality of genomic DNA extracted from tumor and PB T cells was evaluated by Agilent 4200 Tape Station using Genomic DNA ScreenTape system (Agilent, USA), and DNA concentration quantified by Qubit System (Invitrogen, USA). Genomic DNA was captured for each sample in a 10X Chromium instrument using the Chromium Genome Reagent Kit V2 for Exome Assays (10X Genomics, USA). DNA was then fragmented to an average size of 225 bp using a Covaris S220 ultrasonicator (Covaris, USA) and subjected to DNA library construction using Chromium Genome Reagent Kit V2 for Exome Assays (10X Genomics, USA). Target enrichment was performed with SureSelectXT Human All Exon V6 Capture Library (Agilent Technologies, USA) and sequence targets were captured and amplified in accordance with manufacturer's recommendations. Enriched libraries were used for 150 base sequencing in a NovaSeq 6000 (Illumina, USA) following manufacturer's instructions. Raw FASTQ files were processed using LongRanger (v2.2.2, 10X Genomics) with default parameters. Variants were annotated using the bioinformatics software HD Genome One (DREAMgenics, Oviedo, Spain), using several databases containing functional (Ensembl, CCDS, RefSeq, Pfam), populational (dbSNP, 1000 Genomes, ESP6500, ExAC) and cancer-related (COSMIC – Release 87, ICGC – Release 27) information. In addition, 9 scores from algorithms for prediction of the impact caused by non-synonymous variants on the structure and function of the protein were used (SIFT, PROVEAN, Mutation Assessor, Mutation Taster, LRT, MetaLR, MetaSVM, FATHMM and FATHMM-MKL), and 1 score (GERP++) for evolutionary conservation of the affected nucleotide. Indel realignment was performed to correct underestimated allele frequencies.

Variants with a population allele frequency higher than 0.01 were excluded. Variants detected in germline DNA (i.e., T cells) were excluded. Only mutations with a coverage higher than 6 in all samples from a patient were selected. Only variants detected in a sample with a variant frequency >= 0.15, with a mutated allele count >= 4 and droplet count >= 4 were selected. Class A HLA haplotypes were identified using optiType (v1.3.3) genotyping algorithm.[176]

4.15. Prediction of TCR-peptide binding with deep neural networks

A customized deep neural network (DNN) was developed to determine the probability of each TCR to bind specific peptide sequences obtained from WES. The DNN is based on the ERGO (pEptide tcR matchinG predictiOn) Recurrent Neural Network[177] but, differently from it, both α and β chains of the TCR were used as input. The performance of the DNN was evaluated both in terms of loss function computed on the train set, and Area Under Curve (AUC) of the Receiving Operator Curve (ROC) computed on the train set and the validation set.

The DNN model was trained with a subset of VDJDB[178] by including only the paired TCRα and TCRβ that are related to the human species. The obtained dataset is composed of 22,317 positive samples, i.e., TCR chains that have been experimentally demonstrated to bind the respective peptides. To improve the performance, negative samples were generated by assuming that if a TCR chain of the dataset binds to a peptide, then such a pair should be present in the dataset as positive binding, otherwise this TCR does not bind to the peptide (negative sample). Ten samples were randomly extracted from the negative pool for each positive sample, to generate a dataset with both positive and negative examples. The final training dataset was composed of approximately 240,000 samples. An unbalanced distribution of the classes was used (i.e. the chains bind or do not bind the epitope) to better represent the fact that TCRs are highly specific to the peptide they bind.

The class weights in the loss of function computation was introduced to effectively handle the unbalanced dataset, and prevent the DNN from predicting only the negative class. Due to the dimension of the dataset, it was reasoned that a cross validation process was not mandatory to assess the model's performance, so the DNN model was trained with 80% of

samples, while the remaining 20% was used for validation. The training process was run for 65 epochs to avoid possible overfitting scenarios.

During the training process, the loss of function decreased and the AUC on the training set increased accordingly, meaning that the DNN learnt which amino acid sequences are relevant to predict a binding between the considered samples. The AUC on the validation set, after a first increment, leveled off at 0.98 presenting only a very slight decrease, meaning that the DNN can successfully predict bindings between new pairs of TCRs and peptides.

4.16. Combined single-cell RNA and TCR sequencing in mice

B6(Cg)-*Gt(ROSA)26Sor*$^{tm4(Ikbkb)Rsky}$/J mice with constitutively active NF-κB signaling by IKK2 expression and a green fluorescent protein (GFP) reporter,[179] B6.Cg-Tg(BCL2)22Wehi/J mice with BCL2 expression,[180] and B6.129P2-*Trp53*^{tm1Brn}/J mice with p53 deletion[181] were obtained from The Jackson Laboratory (Bar Harbor, ME, USA). Transgenic activation in germinal center B lymphocytes was obtained by crossing mice with the cre-recombinase mouse line cγ1-cre (B6.129P2(Cg)-*Ighg1*$^{tm1(cre)Cgn}$/J) obtained from the Jackson laboratory.[182] Strains were intercrossed by conventional breeding to obtain the corresponding compound mice with heterozygous alleles, termed $BI_{cγ1}$, as this carries BCL2 and IKK2 expression by the cγ1-cre allele, and P53-$BI_{cγ1}$, which also carries P53 deletion. $BI_{cγ1}$ mice (N = 20) and P53-$BI_{cγ1}$ mice (N = 20) consistently developed human-like MM, with a median OS of 296 and 258 days, respectively. As controls, cγ1-cre mice crossed to B6.129X1-Gt(ROSA)*26Sor*$^{tm1(EYFP)Cos}$/J mice (The Jackson Laboratory), which carry a yellow fluorescent protein (YFP) reporter, were also generated (N = 20).[183] All mice were maintained in a hybrid C57BL6/129Sv genetic background under specific pathogen-free conditions in the animal facilities of the Center for Applied Medical Research CIMA at the University of Navarra. To induce the formation of GFP+ transgenic PCs, animals were subjected to T cell-mediated immunization with sheep red blood cells (SRBCs) intraperitoneally administered at eight weeks of age, and then repeated every 21 days for 4 months. After immunization, mice were monitored and sacrificed when signs of disease appeared, being then characterized. To this end, flow cytometry was applied to cell suspensions from BM (flushed from femurs with DPBS) with the following murine monoclonal antibodies to detect tumor and immune cell subpopulations: CD138-PE, B220-

APC, CD19-APC-Cy7, IgM-BV421, CD3-PE-Cy7, CD4-APC, CD8-BV510, NK1.1-BV421, FoxP3-PE, CD25-BV510, PD1-BV421, TIGIT-PE, LAG3-APC-Cy7. Data acquisition was performed in a FACS CantoII flow cytometer (BD Biosciences) and analyzed using FlowJo™ V10.7.1 software. In addition, serum protein electrophoresis of blood samples was used to measure the gamma-globulin (γ) fraction in a semi-automated Hydrasys 2 device, along with an isotyping multiplex assay to quantify Ig isotypes in serum using the MILLIPLEX® Mouse Immunoglobulin Isotyping kit on the Luminex® xMAP® platform. Tumor clonality was determined by genomic amplification of *IgHV* gene sequences by PCR in DNA isolated from GFP+-sorted MM cells in diseased mice, using specific VHA, VHE, and VHB forward primers and a reverse primer for JH4. Survival rates of mice were estimated using Kaplan–Meier overall survival curves. Animal experimentation was approved by the Ethical Committee of Animal Experimentation of the University of Navarra and by the Health Department of the Navarra Government.

4.17. *In vivo* testing of immune checkpoint inhibitors in syngeneic mice

The MM-derived MM5080 cell line was established from an original MM developed in P53-$BI_{cγ1}$ mice. Establishment of syngeneic transplants was performed by injecting $10x10^6$ MM5080 cells in DPBS into the tail veins of 8- to 10-week-old immunocompetent C57BL/6J mice (Envigo). Three days upon injection of MM cells, animals of both sexes were randomly divided into experimental groups, which received anti-PD1 (200 µg; RMP1-14), anti-TIGIT (200 µg; 1G9), or anti-LAG3 (200 µg; C9B7W) administered intraperitoneally alone or in combination for the following three weeks, while control mice received vehicle. Therapy responses were estimated by Kaplan-Meier survival curves, which were compared using the log-rank test using v7 GraphPad Prism software.

4.18. Statistical analysis

The Kruskal-Wallis test was used to estimate the statistical significance observed between groups in T-cell immunosuppression assays and in the comparison between T cells ranging from HA to relapsed/refractory MM. The Student's T test was used to evaluate differences between groups in experiments measuring T-cell proliferation, significant associations

between patients' clinical data and the distribution of various granulocytic subsets, to assess differences between groups in the 3-dimensional culture experiments and in the comparison of PB samples from patients who have progressed to active MM.

Survival probabilities were estimated by using the Kaplan-Meier method and compared with the use of a two-sided stratified log-rank test. Patients were stratified into groups according to the median value of each cell type (or cell ratio) in the whole population. The effect of CD27 ratio on the risk of PFS and OS (hazard ratio [HR]), with its two-sided 95% confidence interval (CI), were estimated with a logistic Cox regression model. PFS was defined from the time of MFC assessment at diagnosis until disease progression or death from any cause. OS was defined from the time of MFC assessment at diagnosis until death. In patients with SMM, time to progression was defined from the time of MFC assessment until disease progression. A multivariate Cox proportional hazard model was developed to explore the independent effect on PFS of prognostic factors defining the R-ISS: ISS stage, LDH levels, and FISH cytogenetics. Patients were stratified into groups according to the median value of the CD27 ratio or the abundance of T cell subsets in the whole population.

Statistical analyses were performed using the GraphPad Prism software (version 7, San Diego, CA), R version 4.0 and SPSS (version 25.0.0, IBM, Chicago, IL). *P* values <.05 were considered as statistically significant.

5. Results

Immunogenomic identification and characterization of granulocytic myeloid-derived suppressor cells in multiple myeloma

Perez C & Botta C. et al. Blood. 2020;136(2):199-209.

5.1.1. Characterization of G-MDSCs based on conventional criteria

In humans, G-MDSCs have been previously defined as a unique (rare) population displaying a $CD11b^{+}CD14^{-}CD15^{+}CD33^{+}HLADR^{-}$ phenotype, comprising ~1% of BM nucleated cells in HA and up to 25% in MM patients.[95] However, the frequency of $CD11b^{+}CD14^{-}CD15^{+}CD33^{+}HLADR^{-}$ cells (gating strategy shown in Supplemental Figure 2) among total BM nucleated cells was similar between HA (N = 7) and MM patients (N = 10; median, 28% vs 24%, respectively; *P* = .49; Figure 6A). Moreover, rather than defining a unique population, $CD11b^{+}CD14^{-}CD15^{+}CD33^{+}HLADR^{-}$ cells included a mixture of neutrophil subsets (i.e. metamyelocytes, band/ mature neutrophils) plus eosinophils (Supplemental Figure 2).

Because various granulocytic subsets were identified within putative G-MDSCs according to conventional phenotypic criteria, an unbiased analysis based on automated clustering using the antigens described above and others reported as potentially relevant[96] for MDSC isolation, was performed to reveal how many granulocytic clusters were present in BM samples from HA and MM patients. This strategy led to the identification of eosinophils, basophils, and three well-defined neutrophil maturation stages according to differential expression of CD11b, CD13, and CD16 in HA and MM patients: immature ($CD11b^{-}CD13^{-/lo}CD16^{-}$), intermediate ($CD11b^{+}CD13^{-/lo}CD16^{-}$), and mature ($CD11b^{+}CD13^{+}CD16^{+}$) neutrophils as confirmed by the expected shape of their nuclei (Figure 6B-C). Of note, the mean frequency of each of the five granulocytic subsets was similar between HA and MM patients (Figure 6D), as was the percentage of each neutrophil subset within total neutrophils (data not shown). There were no differences in the phenotypic profile of mature neutrophils present in matched BM and PB samples from MM patients (N = 5), although as expected, immature and intermediate neutrophils were absent in PB (Supplemental Figure 3A-B). On transcriptional grounds, mature neutrophils from BM and PB of MM patients clustered together and apart from those of HA (Supplemental Figure 3C).

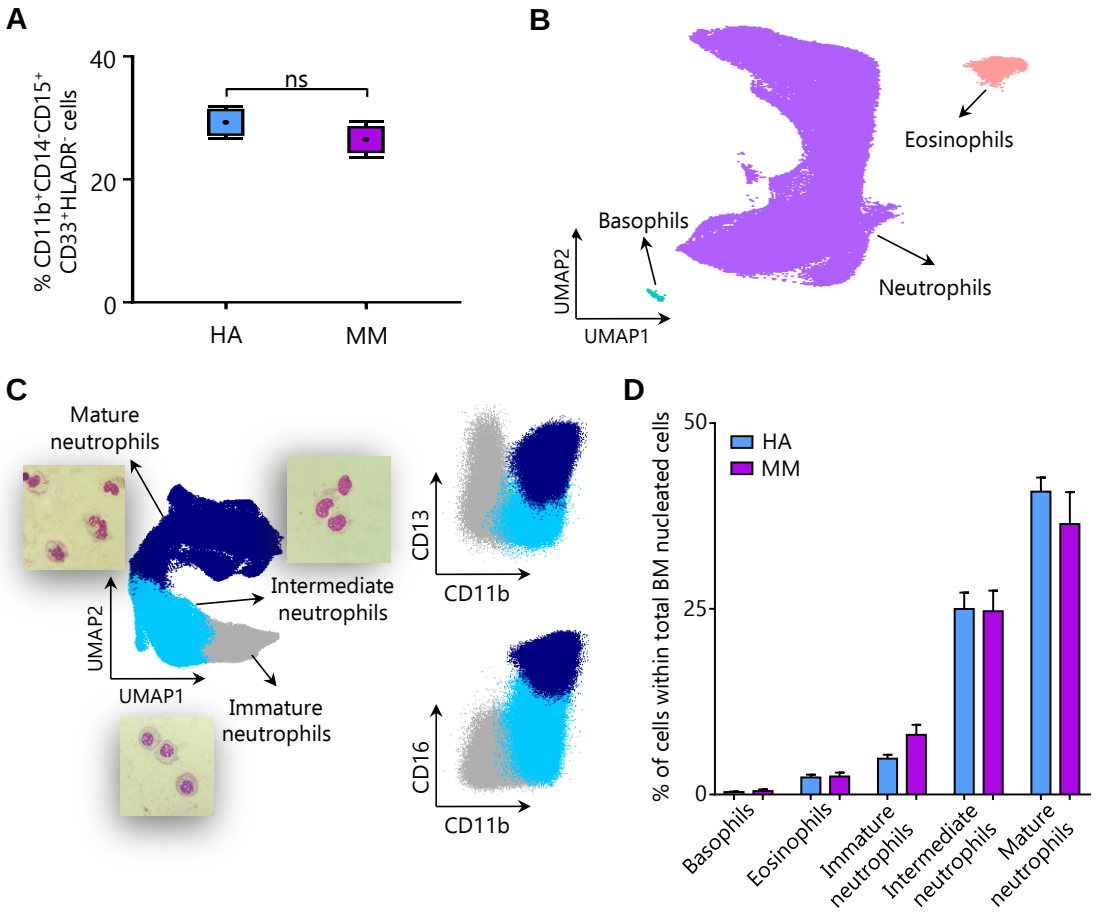

Figure 6. Characterization of G-MDSCs based on conventional criteria. (A) BM samples from MM patients (N = 10) and HA (N = 7) were stained with HLADR-BV421, CD45-OC515, CD15-FITC, CD13-PE, CD33-PerCPCy5.5, CD16-PECy7, CD11b-APC, and CD14-APCH7 monoclonal antibodies. Cells with a $CD11b^{+}CD14^{-}CD15^{+}CD33^{+}HLADR^{-}$ phenotype represent ~25% of total BM nucleated cells both in HA and MM patients. **(B)** Unbiased analysis based on uniform manifold approximation and projection (UMAP) according to expression levels of HLADR, CD45, CD15, CD13, CD33, CD16, CD11b, and CD14 revealed various granulocytic subsets (neutrophils, eosinophils, and basophils) in BM samples from HA and MM patients. **(C)** UMAP of the neutrophil population led to the identification of three neutrophil maturation stages according to differential expression of CD11b, CD13, and CD16: immature ($CD11b^{-}CD13^{-/lo}CD16^{-}$), intermediate ($CD11b^{+}CD13^{-/lo}CD16^{-}$), and mature ($CD11b^{+}CD13^{+}CD16^{+}$) neutrophils. Cellular maturation was confirmed on cytospinned cells from the three different populations by evidencing the classic changes in nuclear shape. Images are shown with a x400 magnification. **(D)** Frequency of each granulocytic subset was similar between HA and MM patients. Bars represent the mean and lines the standard deviation.

5.1.2. Daratumumab has no long-term *in vitro* effect on BM granulocytes from MM patients

Based on previous data indicating that daratumumab depletes G-MDSCs,[184] primary BM aspirates from MM patients (N = 3) were treated with daratumumab to compare the number

and phenotype of granulocytic cells before vs after treatment and thereby infer the antigen expression of putative G-MDSCs depleted by the drug. Samples were cultured in an organoid 3-dimensional model to enable long-term treatment (Supplemental Figure 4A). As expected, daratumumab induced a significant depletion of tumor PCs (Supplemental Figure 4B), but no differences were found regarding the percentage of $CD11b^{+}CD14^{-}CD15^{+}CD33^{+}HLADR^{-}$ cells (Supplemental Figure 4C) or various granulocytic subsets (Supplemental Figure 4D) after 10-day treatment with daratumumab. These results were confirmed *ex vivo*, where the percentage of various granulocytic subsets was similar in paired BM samples from MM patients (N = 36) analyzed before and after treatment with daratumumab (Supplemental Figure 4E).

5.1.3. Clinical significance of granulocytes in the tumor microenvironment

Because the pre-established phenotype of human G-MDSCs did not allow for the identification of a unique population of myeloid cells in the BM of HA and MM patients (nor in different percentages), and because no myeloid cells were depleted by daratumumab *in vitro* to allow for identification of the phenotype of G-MDSCs, the identification of granulocyte subsets of clinical significance in patients with newly diagnosed MM (N = 267) was subsequently investigated as an alternative strategy to define the phenotypic profile of G-MDSCs. Overall, the frequency of basophils, eosinophils, and immature ($CD11b^{-}CD13^{-/lo}CD16^{-}$), intermediate ($CD11b^{+}CD13^{-/lo}CD16^{-}$), and mature ($CD11b^{+}CD13^{+}CD16^{+}$) neutrophils had no significant association with clinical parameters, including cytogenetic alterations (Supplemental Figure 5A). However, the presence of unique patient subgroups based on differential predominance of neutrophils, nucleated red blood cells, tumor cells, and T cells in the tumor microenvironment was noted (Figure 7A-B). On prognostic grounds, only the percentage of mature neutrophils and not any other granulocytic subset had a significant impact on PFS (Supplemental Figure 5B); patients with >32% $CD11b^{+}CD13^{+}CD16^{+}$ BM cells had 3-year PFS rates of 66% vs 79% in cases with ≤32% mature neutrophils (Figure 7C). Because of the relationship between MDSCs and T-cell immunosuppression, the prognostic value of the mature neutrophil/T-lymphocyte ratio was further investigated. Accordingly, patients with higher ratios (>3.4) had significantly inferior

PFS when compared with cases with lower ratios (3-year PFS rate, 85% vs 60%, respectively; *P* < .001; Figure 7D).

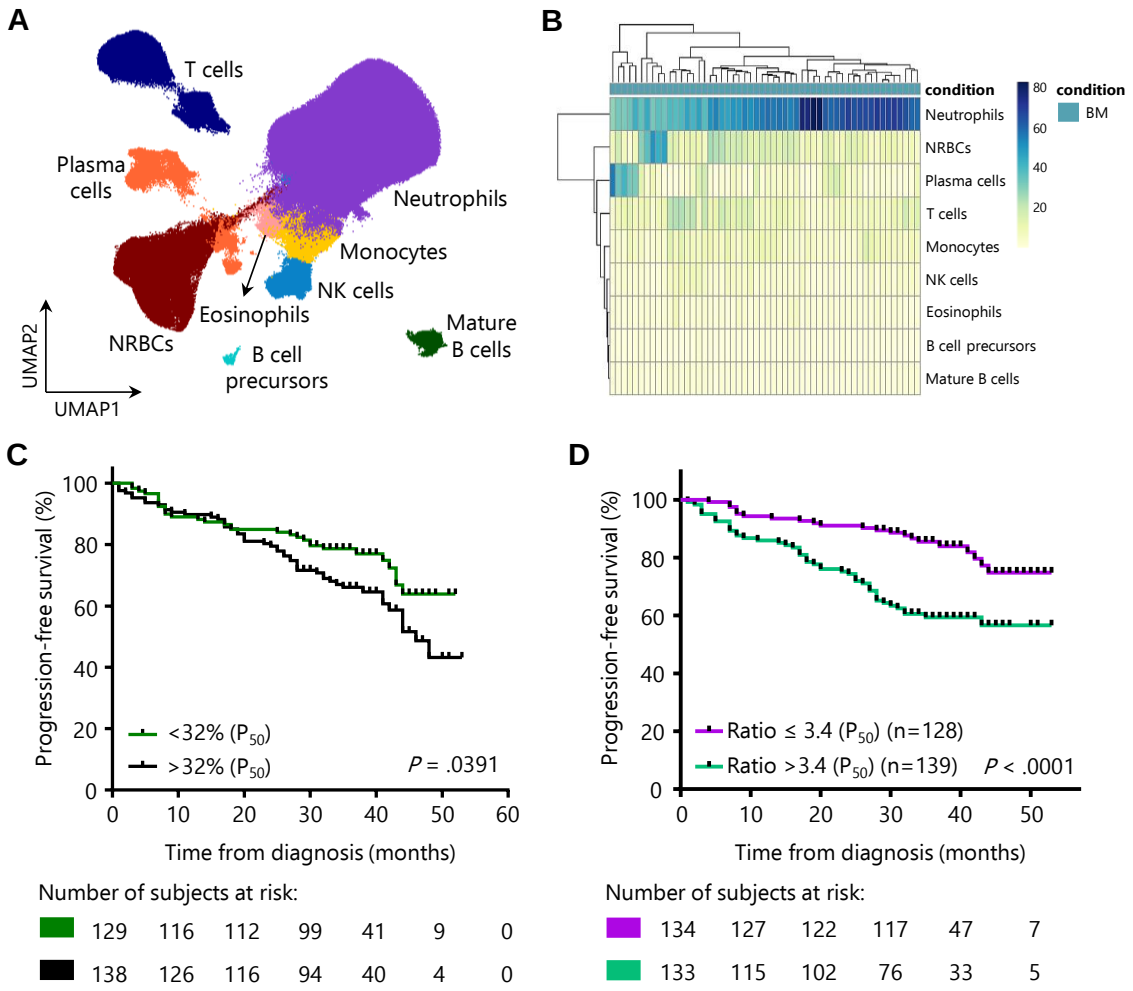

Figure 7. Clinical significance of granulocytes in the tumor microenvironment. (A) Unbiased immune monitoring of the tumor microenvironment based on UMAP of BM samples of newly diagnosed MM patients (N = 55). **(B)** Unsupervised clustering of MM patients based on cellular composition of the tumor microenvironment. **(C)** PFS according to high (> 32%) vs low (≤ 32%) abundance of mature ($CD11b^+CD13^+CD16^+$) neutrophils (3-year PFS rate, 66% vs 79%, respectively; *P* = .0391). **(D)** PFS according to high (> 3.4) vs low (≤ 3.4) mature neutrophil/T-lymphocyte ratio (3-year PFS rate, 60% vs 85%, respectively; *P* > .0001). NK, natural killer; NRBC, nucleated red blood cell.

5.1.4. Progressive immunosuppression from immature to mature neutrophils

As a result of the prognostic value found in regard to the frequency of mature neutrophils in the tumor microenvironment of MM patients, the immunosuppressive potential of these cells

was investigated with two functional assays: the proliferation rate of autologous T cells in the presence of CD3/CD28 stimulatory beads (N = 14; Figure 8A), and the cytotoxic potential of autologous T cells against MM cells using a BCMAxCD3-bispecific antibody (N = 10; Figure 8B). Interestingly, a significant decrease in T-cell proliferation was observed when these were stimulated in the presence of mature neutrophils from MM patients (0.5-fold; *P* = .016) but not from HA (Figure 8C). By contrast, immature and intermediate neutrophil subsets from MM patients or HA had no impact on T-cell proliferation. In addition, the cytotoxic potential of T cells engaged by a BCMAxCD3-bispecific antibody progressively increased with the depletion of immature, intermediate, and mature neutrophils (two-, three-, and four-fold, respectively; *P* ≤ .03; Figure 8D).

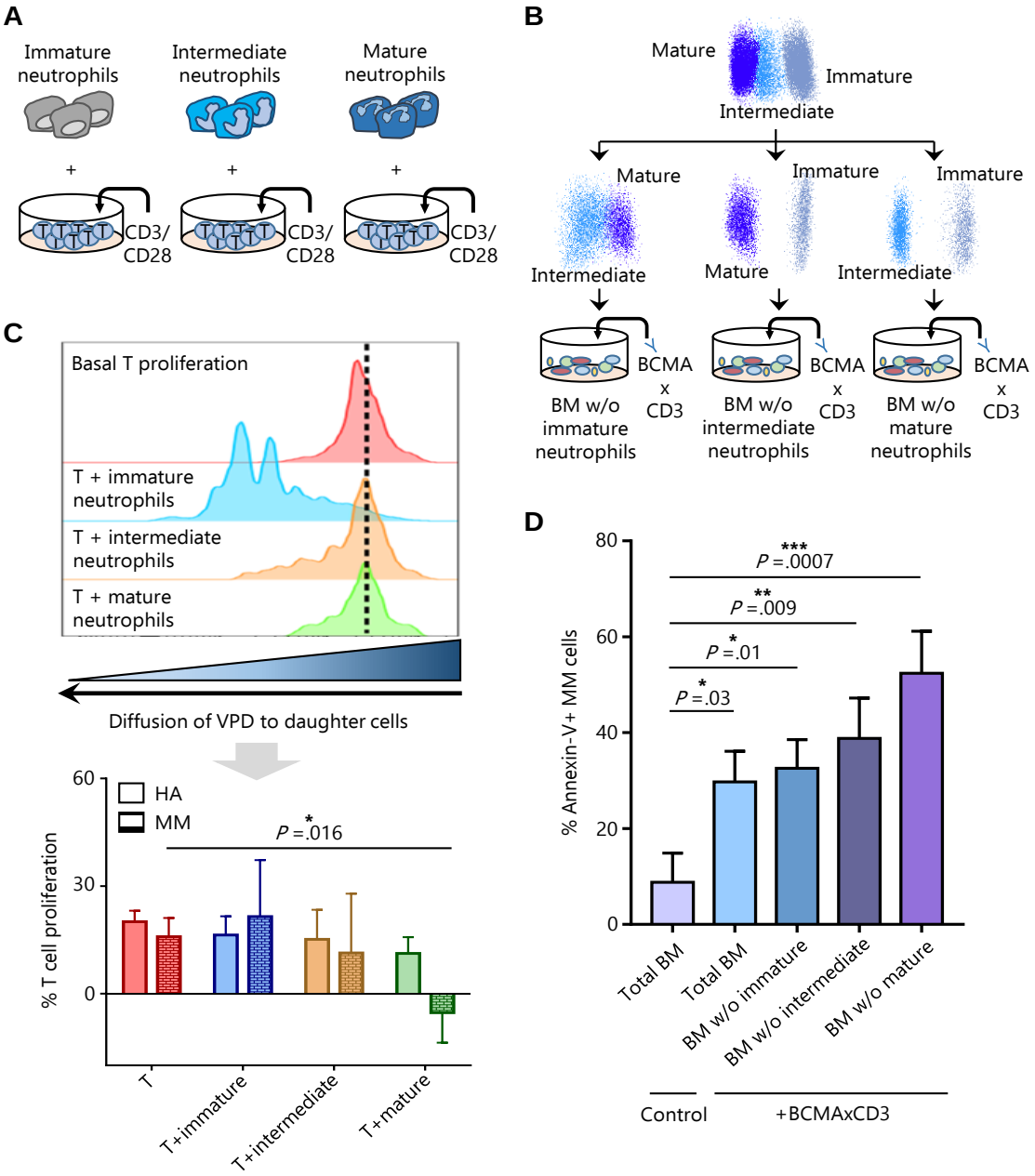

Figure 8. Progressive immunosuppression from immature to mature neutrophils. (A) Fluorescence-activated cell sorting of the three neutrophil subsets from BM samples of MM patients (N = 10) and HA (N = 4) was performed to culture each subset with autologous T cells previously stimulated with CD3/CD28 antibodies and labeled with VPD. After a 4-day incubation, VPD intensity was measured on total T cells. **(B)** Total BM samples vs BM samples depleted of each neutrophil subset (i.e. without $CD11b^{-}CD13^{-/lo}CD16^{-}$, without $CD11b^{+}CD13^{-/lo}CD16^{-}$, and without $CD11b^{+}CD13^{+}CD16^{+}$) from MM patients (N = 10) were treated with 30 nM of a BCMAxCD3-bispecific antibody and left in culture for 24 hours. **(C)** Significant decrease in T-cell proliferation when these were stimulated in the presence of mature neutrophils from MM patients (0.5-fold; *P* = .016), but not the immature or intermediate subsets from MM patients or HA. **(D)** Cytotoxic potential of T cells engaged by a BCMAxCD3-bispecific antibody progressively increased with the depletion of immature, intermediate, and mature neutrophils (two-, three-, and four-fold, respectively; P≤.03). Bars represent the mean and lines the standard error of the mean. Statistical significance was evaluated using the Student t test for proliferation analysis and the Kruskal-Wallis test for the immunosuppression assay. **P* < .05, ***P* < .01, ****P* < .001.

5.1.5. Molecular characterization of neutrophil differentiation in normal and tumor BM

The progressively increasing gradient of immunosuppression from immature to mature neutrophils triggered additional research to understand if differences in the functional behavior of each neutrophil subset were related to transcriptional modulation after their differentiation. Unsupervised clustering after RNA-seq of immature, intermediate, and mature neutrophils from HA and MM patients (N = 8, each) showed accurate segregation per cell type and not participant (Figure 9A), thereby validating CD11b, CD13, and CD16 as robust markers to identify and isolate neutrophil stages with different transcriptional profiles. Specific analysis of genes coding for cytokine/chemokine-soluble mediators based on the KEGG cytokine-cytokine receptor interaction pathway list (Supplemental Table 1) revealed significantly different levels in 21 genes and various patterns of differential expression in immature, intermediate, and mature neutrophils (Supplemental Figure 6A-B). Notably, most of these patterns were identical in HA and MM patients, except for the *CXCL1, PTGS2, TGFB1, TNFSF13B, VEGFA, CCL4*, and *IL1B* genes, because their expression levels were significantly altered in mature neutrophils from MM patients (Supplemental Figure 6C). Accordingly, unsupervised clustering at the subset level showed incomplete segregation between HA and MM patients regarding the transcriptional profiles of immature and intermediate (Supplemental Figure 7) but not mature neutrophils (Figure 9B), which segregated all HA and MM patients based on differentially expressed genes. Interestingly,

gene set enrichment analysis revealed that mature neutrophils from MM patients displayed reduced antiviral and anticancer type 1 and 2 interferon transcriptional response, as well as increased activation of transcriptional pathways related to inflammation, such as tumor necrosis factor a, IL-2–STAT5, and TGF-β signaling (Figure 9C).

5.1.6. TGF-β transcriptionally rewires mature neutrophils

Based on the transcriptomic findings and on the prominent role of TGF-β in the MM tumor microenvironment,[185,186] mature neutrophils from HA (N = 3) were exposed to TGF-β in order to investigate if this cytokine could contribute to a shift in their transcriptional profile to a program similar to that found in mature neutrophils from MM patients. Therefore, the mRNA counts of the top-10 differentially expressed genes between mature neutrophils from HA and MM patients identified above, were specifically compared in MM patients vs mature neutrophils from HA after treatment with TGF-β (Figure 9D). Accordingly, no significant differences ($P > .05$) were found in the expression of these genes, suggesting that TGF-β significantly contributes to the molecular reprogramming of mature neutrophils. Interestingly, MSCs from MM patients (N = 56) had similar expression levels of TGF-β as compared with those from age-matched HA (N = 8), but genes coding for proinflammatory molecules (*CXCL2, CXCL3*, and *PTGS2*), growth factors (*IL-6, BAFF*), and angiogenetic mediators (*IL-8*), which eventually may also shift the transcriptome of mature neutrophils, were found to be upregulated in MSCs from MM patients (Supplemental Figure 8).

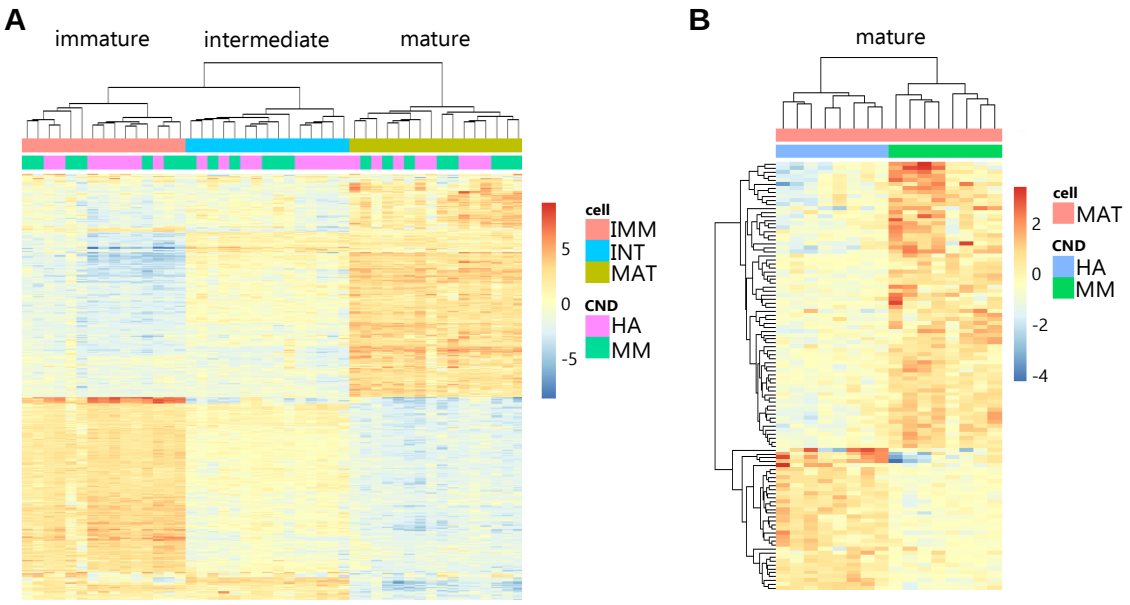

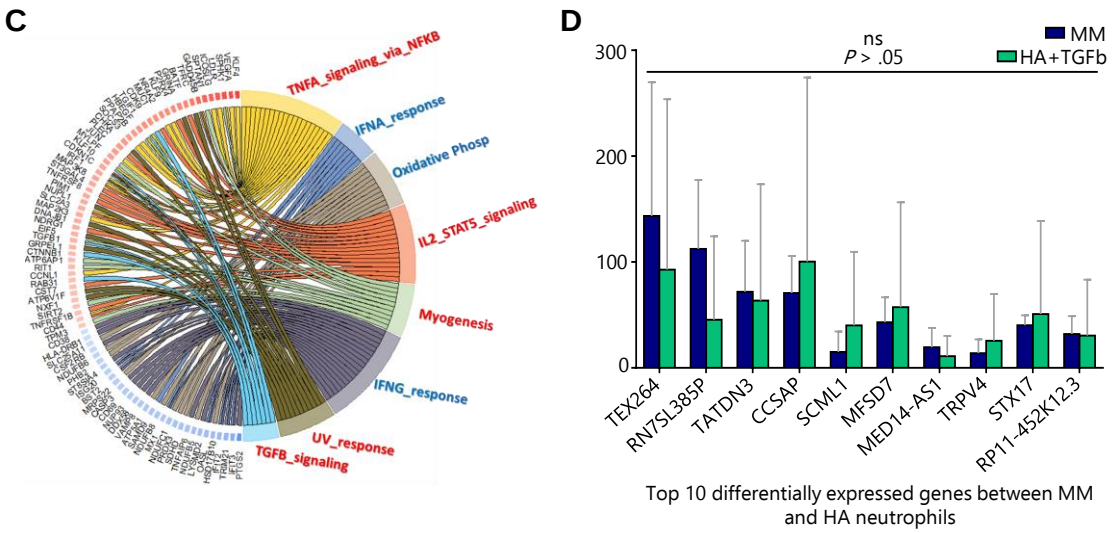

Figure 9. Molecular characterization of neutrophil differentiation in normal and tumor BM. (A) Unsupervised clustering after RNAseq of immature, intermediate, and mature neutrophils from HA and MM patients (N = 8 each) showed accurate segregation per cell type and not participant. **(B)** Whole-transcriptome profiling through RNAseq segregates mature neutrophils from HA and MM patients according to 108 genes differentially expressed (*P* < .05). **(C)** Gene set enrichment analysis showed that mature granulocytes from MM patients increased activation of pathways related to inflammation and reduced antiviral and anticancer type 1 and 2 interferon transcriptional response. **(D)** Mature neutrophils from HA (N = 3) were treated with TGF-β, and expression levels of the top-10 differentially expressed genes between MM and HA neutrophils (panel B) were analyzed. There were no significant differences when comparing mature neutrophils from MM patients vs HA treated with TGF-β (*P* < .05). CND, condition; ns, not significant; TNFA, tumor necrosis factor α.

5.1.7. Transcriptional network of mature neutrophils is epigenetically deregulated in MM

Under the hypothesis that the transcriptional changes found in mature neutrophils from MM patients resulted from epigenetic modulation as a consequence of the altered cellular and cytokine content in the tumor microenvironment, RNA-seq data was integrated with chromatin accessibility profiling through ATAC-seq in mature neutrophils from BM aspirates of HA (N = 3) and MM patients (N = 3). A mean of 23,214 open chromatin sites (peaks) in nucleosome-free regions in the 6 different samples was reported, and using a generalized linear model (DESeq2; adjusted *P* < .1), 1,445 differentially accessible peaks between mature neutrophils from HA vs MM patients were identified. Among these peaks, 678 showed an increase and 767 showed a decrease in chromatin accessibility in MM. To assess their biological relevance, differential peaks were annotated to the nearest gene

based on their distance to transcription start sites (TSSs). Of note, 50% of these peaks were in potential promoter regions within 3 kb of a TSS, suggesting that these gains/losses in accessibility could exert regulatory activity (Supplemental Figure 9A). Accordingly, a gene ontology enrichment analysis was performed with genes that were closing or opening in MM derived mature neutrophils. Interestingly, several functions (the top 10 are described in Table 2) were associated with closed regions that predicted for altered neutrophil immunity in MM, whereas no significant functions were found associated with open regions.

Based on paired ATAC-seq and RNA-seq data, a significant correlation was found between gains or losses of chromatin accessibility near TSSs and gene expression for each normal and tumor-derived neutrophil sample (Supplemental Figure 9B). *CD83*, which showed significantly higher mRNA expression in MM patients vs HA, as well as concordant transcriptional and chromatin accessibility data, was selected to confirm these results using flow cytometry that confirmed the increased CD83 expression in MM (Supplemental Figure 9C). Most importantly, a significant positive correlation between MM-specific changes in gene expression levels and chromatin accessibility was observed in gene promoters of mature neutrophils (P = 8.17e^{-6}; Figure 10A). Furthermore, gene ontology enrichment analysis of differentially expressed genes in mature neutrophils from MM patients revealed a significant downregulation in functions related to neutrophil immune activation, in accordance with chromatin accessibility (Figure 10B).

These results led to additional experiments to investigate if DNA demethylation induced by CM-272, a selective and reversible inhibitor of histone methyltransferase G9a and DNA methyltransferase,[172] could open chromatin regions that were closed in mature neutrophils from MM patients and induce expression of genes related to neutrophil immune activation. Accordingly, dose-dependent transcriptional changes in mature neutrophils from MM patients were observed after treatment with CM-272 (Figure 10C) and its mode of action was validated by confirming increased expression of several type 1 interferon–related genes (Supplemental Figure 10).[172] Most importantly, a significant enrichment of upregulated genes related with neutrophil activation was noted (Figure 10D), which suggests that hypomethylating agents could potentially be used to revert the immunosuppressive signature of mature neutrophils present in the tumor microenvironment. Accordingly, the cytotoxic potential of T cells engaged by a BCMAxCD3-bispecific antibody was restored and

even enhanced when mature neutrophils were pretreated with CM-272 (Supplemental Figure 11).

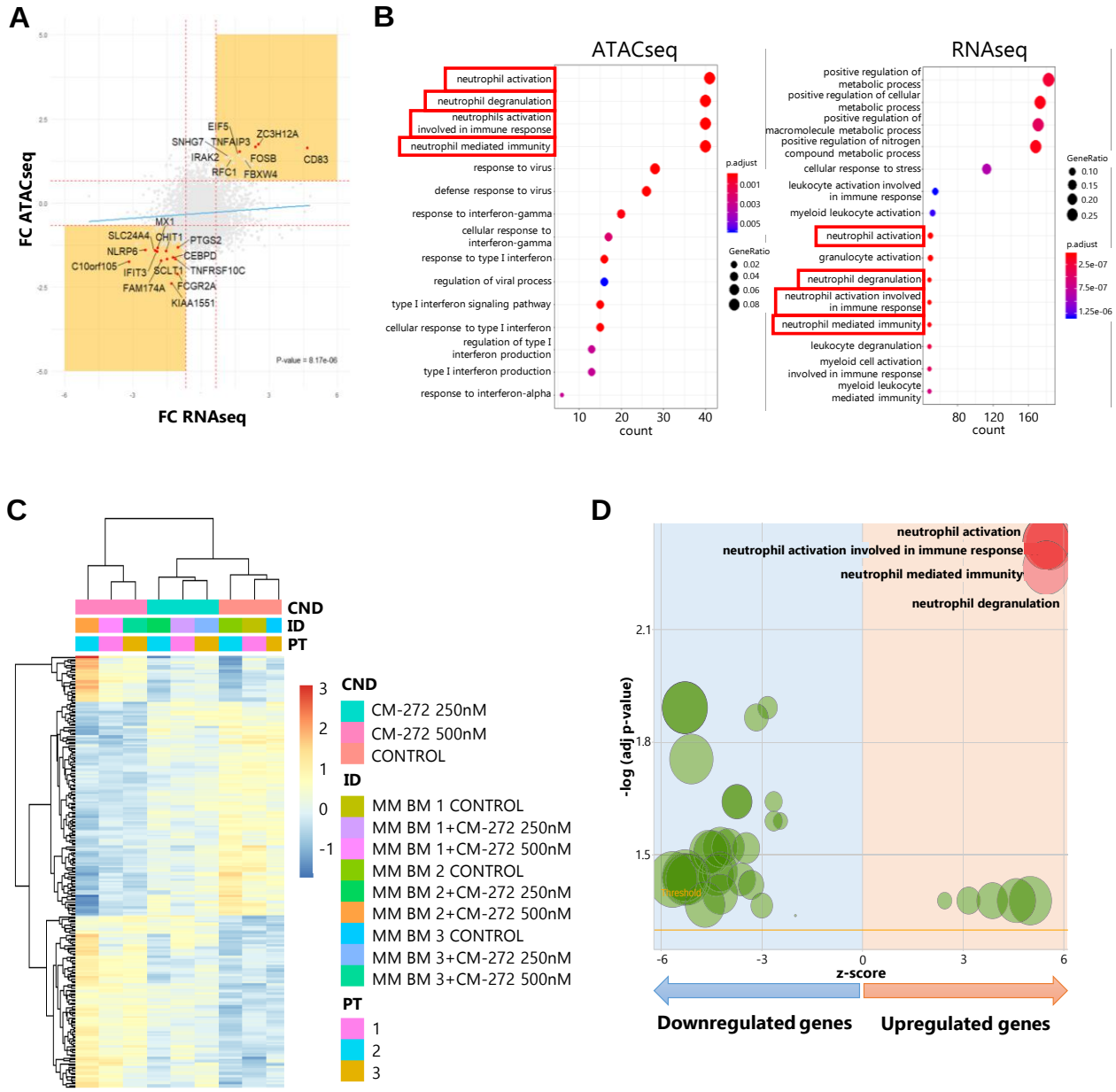

Figure 10. Transcriptional network of mature neutrophils is epigenetically deregulated in MM. (A) Correlation between gains and losses of chromatin accessibility near TSSs and gene expression for each sample. Significant positive correlation between MM-induced changes in gene expression level and chromatin accessibility at gene promoters in mature granulocytes (P = 8.17e^{-6}). **(B)** Gene ontology enrichment analysis of differentially expressed genes underscores functions related to neutrophil activation in MM. **(C)** Transcriptional analysis of mature neutrophils from MM patients (N = 3) treated with CM-272–segregated samples according to exposure and concentration of the drug. **(D)** Gene ontology enrichment analysis based on upregulated genes in mature neutrophils from MM patients after treatment with CM-272. FC, fold-change.

ID	Description	p value	p.adjust
GO:0042119	neutrophil activation	1.72e-11	3.56e-8
GO:0043312	neutrophil degranulation	2.27e-11	3.56e-8
GO:0002283	neutrophil activation involved in immune response	2.82e-11	3.56e-8
GO:0036230	granulocyte activation	2.83e-11	3.56e-8
GO:0002446	neutrophil mediated immunity	6.15e-11	6.18e-8
GO:0031325	positive regulation of cellular metabolic process	1.08e-10	8.60e-8
GO:0051173	positive regulation of nitrogen compound metabolic process	1.20e-10	8.60e-8
GO:0009893	positive regulation of metabolic process	3.33e-10	2.09e-7
GO:0043299	leukocyte degranulation	5.13e-10	2.87e-7
GO:0002275	myeloid cell activation involved in immune response	9.00e-10	4.29e-7

Table 2. Gene ontology enrichment analysis of genes closing or opening in mature neutrophils of MM patients vs HA.

Single T cell profiles in multiple myeloma and precursor states reveals early exhaustion and phenotypic determinants of immunotherapy response

Botta C & Perez C. et al. *Manuscript in review*

5.2.1. Clonal T cell expansions in healthy, benign and malignant BM

FACSorting was performed to isolate BM T cells from three HA, five cases with the precursor states of MGUS and SMM (MGUS/SMM), and nine patients with active, newly-diagnosed MM (Figure 11A, Supplemental Table 2). Droplet-based 5′ scRNA-seq and paired scTCR-seq was performed to analyze clonal relationship and functional states among BM T cells. After stringent quality control filtering, scTCR-seq yielded one or more complementarity-determining region 3 (CDR3) of α- or β-chains in 75,753 T cells with paired transcriptomes. These T cells were grouped into 541 distinct clonotypes, defined by a unique CDR3 being present in at least three single-cells, with a representation among total T cells ≥ 0.2% (Figure 11B and Supplemental Table 3 available in the shared folder).

The average number of clonal T cell expansions was 31 in HA, 30 in MGUS/SMM and 31 in MM (P = .9799) (Figure 11C). The ratio between non-clonotypic and clonotypic T cells was 3:1 in HA and MGUS/SMM, and 2:1 in MM (Figure 11D). HA showed significantly higher TCR diversity when compared to MGUS/SMM and MM patients (Figure 11E-F), as measured by the index scores of Chao1 (1937, 1399 and 1179, respectively; P = .0036) and ACE (2027, 1101 and 1170, respectively; P = .0036).[187,188] Elicited by these findings, WES and RNA-seq of tumor cells was performed in two (of the nine) MM patients to investigate the likelihood of neoantigen expression. After determining non-synonymous somatic mutations (12 and 15 in each patient), those being expressed were selected for analysis (5/12 and 4/15) (Figure 11G). HLA-A haplotypes were subsequently determined in both patients using the optiType algorithm,[176] before investigating with netMHC, the probability that mutated peptides had of being presented by patients' MHC. Overall, 2/5 and 2/4 of expressed mutations are potentially presented by patient'-specific HLA molecules (Figure 11G). Next, a deep learning model based on recurrent neural networks trained with available VDJDB and 10X databases, was developed to estimate the strength of the association between the TCR α- and β-chains of clonal T cells and the peptide-MHC cognates identified above in each patient (Figure 11H). Two positive predictions were identified in each of the

two patients, with similar results being observed using ERGO (Supplemental Table 4).[177] Collectively, reduced diversity of clonal T cells in benign and malignant BM, together with partial displacement of non-clonotypic by clonotypic T cells in MM, appeared to be the result of local recognition of tumor antigens.

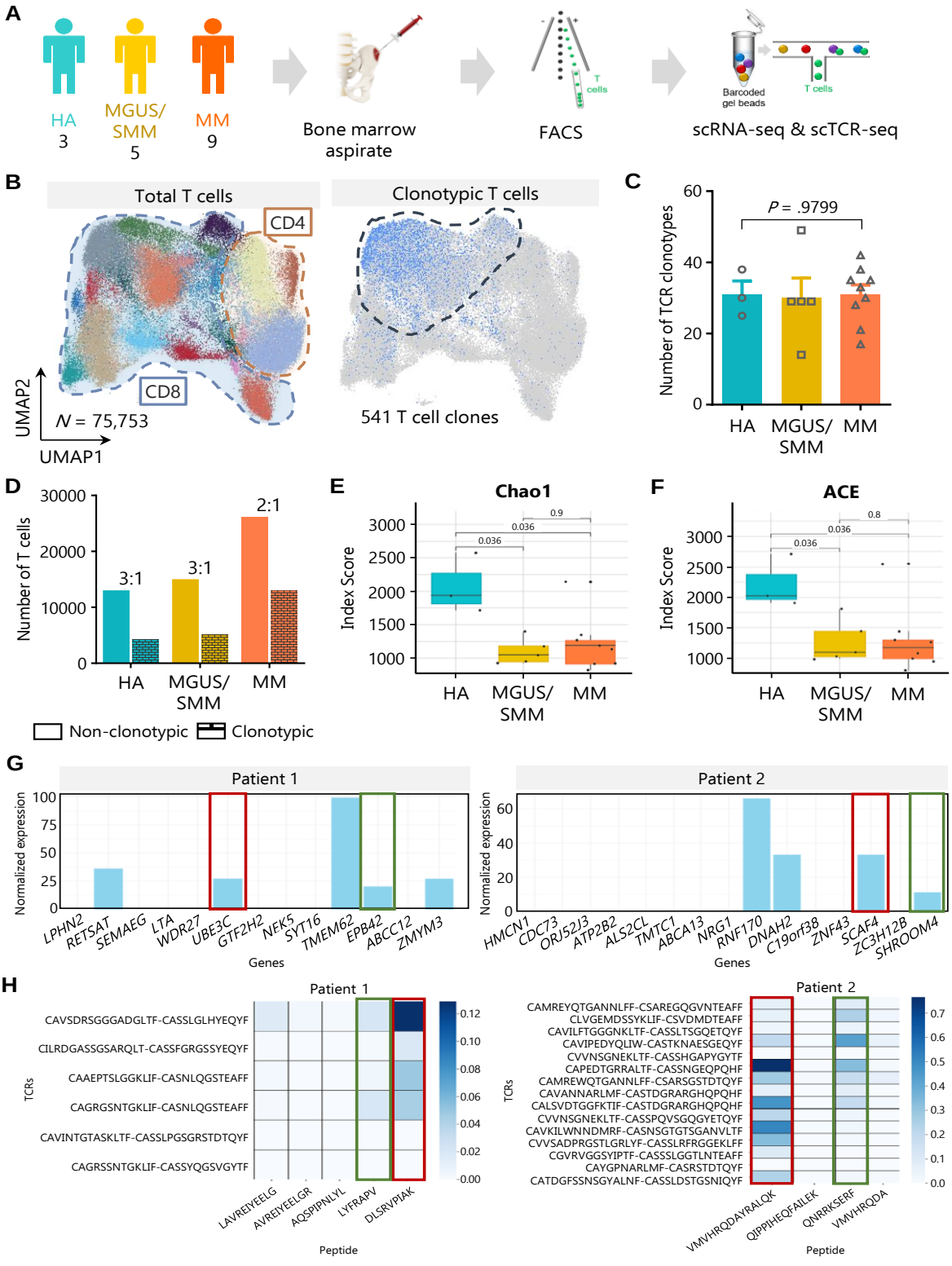

Figure 11. Clonal T cell expansions in healthy, benign and malignant BM. (A) Experimental design. BM aspirates were collected from three HA, five patients with the precursor states of MGUS or SMM, and nine patients with active, newly-diagnosed MM. T cells were isolated using FACSorting, followed by simultaneous scRNA-seq and scTCR-seq. **(B)** UMAP of 75,753 BM T cells from the subjects described above. Among these, 541 T cell clones were detected according to the following criteria: a unique complementarity determining region 3 being present in at least three single-cells, with a representation among total T cells ≥ 0.2%. **(C)** Average number of clonotypic T cells in HA, MGUS/SMM and MM patients. Error bars represent mean ± standard error mean (SEM). **(D)** Absolute number of non-clonotypic and clonotypic T cells in HA, MGUS/SMM and MM patients. The ratio between both is shown for each group. **(E)** TCR diversity in HA, MGUS/SMM and MM patients using the Chao1 index score. Error bars represent mean ± SEM. **(F)** TCR diversity in HA, MGUS/SMM and MM patients using the ACE index score. Error bars represent mean ± SEM. **(G)** Normalized mRNA expression of genes carrying somatic mutations in two of the nine MM patients described above. Those with higher probability of being presented by patients' major histocompatibility complex were highlighted with red and green rectangles. **(H)** Estimation of the strength of the association between the TCR α- and β-chains of clonal T cells and cognate peptide-MHC. Two positive predictions were identified in the two respective patients.

5.2.2. Evolving phenotype of clonal T cells during disease progression

Because there is very limited data on the effect of tumor progression in global T cell phenotypes determined by scRNA-seq,[105] BM T cell states across HA, MGUS/SMM and MM patients were therefore mapped. Overall, 116 million mRNA transcripts in 75,753 T cells from the 17 subjects described above, were sequenced. Transcriptional profiles of individual T cells allowed grouping of similar cells into clusters, which were characterized by profiling genes found to be cluster-specific (Supplemental Figure 12A, Supplemental Table 5 available in the shared folder). Thus, 17 subsets were identified including γδ T cells, double negative T cells, Tregs, five $CD4^+$ T cell clusters (naïve, stem cell memory [SCM], central memory [CM], effector memory [EM], effector and resting $CD4^+$ T cells), and eight $CD8^+$ T cell subsets (naïve, SCM, mucosal-associated invariant T [MAIT], interferon-induced proteins with tetratricopeptide repeats [IFIT], granzyme B [GZMB], H [GZMH] and K [GZMK] cells, plus an additional subset of $CD8^+$ T cells with increased expression of CD94) (Figure 12A). All 17 clusters were present in HA, MGUS/SMM and MM patients (Figure 12B, Supplemental Table 6). Furthermore, their relative distribution within the T cell compartment was similar across normal, benign and malignant BM, with significant differences being observed in only three subsets (MAIT and GZMH $CD8^+$ T cells, and double negative T cells). One possible explanation for the unexpected similarity could be that in MGUS/SMM and MM, bystander T cells (i.e., non-clonotypic) predominated over potential tumor-reactive

clonotypes (Figure 11D), which urged investigating transcriptomes at the level of clones rather than individual T cells.

Combined scTCR-seq and scRNA-seq analyses of non-clonotypic T cells (N = 63,953) and clonal T cells (N = 11,800) revealed significant enrichment of the $GZMB^+$, $GZMK^+$, naïve and $CD94^+$ $CD8^+$ clusters, counterbalanced by absent or nearly absent Treg, naïve, SCM, resting and CM $CD4^+$ T cells, as well as naïve and MAIT $CD8^+$ T cells (Figure 12C, Supplemental Figure 12B, Supplemental Table 7). Because clonotypic T cells comprised a mixture of T cell phenotypes (Figure 12D, Supplemental Table 8 available in the shared folder), including the $PD1^+GZMK^+CD8^+$, $TIGIT^+GZMB^+CD8^+$, Lysosomal-associated membrane protein 1 (LAMP1) or $CD107a^+CD8^+$ and $PD1^+$effector$CD4^+$ clusters, their transcriptional diversity was further analyzed during disease progression (Figure 12E, Supplemental Table 9). When compared to clonal T cells in healthy BM, intratumoral T-cell clones (i.e., in MGUS/SMM and MM) were characterized by decreased percentages of double negative T cells and $CD4^+$ T cells with effector phenotype. The progression from a normal to benign and malignant tumor microenvironment (i.e., HA vs MGUS/SMM vs MM) was further depicted by a progressive increment in $GZMK^+CD8^+$ and $GZMK^+PD1^+CD8^+$ T cells. A marked enrichment of clonotypic $LAMP1^+CD8^+$ T cells was observed exclusively in MM patients.

Next, gene expression and TCR data was combined to dissect the phenotypic trajectories of clonal T cell expansions throughout disease progression (Figure 12F). In HA, these cells were predominantly in an effector state, as defined by the expression of genes such as *GZMB* and *GZMK*. In MGUS/SMM, clonotypic T cells showed an intermediate phenotype between effector and exhausted states, with similar expression levels of *GZMB* and *GZMK* but higher mRNA counts of *IFIT2*. In MM patients, there was predominant clustering in terminal and exhausted differentiation stages, characterized by overexpression of *LAG3*, *LAMP1*, *TIGIT* and *TOX* (Figure 12F, Supplemental Figure 12C). There were trends of progressively increased expression of *PD1* and *LAG3* in clonal T cells from HA, MGUS/SMM and MM patients, as well as of reduced expression of *GZMB* and *PRF1* genes (Figure 12G and Supplemental Figure 12D). Taken together, the trajectory analysis of clonotypic T cells suggested the presence of continuously differentiating T cell states towards an exhausted phenotype ($GZMB^-GZMK^+PRF1^-TOX1^+$), which started in MGUS/SMM and peaked in MM. Because this was concomitant to reduced TCR diversity in benign and malignant BM (Figure 11E-F), the combined scRNA-seq and scTCR-seq data urged investigating if patients with

precursor conditions showing accumulation of potential tumor-reactive T cells with an exhausted phenotype, could be of greater risk of immune escape and malignant transformation.

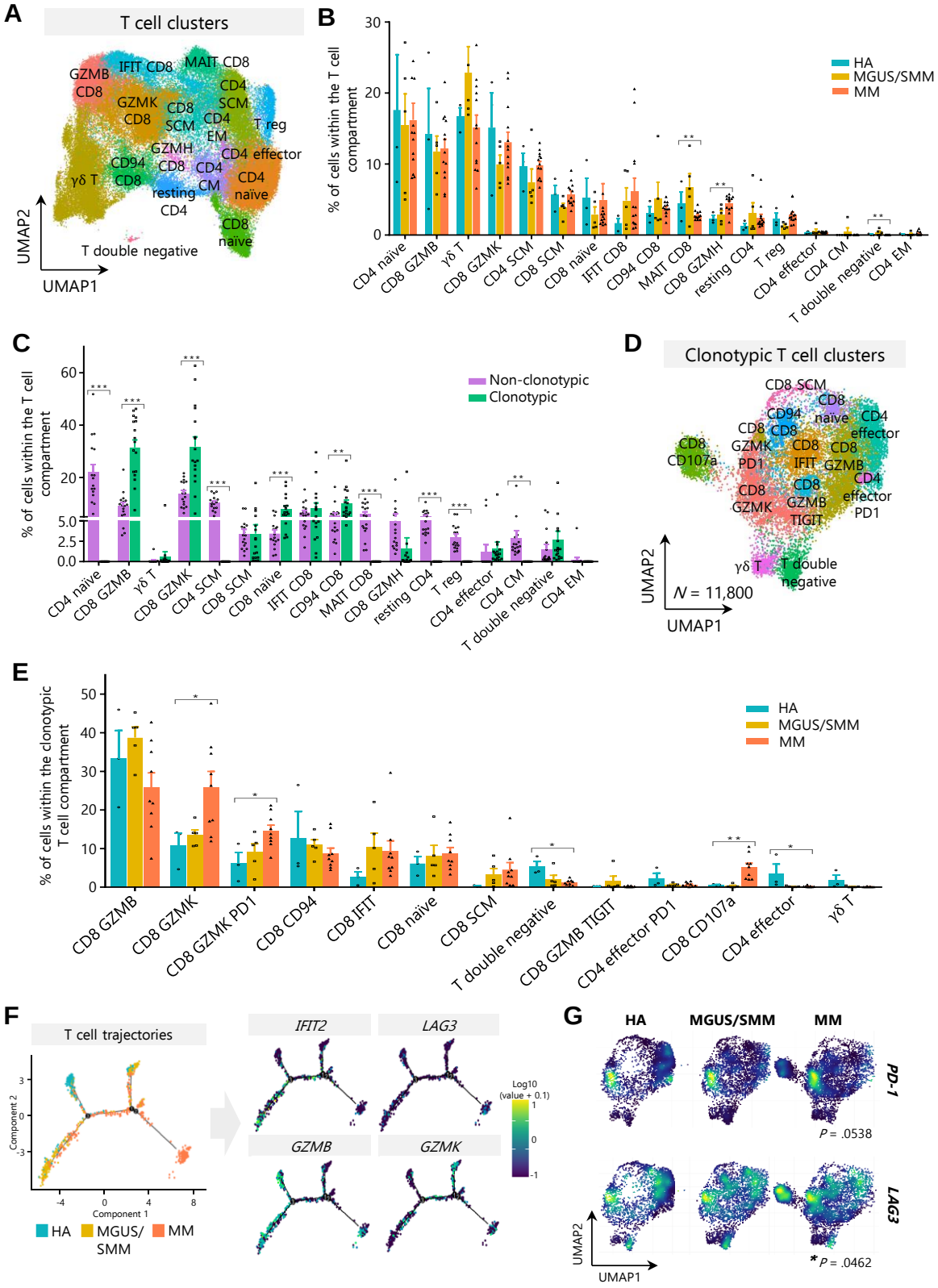

Figure 12. Evolving phenotype of clonal T cells during disease progression. (A) UMAP of 17 T cell clusters identified with scRNA-seq, in BM aspirates from three HA, five patients with benign MGUS/SMM, and nine patients with active, newly-diagnosed MM. **(B)** Relative distribution of the 17 clusters within the T cell compartment of HA, MGUS/SMM and MM patients. Error bars represent mean ± SEM, ***P* < .01. **(C)** Relative distribution of clusters within non-clonotypic and clonotypic BM T cells, identified with single-cell sequencing of T cell receptors following the criteria described in the main text and the legend of Figure 1. Error bars represent mean ± SEM, ***P* < .01, ****P* < .001. **(D)** UMAP of 13 clusters identified within clonotypic T cells from HA, MGUS/SMM and MM patients. **(E)** Relative distribution of the 13 clusters of clonotypic T cells in HA, MGUS/SMM and MM patients. Error bars represent mean ± SEM, **P* < .05, ***P* < .01. **(F)** Phenotypic trajectory of T cell clones, colored according to their respective origin: HA (green), MGUS/SMM (orange) and MM (dark orange) patients. The expression of genes such as *IFIT2*, *LAG3*, *GZMB* and *GZMK* are shown. **(H)** UMAP of mRNA expression of *PD-1* and *LAG3* in clonotypic T cells from HA, MGUS/SMM and MM patients. *P* values of the comparison between HA vs MGUS/SMM and MM.

5.2.3. Correlative markers of tumor reactive T cells to predict disease progression

The unaffordable costs of performing single-cell multiomic studies in larger series of patients urged the identification of phenotypic hallmarks of potential MM-reactive T cells that could be leveraged for MFC immune monitoring. Among 1,550 deregulated genes between non-clonotypic and T-cell clones from MGUS/SMM and MM patients (Supplemental Table 10 available in the shared folder), 71 coded for cell surface proteins; these included *CD2, CD3, CD8, CD27, CD28, CD52, CD55, CD62L, CD63, CD69, CD74, CD127, CD320, CCR6, CCR7, CXCR3*, and *LAG3*, amongst the most differentially expressed ones (Figure 13A, Supplemental Table 11). Namely, clonal T cells showed increased expression of *CD2, CD3, CD8, CD52, CD63, CD74, CD320, CXCR3* and *LAG3*, as well as reduced mRNA levels of *CD27, CD28, CD55, CD62L, CD69, CD127, CCR6* and *CCR7*. Selected markers were subsequently investigated according to their availability in antibody panels being used for immune profiling of intratumoral T cells in precursor states (Figure 13B).

Following the phenotypic hallmarks of potential tumor-reactive T cells identified above, the abundance of $CD8^+CD27^-CD62L^-CCR6^-CXCR3^+$ and $CD8^+CD28^-CD127^-$ T cells was measured in the tumor microenvironment of 90 SMM patients (Figure 13B, Supplemental Table 12). Percentages of both T-cell subsets above the respective median value in the whole series were significantly associated with shorter time-to progression from SMM to active MM (Figure 13C). Patients with >15.4% $CD8^+CD27^-CD62L^-CCR6^-CXCR3^+$ or with >5.5% $CD8^+CD28^-CD127^-$ cells within the BM T cell compartment, had median time-to

progression of 24 months vs not reached in the remaining cases. The concordance between patients identified according to the percentages of the two T-cell populations was high (N = 45/47, 96%), suggesting that both phenotypic profiles were identifying a similar subset of effector T-cells, possibly expanded in response to the tumor, but incapable of controlling it.

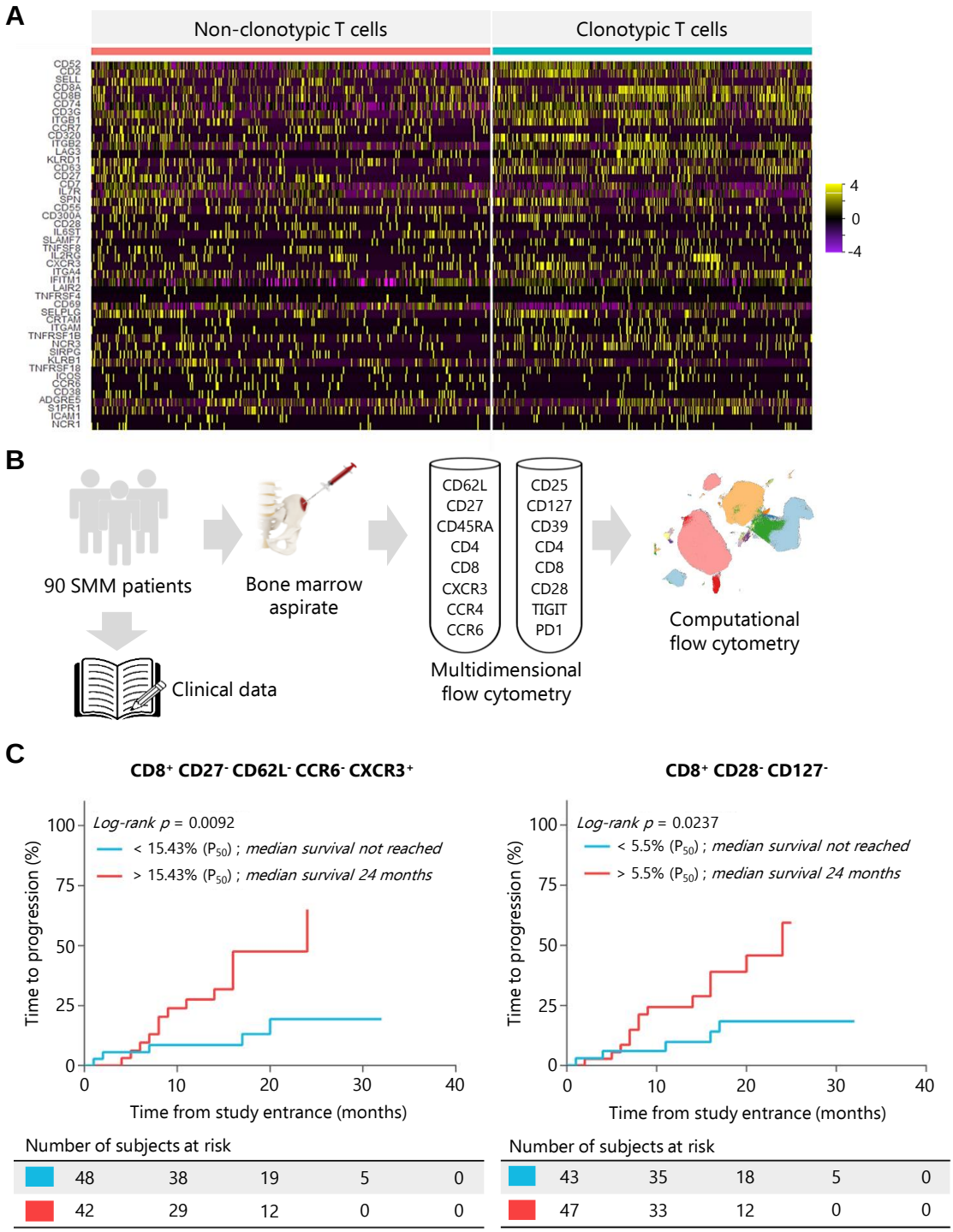

Figure 13. Correlative markers of tumor reactive T cells to predict disease progression. (A) Heatmap of the most differentially expressed genes between non-clonotypic and clonotypic intratumoral T cells from five patients with benign MGUS/SMM and nine patients with active, newly-diagnosed MM. A log-transformed fold-

change was used to measure gene expression. **(B)** Experimental design to assess in 90 patients with SMM, the prognostic value of BM T cell phenotypes previously found to be enriched in clonotypic T cells. **(C)** Time to progression of SMM patients stratified according to percentages equal or greater vs below the median values of $CD8^+CD27^-CD62L^-CCR6^-CXCR3^-$ (left) and $CD8^+CD28^-CD127^-$ (right) T cell percentages, within the BM T cell compartment.

5.2.4. Enhanced T-cell anticancer immunity using data-driven immunocheckpoint blockade (ICB)

To corroborate the association between progressive exhaustion of clonotypic T cells and tumor escape, intratumoral T cells in a genetically engineered $BI_{cγ1}$ mouse model that results from transgenic BCL2 and $IKK2^{NF\text{-}κB}$ expression in mature germinal center B lymphocytes by the cγ1-cre allele were characterized. Upon T-cell driven immunization with sheep red blood cells (SRBCs), mice spontaneously develop MM fulfilling two important characteristics of human disease: the evolution of pre-malignant MGUS into full-blown MM, and the interplay between tumor and the BM immune microenvironment during progression. A total of 31,088 BM T cells from control, MGUS and MM bearing mice were characterized by scRNA-seq and scTCR-seq (Figure 14A, Supplemental Figure 13, Supplemental Table 13). MGUS was defined as < 10% $GFP^+CD138^+B220^-sIgM^-$ BM PCs and no CRAB-like clinical features (hypercalcemia, renal disease, anemia, and bone disease), whereas MM was diagnosed when mice presented >10% tumor cells and/or CRAB.

Similarly to humans, the ratio between non-clonotypic and clonotypic T cells was higher in controls (2:1) and MGUS (2:1) than in MM (1:1) mice (Figure 14B-C). By contrast, TCR diversity peaked in MGUS and dropped significantly in MM (Figure 14D). This is possibly related to the pathogen-free environment where control (and tumor) mice were breed, as well as to the initial oligoclonal tumor expansion followed by clonal selection and uncontrolled proliferation (Supplemental Figure 13). In MGUS and MM mice, T cell clones showed increased expression of *CD8, CD38, Pd1, Lag3* and *Tigit* when compared to non-clonotypic cells (Figure 14E). Another similitude of clonotypic T cells with humans was the progressive differentiation from effector to exhausted states in MGUS and MM mice, including the higher expression of the immune checkpoints *Lag3, Pd1* and *Tigit* (Figure 14F, Supplemental Figure 14). Collectively, tumor progression in immunocompetent mice that spontaneously develop MM showed similarities with human cancer, and could therefore be

used as a model to enhance T-cell anticancer immunity with immunotherapy tailored to the dynamic phenotype of tumor-reactive T cells.

Because intratumoral clonotypic T cells showed, both in humans and in mice, both in precursor and malignant stages, co-expression of multiple immune checkpoints, the combined administration of anti-PD1 plus anti-LAG3 or anti-TIGIT was tested in immunocompetent C57BL/6 mice intravenously injected with the MM5080 murine MM cell line, which was established from BI_{cY1} mice with an additional P53 deletion (Figure 14G and Supplemental Figure 15). This model is characterized by the progressive accumulation of tumor cells in the BM, together with increased percentages of $CD8^+$ T cells overexpressing *Pd1, Lag3* and *Tigit* (Supplemental Figure 15). Therefore, this model was leveraged to enhance the antitumor effects of tumor-naïve T cells with combined ICB. Mice were treated with ICB (single-agent or dual combinations) at days +3, +10 and +17. Interestingly, none of the ICB used in monotherapy prolonged survival; by contrast, the co-administration of anti-PD1 plus anti-LAG3, or anti-PD1 plus anti-TIGIT, resulted in longer overall survival (Figure 14G). Thus, preemptive blockade of two immune checkpoints at the onset of the disease and before T cell exhaustion, significantly delayed MM growth.

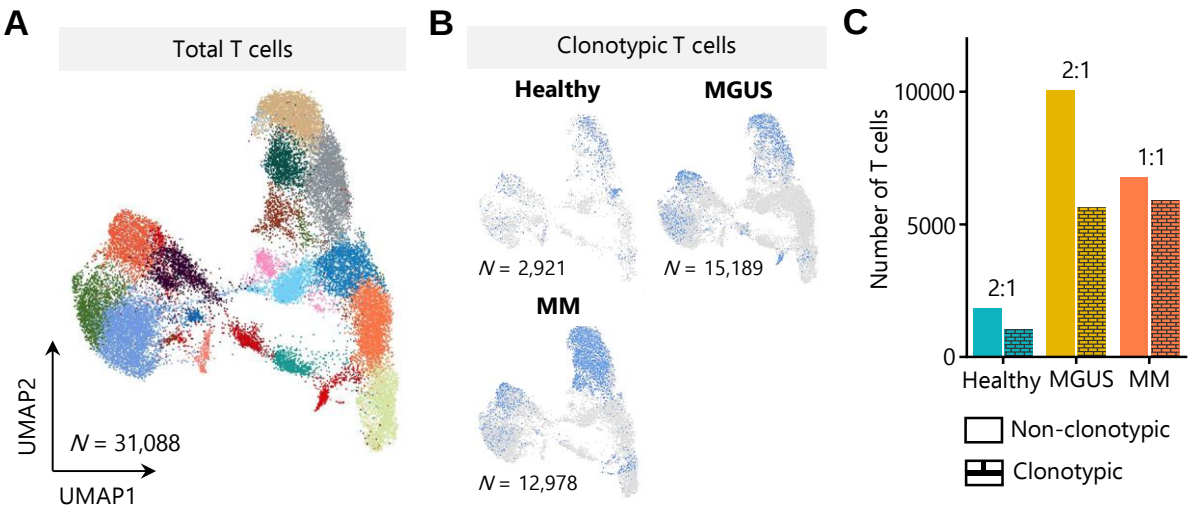

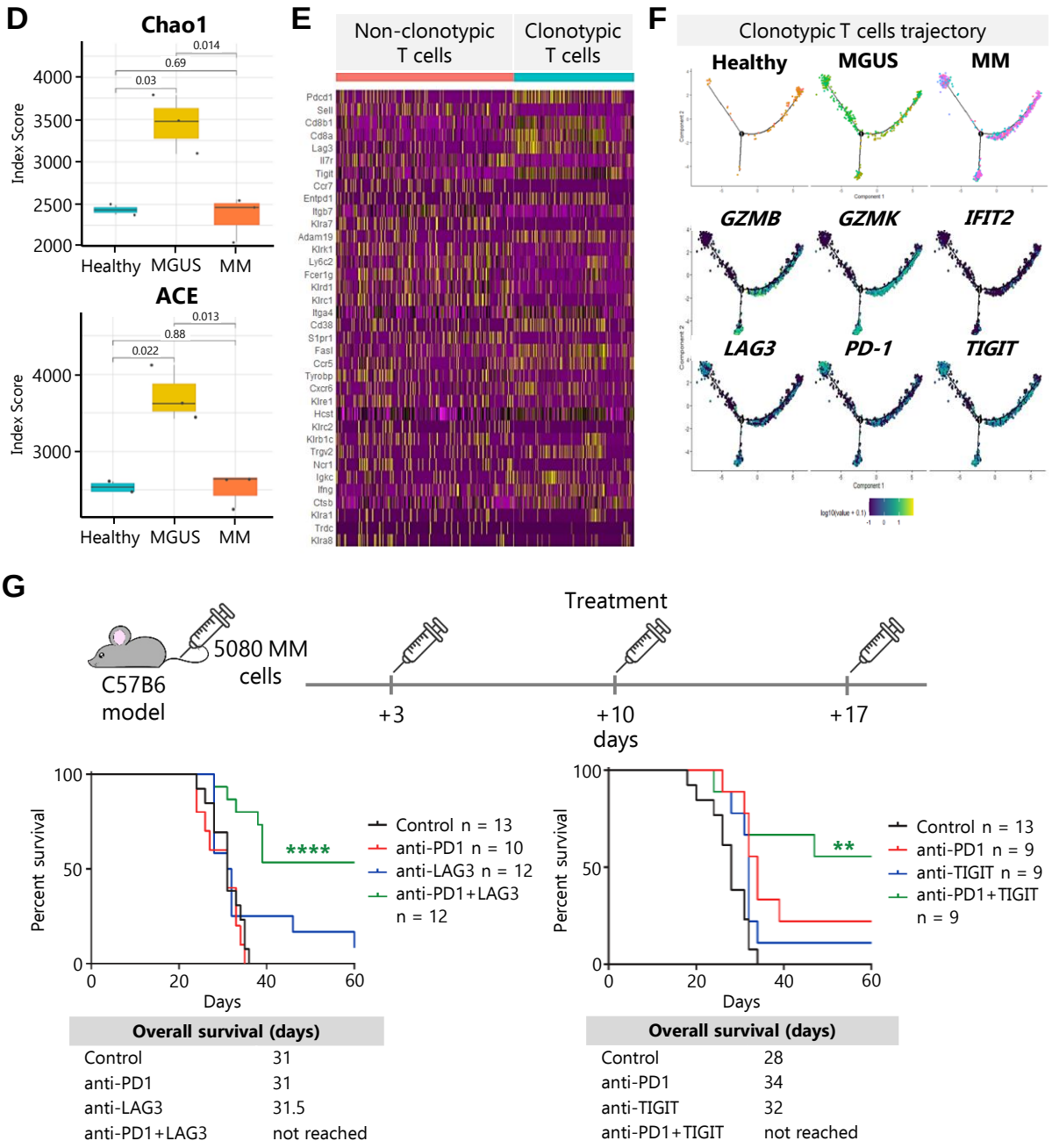

Figure 14. Enhanced T-cell anticancer immunity using data-driven ICB in experimental mice. (A) UMAP of 31,088 BM T cells from control, MGUS and MM bearing mice. This model is termed $BI_{cγ1}$, as it carries transgenic BCL2 and IKK2$^{NF\text{-}κB}$ expression in mature germinal center B lymphocytes by the cγ1-cre allele, and spontaneously develops MM at 11 months of age, which is preceded by a precursor MGUS stage at 6 months of age **(B)** UMAP of clonotypic T cells in the BM of healthy, MGUS and MM $BI_{cγ1}$ mice. T cell clones were defined using the same criteria as in humans: a unique complementarity determining region 3 being present in at least three single-cells, with a representation among total T cells ≥ 0.2%. **(C)** Absolute number of non-clonotypic and clonotypic T cells in healthy, MGUS and MM $BI_{cγ1}$ mice. The ratio between both is shown for each group. **(D)** T cell receptor (TCR) diversity in healthy, MGUS and MM $BI_{cγ1}$ mice using the Chao1 and ACE index scores. Error bars represent mean ± standard error mean (SEM). **(E)** Heatmap showing top differentially expressed genes

between non-clonotypic and clonotypic BM T cells in $BI_{cγ1}$ mice, measured with log-transformed fold-change. **(F)** Phenotypic trajectories of clonal T cells in healthy, MGUS and MM $BI_{cγ1}$ mice. The expression of genes such as *IFIT2*, *LAG3*, granzyme B (*GZMB*) and K (*GZMK*), *PD-1* and *TIGIT*, are shown. **(G)** A total of $10x10^6$ cells from the MM5080 cell line were intravenously injected into 8-week-old C57BL/6 mice. This cell line was established from BM MM cells from a P53-$BI_{cγ1}$ mouse, which results from the addition of a heterozygous P53 deletion to $BI_{cγ1}$ mice. Three days after cell injection, mice were randomly divided into experimental groups and received a weekly dose of anti-PD1 (200 µg; RMP1-14), anti-LAG3 (200 µg; C9B7W) or anti-TIGIT (200 µg; 1G9), as monotherapy or in combination for the three following weeks. Kaplan-Meier OS for each group of mice is shown at the bottom of the panel.

5.2.5. The ratio between CD27 negative and positive T cells as a surrogate of T cell clonality throughout disease progression

One of the antigens being differentially expressed between non-clonotypic and clonotypic T cells was CD27; the latter showing significantly lower mRNA levels (Figure 15A). As such, there was a significant association between increasing numbers of T-cell clones and a higher ratio between CD27 negative and positive T cells (CD27 ratio), after defining the latter as those showing >10 counts of CD27 mRNA (Figure 15B). This was an important observation, because CD27 is amongst the markers that are routinely evaluated through MFC for the screening of PCs clonality in patients with monoclonal gammopathies.[189] Indeed, the association between T cell clonality and the CD27 ratio was similarly observed by MFC (Figure 15C). Thus, the putative abundance of clonotypic T cells could be estimated in larger series of patients with available immunophenotypic data, according to the CD27 ratio. To this end, FlowCT was used for the simultaneous and semi-automated analysis of BM immune cell types, including CD27 negative and positive T cells (Figure 15D and Supplemental Figure 16), from HA (N = 26), MGUS (N = 108), SMM (N = 160), newly-diagnosed (N = 384) and relapsed MM (N = 175) patients, all of whom tested with the same standardized antibody combination including CD27 (Figure 15D). The CD27 ratio increased from HA to MGUS and SMM, further augmented in newly-diagnosed MM, and peaked in relapsed patients (Figure 15E). A progressive increment of the CD27 ratio was similarly observed using scRNA-seq (Figure 15F).

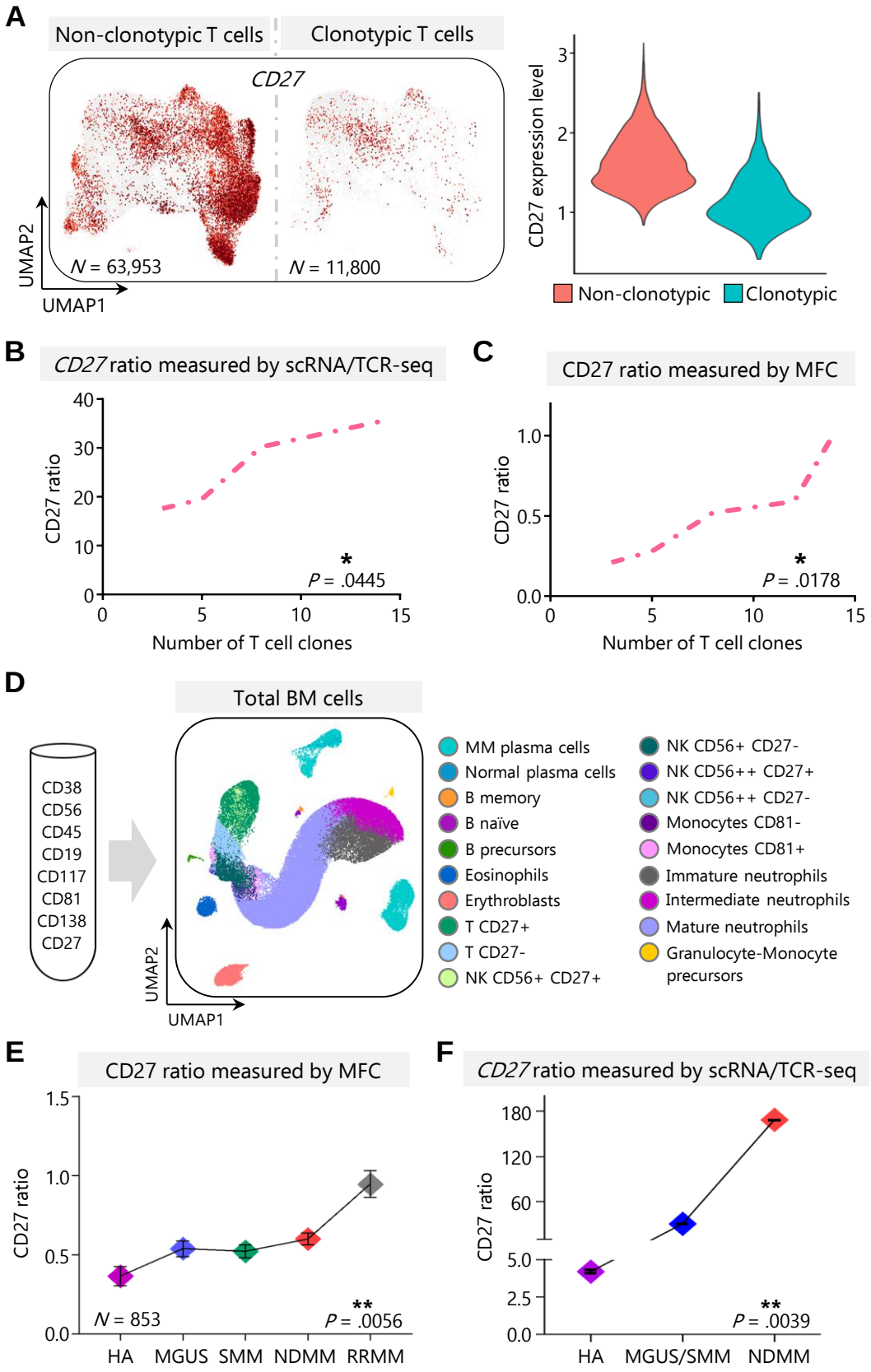

Figure 15. The ratio between CD27 negative and positive T cells as a surrogate of T cell clonality throughout disease progression. (A) mRNA expression of CD27 in non-clonotypic vs clonotypic BM T cells, shown in a UMAP and violin plots. **(B)** Association between the ratio of CD27 negative and positive T cells with

the number of T cell clones analyzed by scRNA/TCR-seq. *P < .05. **(C)** Association between the ratio of CD27 negative and positive T cells with the number of T cell clones analyzed by MFC. *P < .05. **(D)** UMAP of BM immune cells using computational flow cytometry analysis. All samples were stained with the eight-color monoclonal antibody combination described in the panel, using standardized methods for batch and semi-automated analysis. A total of 19 clusters were identified, including CD27 negative and positive T cells. **(E)** The CD27 ratio measured by MFC in HA (N = 26), patients with MGUS (N = 108), SMM (N = 160), newly-diagnosed (NDMM, N = 384) and relapsed/refractory MM (RRMM, N = 175). "N" represents the total number of cases. Error bars represent mean ± SEM, **P < .01. **(F)** The CD27 ratio measured by scRNA-seq in HA, MGUS/SMM and NDMM patients. Error bars represent mean ± SEM, **P < .01.

5.2.6. The ratio between CD27 negative and positive T cells prior lenalidomide combination therapy predicts survival

Among MM patients with diagnostic MFC assessment, 271 and 272 were respectively enrolled in the transplant-ineligible GEM-CLARIDEX[18] and transplant-eligible GEM2012MENOS65[16] phase 3 clinical trials. Both series yielded unique opportunities to investigate the prognostic value of the CD27 ratio as a surrogate of clonotypic T cell abundance in patients treated with regimens including lenalidomide, an IMID that requires tumor-reactive T cells to mediate its anti-MM effect.[26]

Using computational flow cytometry, 22 BM clusters were identified, including CD27 negative and positive T cell subsets (Figure 16A). The presence of a CD27 ratio higher than the median value (i.e., ≥ 0.3) was significantly associated with longer PFS in both transplant-ineligible (HR: 0.597, 95% confidence interval: 0.366 – 0.975; P = 0.0402) (Figure 16B) and transplant-eligible patients (HR: 0.493, 95% confidence interval: 0.289 – 0.840; P = 0.0052) (Figure 16C), and with OS in the latter (Supplemental Figure 17). Furthermore, multivariate analysis including classical MM prognostic factors such as the International Staging System, LDH and cytogenetic risk demonstrated that the CD27 ratio showed independent prognostic value for PFS (Supplemental Table 14). Indeed, the CD27 ratio was not associated with patients' staging and LDH levels (Supplemental Table 15), nor the presence of cytogenetic abnormalities such as +1q, del(1p), del(17p) and IgH chromosomal translocations (Supplemental Table 16). Furthermore, there were no differences in the mutational burden and transcriptional profile of tumor cells, respectively assessed by whole-exome sequencing (N = 23) and RNA-seq (N = 102), between patients with < 0.3 and ≥ 0.3 CD27 ratio (Supplemental Figure 18).

Additional studies were performed to gain further insight into a putative association between increased numbers of clonotypic T cells in the tumor microenvironment (i.e., high CD27 ratio) and their re-activation upon exposure to lenalidomide. First, mRNA expression of HLA class I and II molecules was analyzed through RNA-seq in normal PCs from HA (N = 25) and tumor cells from MGUS (N = 12) and MM patients (N = 216). Whereas HLA class II molecules were downregulated in tumor cells, the expression of HLA-A, HLA-B, HLA-C, HLA-E and β2-microglobulin was higher in patients vs controls (Figure 16D). Next, whole BM aspirates from MM patients (N = 3) were cultured in an organoid 3-dimensional model during five days, and treated with 1 µM lenalidomide +/- an anti-HLA antibody to block TCR-MHC interactions. The significant tumor cell killing induced by lenalidomide was nearly abrogated in the presence of HLA blocking (Figure 16E). Lastly, the immunomodulatory effects of lenalidomide were measured in PB T cells of 54 MM patients enrolled in the GEM-CLARIDEX trial, before and after three induction courses (C3). Using computational flow cytometry and an antibody combination specifically designed to characterize T cell differentiation upon antigen recognition, 39 clusters were systematically identified at diagnosis and C3 (Figure 16F and Supplemental Figure 19A). This analysis showed a significant reduction of naïve Treg, naïve and terminally effector memory CD45RA^{+}CD127^{lo}PD-1^{-} CD4^{+} T cells, counterbalanced by an expansion of central memory CD127^{+}PD-1^{-} CD4^{+} T cells, as well as of effector memory CD127^{lo} (PD-1^{-} and PD-1^{+}) and CD127^{+}PD-1^{+} CD8^{+} T cells (Figure 16G, Supplemental Figure 19B). Collectively, these data reinforce the association between the prognostic value of the CD27 ratio and the re-activation of clonotypic T cells upon lenalidomide combination therapy.

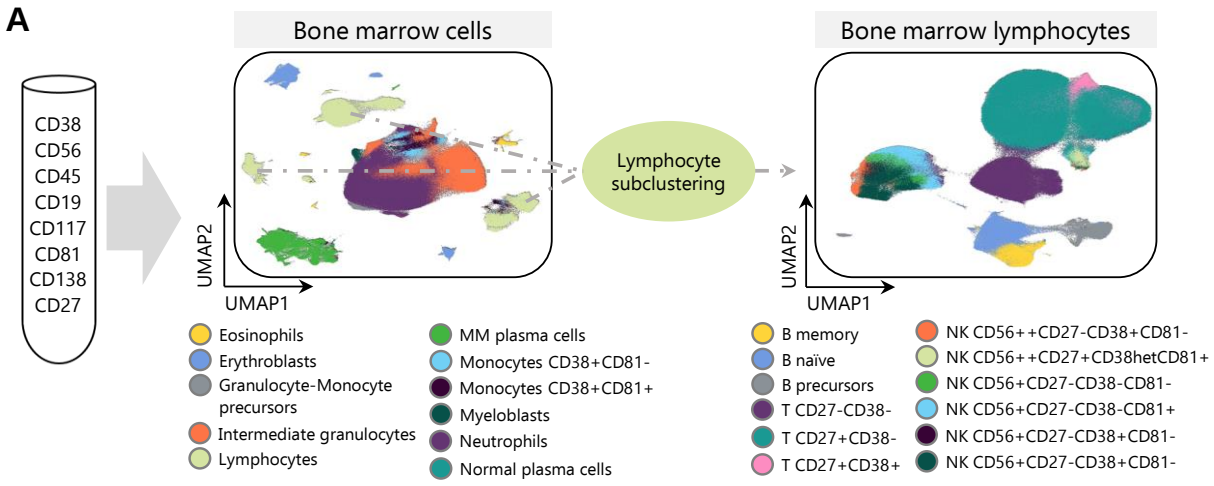

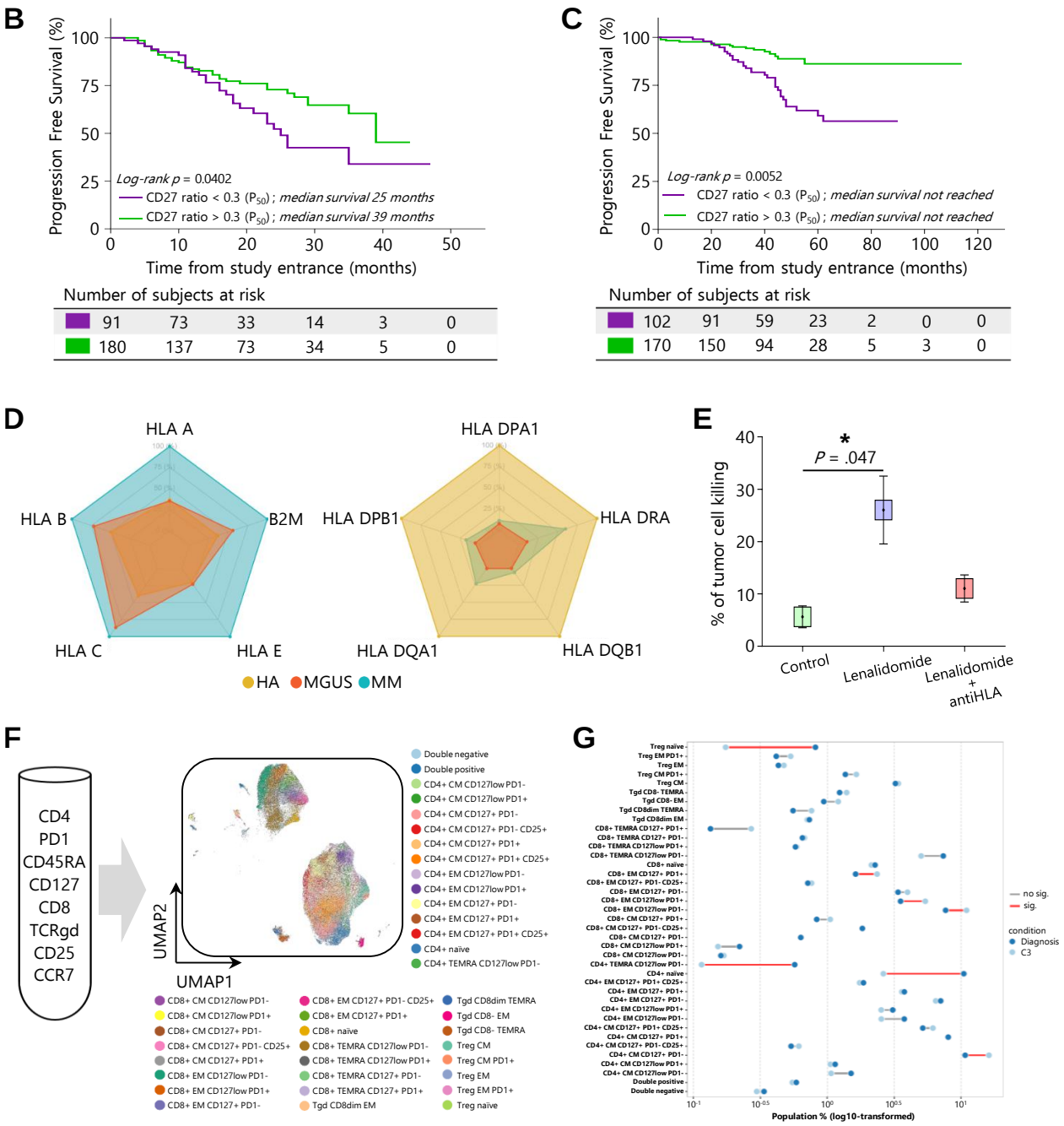

Figure 16. The ratio between CD27 negative and positive T cells prior lenalidomide combination therapy predicts survival. (A) UMAP of BM cells from newly-diagnosed MM patients. All samples were stained with the same eight-color monoclonal antibody combination described in the panel, and processed using standardized protocols. Computational flow cytometry was used to cluster BM cells and to subcluster lymphocytes. A total of 22 clusters and subclusters were identified, including CD27 negative and positive T cells. **(B)** PFS of 271 transplant-ineligible MM patients enrolled in the PETHEMA/GEM-CLARIDEX clinical trial, stratified according to values of CD27 ratio below vs equal or greater than the median value observed in the entire MM series (0.3). **(C)** PFS of 272 transplant-eligible MM patients enrolled in the PETHEMA/GEM2012MENOS65 clinical trial, stratified according to values of the ratio between CD27 negative and positive T cells below vs equal or greater

than the median value observed in the entire MM series (0.3). **(D)** Radar charts of mRNA expression of HLA class I and II molecules in PCs from HA (N = 25), MGUS (N = 12) and MM (N = 216) patients. **(E)** Boxplots representing the percentage of tumor cell killing after culture in a 3-dimensional organoid model and treatment with 1 μM lenalidomide +/- an anti-HLA antibody to block TCR-MHC interactions. Error bars represent mean ± SEM, *P < .05. **(F)** UMAP of PB T cells from 54 MM patients enrolled in the PETHEMA/GEM-CLARIDEX clinical trial. All samples were stained with the same eight-color monoclonal antibody combination described in the panel, and processed using standardized protocols. **(G)** Dumbbell plot showing variation in the relative distribution of 39 T cell clusters in patient-matched samples at diagnosis and after three induction courses. Significant differences (P < .05) were highlighted with red lines.

6. Discussion

Emerging immunotherapies have shown efficacy in the treatment of early- and late-stage MM.[109,190,191] Therefore, better understanding of the complexity and diversity of the tumor immune milieu is warranted to improve the ability to predict, monitor, and guide immunotherapeutic responsiveness. Next-generation techniques have given the opportunity to study immune cell populations with unprecedented resolution, and such knowledge must have clinical translation to improve patient care.

Nowadays, there is growing interest in targeting immunosuppressive cells to optimize T-cell activity and immunotherapy efficacy in MM. However, the ability to specifically target immunosuppressive cells while preserving the function of antitumor immune cells remains a challenge in the absence of specific cell markers, and MDSCs are a good example of this conundrum. MDSCs were first described in 2007,[192] but since then, the few studies performed in humans have commonly required isolation by density centrifugation of PB samples because of the lack of markers to isolate G-MDSCs from other cells in the tumor microenvironment.[96] Interestingly, these low-density granulocytes were found to be a heterogeneous mix of both banded and segmented neutrophils,[96,193] but not of more immature stages. These findings are consistent with the observation made during the PhD thesis, that there is a gradient of progressive immunosuppression from immature to mature neutrophils, reaching its maximum at the banded/segmented stage.

The G-MDSC–specific Gr-1 surface antigen is only present in mice, and therefore, human G-MDSCs have been attributed to a broader $CD11b^{+}CD14^{-}CD15^{+}CD33^{+}HLADR^{-}$ phenotype. However, this combination of markers could not distinguish G-MDSCs from common neutrophils in the analysis shown above; in fact, most maturing granulocytes are $CD11b^{+}$, CD15 is also expressed in eosinophils, and CD33 is present in all myeloid cells. CD16 has been proposed as an additional marker[194] to identify G-MDSCs, but alone it is not sufficient, because it is also expressed in non-classic monocytes that coincidently downregulate CD14.[195] Therefore, in the absence of established markers, human G-MDSCs can only be defined by their functional hallmarks (T-cell suppression and arginase 1 expression). The analysis of which granulocytic subset had prognostic value showed that only mature neutrophils (and no other granulocytic subset) present in the MM tumor microenvironment correlate with patient outcome. Furthermore, these cells exerted the strongest T-cell immunosuppression and expressed higher levels of inflammatory cytokines, such as TGFβ1, TNF, and VEGFA, together with an increase in NF-κB and other G-MDSC-

associated markers (e.g. PTGS2, CSF1, IL-8, IRF1, IL4R, STAT1, STAT3, STAT6) when compared with intermediate and immature neutrophils.[196–198] Therefore, one of the outputs of the PhD thesis was the phenotypic identification of G-MDSCs in MM: $CD11b^{+}CD13^{+}CD16^{+}$ neutrophils.

Structured models of transcriptional, phenotypic, and functional diversity are instrumental for better understanding of immune cell biology. However, unlike in other myeloid cells, in which diverse functional properties have been linked to specific molecular programs, the transcriptional heterogeneity behind the functional diversity of neutrophils remains largely unknown.[199] As noted above, the identification of surface markers enabling the tracking of immunosuppressive neutrophils (i.e. G-MDSCs) within the MM tumor microenvironment, elicited subsequent studies showing that maturing neutrophil subsets have unique gene expression profiles that are rewired into an immunosuppressive state through epigenetic modulation in the BM of patients with cancer. It has been suggested that TGF-β, an immunosuppressive cytokine produced by tumor cells from various cancer types, polarizes neutrophils to a protumorigenic phenotype.[200,201] The results of the PhD thesis show that exposure to TGF-β is able to shift the transcriptional profile of mature neutrophils from HA to a program similar to that found in MM, and future studies are warranted to investigate a possible correlation between TGF-β level and the immunosuppressive potential of G-MDSCs in BM aspirates. Additional research should also be performed to identify which other players in the BM milieu may contribute to this phenomenon. Another important observation was that the molecular network of mature neutrophils from MM patients could be modified by epigenetic drugs and thereby prevent their immunosuppressive effect in T cells engaged by a BCMAxCD3-bispecific antibody. Therefore, these results propose further investigation of their biology to identify targeted therapies for the rewiring of G-MDSCs and increase the successful application of immunotherapy in MM and other tumors.

Tumor recognition by T cells is essential for anticancer immunity, and identification of cell states that indicate the presence of a tumor-specific T cell repertoire is needed for informative immune profiling of patients. However, a major limitation to understand the origin and fate of T cells in tumor immunity is the lack of quantitative and qualitative information on the distribution of individual T-cell clones.[202] The results of the PhD thesis showed that the number of clonotypic T cells was similar between HA and patients with benign and malignant monoclonal gammopathies. This observation could be partially related to the fact that the

BM acts as a reservoir of memory T cells, as well as a primary lymphoid organ.[203] Accordingly, an increased number of clonotypic T cells was noted in tumor vs control mice, which are bred in a virtually pathogen-free environment. More importantly, reduced clonal diversity was observed the moment that tumor cells started infiltrating the BM (i.e., MGUS/SMM), and a putative displacement of bystander by tumor-reactive T cells in full-blown disease. Because skewed T cell clonality was followed by progressively exhausted and terminally-differentiated T cell states in MM patients and mice, these findings suggest that T cells react at the onset of cancer, but lose control of tumor growth due to a possible lack of T cell replenishment and accumulating dysfunctionality in result of chronic antigen exposure. The fact that cluster distribution of clonotypic vs non-clonotypic T cells was notoriously different, further supports this hypothesis.

TILs include both T cells specific for tumor antigens and bystander T cells with partially overlapping phenotypes.[102,103] Although selected markers have been utilized to exclude T cells recognizing a wide range of epitopes unrelated to cancer (e.g., PD-1, CD39, CD103), these may generate false-negative selection in tumors with limited data about their phenotype. Another output of the PhD thesis was a detailed list of 1,531 genes, including 78 coding for cell surface proteins, differentially expressed between non-clonotypic and clonotypic T cells from patients with monoclonal gammopathies. As expected, clonal T cells showed overexpression of CD8 and markers related to antigen-dependent differentiation such as *CD27, CD52, CD62L, CD63, CD74, CD320* and *CXCR3*; also markers of T-cell exhaustion such as *LAG3*, while *PD-1* was not amongst the top differentially expressed genes. These data confirms and extends previous observations in MM,[204] and help explaining the limited clinical benefits of anti–PD-1 blockade in recent phase 3 clinical trials.[205,206] If, similarly to solid tumors,[207–210] ICB combination therapy is needed to reactivate and expand MM-specific T cells, remains unexplored.

In addition to patients with full-blown disease, anti–PD-1 monotherapy has shown limited efficacy in SMM patients with intermediate/high risk of progression to symptomatic MM.[211] A recently-developed spontaneous MM model that recapitulates the progression from benign to malignant states in immunocompetent mice, yielded a unique opportunity to better understand these negative results. As in humans, murine T cell clones exhibited exhausted phenotypes involving the co-expression of various immune checkpoints at MGUS and MM stages. These results are in agreement with the finding that the CD27 ratio (i.e. possible

surrogate of T cell clonality) increased in MGUS patients, remained stable in SMM, further increased in MM, and peaked in relapsed/refractory patients. Therefore, ICB combination therapy administered at the onset of the disease was evaluated in mice with tumor-naïve T cells, and prolonged survival was observed with anti-PD1 plus anti-LAG3 or anti-TIGIT. These results build upon previous pre-clinical evidence of an immune-inhibitory role of LAG3 and TIGIT in MM, and a possible benefit when blocking these immune checkpoints.[41,212,213] Furthermore, the combined scTCR-seq and scRNA-seq data uncovered an expansion of $CD8^+CD107a^+$ clonotypic T cells in MM, which among other genes, overexpressed the V-Set Immunoregulatory Receptor (VISTA) immune checkpoint (data not shown). Antagonist monoclonal antibodies targeting VISTA are being investigated in solid tumors but not in MM. Because VISTA inhibits T cell activation and contributes to the immunoinhibitory functions of MDSCs, which are relevant to MM immunopathobiology, its therapeutic role in this disease warrants investigation.

Lenalidomide (alone or in combination with dexamethasone) significantly prolonged time-to progression of high risk SMM patients in two phase 3 clinical trials[109,110] and is a backbone of frontline MM therapy.[17,214] IMIDs bind to the E3 ligase substrate-recognition adapter protein cereblon and, therefore, the protein is essential for the therapeutic effect of these drugs. Surprisingly though, more than two thirds of patients do not show point mutations, copy losses/structural variations or specific variant transcripts of cereblon by the time they become refractory to IMIDs. Thus, determinants of response and resistance remain largely unknown and there are no routine biomarkers to predict clinical outcomes prior lenalidomide treatment.[215–218] The results of the PhD thesis suggest that the efficacy of IMIDs could depend on the amount and properties of TILs. Namely, that the ratio between CD27 negative and positive T cells in the tumor microenvironment predicted survival in two independent series of patients, representative of both transplant-eligible and ineligible MM. A strength of the observed novel relationship between CD27 ratio and outcome, is that it is agnostic to the clone target. This is important because the clonal T cell repertoire will vary markedly within and between individuals and thus, a generalized surrogate biomarker is required for translation to patient care. Therefore, similar to colorectal cancer where $CD39^+$ T cells have been hypothesized as a readout of tumor-specific response to anti–PD-1 treatment,[102] future studies will determine the extent to which the CD27 ratio is a useful maker of tumor specificity and response to lenalidomide in MM. Fortunately, CD27 is commonly used to screen for

PCs clonality in patients with monoclonal gammopathies,[189,219] and MFC is considered as an obligatory diagnostics test in MM.[17] Thus, there is potential for the CD27 ratio to become a biomarker of patients with different T cell composition who may display distinct clinical behavior upon treatment with lenalidomide.

The fact that only a small fraction of intratumoral T cells have the capacity to contribute to tumor control, suggests that therapeutic strategies aimed at increasing the frequency and breath of the tumor-specific TCR compartment are poised to show clinical benefit.[103] However, not all immunotherapies that rely on the re-activation and clonal expansion of tumor-reactive T cells have been successful in MM, and even those that are currently approved, are efficacious in a subset of patients. The results of the PhD thesis provide a framework to understand the determinants of success or failure to immunotherapies and which patients may benefit the most. For example, the finding that SMM patients at greater risk of progression had increased percentages of intratumoral T cells with phenotypic hallmarks of possible tumor-antigen recognition, is an interesting observation that builds upon previous data suggesting that the clinical benefit of lenalidomide in high-risk SMM resulted, at least in part, from the immune modulation of T and NK cells.[111] Therefore, the single-cell atlas of TILs in MM and its precursor states made available in this thesis, can be leveraged to identify new immune biomarkers of malignant transformation, and to develop personalized immunotherapies for the prevention of disease progression.

As human cancers arise in an immunocompetent host, tumor development is shaped by immunoediting and malignant cells develop the capacity to escape tumor antigen responses.[220] Indeed, the classical paradigm of host-tumor interaction – i.e. elimination, equilibrium and escape –, is reflected in the clinical behavior of MM which progresses from MGUS and SMM.[203] The results shown above suggest that reduced antigen presentation might not be the predominant mechanism of immune evasion in MM, and that prolonged exposure to tumor antigens during pre-malignant stages induces exhaustion of expanded T cell clones that potentially recognize tumor antigens. Therefore, this PhD thesis illustrates the power of combining transcriptomic with TCR analysis to shed light on the functional impairment of T-cell mediated immunity in the tumor microenvironment, and how the systematic interrogation of TILs is key to future development of immunotherapy, and the prediction of clinical responses in cancer.

7. Conclusions

1. Only the percentage of mature neutrophils and not of any other granulocytic subset had a significant impact in progression-free survival of newly-diagnosed patients with multiple myeloma.
2. T cell proliferation and the cytotoxic potential of T cells exposed to a BCMAxCD3 bispecific antibody, progressively increased with the depletion of immature, intermediate, and mature neutrophils.
3. In multiple myeloma, mature neutrophils defined by the simultaneous expression of CD11b, CD13 and CD16 are the most immunosuppressive granulocytic subset.
4. Amongst other cellular and soluble factors, increased levels of TGF-β in the tumor microenvironment could contribute to the epigenetic deregulation of mature neutrophils in patients with multiple myeloma.
5. Epigenetic drugs may modify the transcriptional network of mature neutrophils from patients with multiple myeloma and thereby, prevent their immunosuppressive effect in T cells exposed to a BCMAxCD3 bispecific antibody.
6. While the number of clonotypic T cells was similar between healthy adults and patients with benign and malignant monoclonal gammopathies, there is a reduced clonal diversity the moment that tumor cells start to infiltrate the bone marrow, and a putative displacement of bystander by tumor-reactive T cells in full-blown disease.
7. Multiple myeloma reactive T cells have a singular phenotype that can be monitored using cost-effective techniques such as multidimensional flow cytometry.
8. The accumulation of T cells with phenotypic traits of tumor-reactivity in the bone marrow of patients with smoldering multiple myeloma, is significantly associated with inferior time-to progression.
9. Preemptive blockade of two immune checkpoints at the onset of the disease and before T cell exhaustion, was able to delay tumor growth in mice resembling human myeloma.
10. The ratio between CD27 negative and positive T cells is significantly associated with T-cell clonality and survival in newly-diagnosed patients with transplant-eligible and –illegible multiple myeloma, treated with lenalidomide combination therapy.

8. Bibliography

1. Bell, D. & Gaillard, F. WHO classification of tumours of haematopoietic and lymphoid tissues. in *Radiopaedia.org* (Radiopaedia.org, 2010). doi:10.53347/rID-9250

2. Kumar, S. K. *et al.* Multiple myeloma. *Nat. Rev. Dis. Prim.* **3**, 17046 (2017).

3. Röllig, C., Knop, S. & Bornhäuser, M. Multiple myeloma. *Lancet* **385**, 2197–2208 (2015).

4. Cancer.gov. Cancer Stat Facts: Myeloma. (2021). Available at: https://seer.cancer.gov/statfacts/html/mulmy.html.

5. Rajkumar, S. V. Multiple myeloma: Every year a new standard? *Hematol. Oncol.* **37**, 62–65 (2019).

6. Rajkumar, S. V. *et al.* International Myeloma Working Group updated criteria for the diagnosis of multiple myeloma. *Lancet Oncol.* **15**, e538–e548 (2014).

7. Greipp, P. R. *et al.* International Staging System for Multiple Myeloma. *J. Clin. Oncol.* **23**, 3412–3420 (2005).

8. Palumbo, A. *et al.* Revised International Staging System for Multiple Myeloma: A Report From International Myeloma Working Group. *J. Clin. Oncol.* **33**, 2863–2869 (2015).

9. Szalat, R., Avet-Loiseau, H. & Munshi, N. C. Gene Expression Profiles in Myeloma: Ready for the Real World? *Clin. Cancer Res.* **22**, 5434–5442 (2016).

10. Black, H. & Glavey, S. Gene expression profiling as a prognostic tool in multiple myeloma. *Cancer Drug Resist.* (2021). doi:10.20517/cdr.2021.83

11. Miller, A. *et al.* High somatic mutation and neoantigen burden are correlated with decreased progression-free survival in multiple myeloma. *Blood Cancer J.* **7**, e612–e612 (2017).

12. Lee, N. *et al.* Prognostic value of integrated cytogenetic, somatic variation, and copy number variation analyses in Korean patients with newly diagnosed multiple myeloma. *PLoS One* **16**, e0246322 (2021).

13. D'Agostino, M. *et al.* Prognostic Implication of Somatic Mutations By Next Generation Sequencing: An Analysis from the Mmrf Commpass Study in Newly Diagnosed Multiple Myeloma Patients. *Blood* **128**, 2079–2079 (2016).

14. Zhaoyun, L. & Rong, F. Predictive Role of Immune Profiling for Survival of Multiple Myeloma Patients. *Front. Immunol.* **12**, (2021).

15. Lahuerta, J.-J. *et al.* Depth of Response in Multiple Myeloma: A Pooled Analysis of Three PETHEMA/GEM Clinical Trials. *J. Clin. Oncol.* **35**, 2900–2910 (2017).

16. Rosiñol, L. *et al.* Bortezomib, lenalidomide, and dexamethasone as induction therapy prior to autologous transplant in multiple myeloma. *Blood* **134**, 1337–1345 (2019).

17. Dimopoulos, M. A. *et al.* Multiple myeloma: EHA-ESMO Clinical Practice Guidelines for diagnosis, treatment and follow-up†. *Ann. Oncol.* **32**, 309–322 (2021).

18. Puig, N. *et al.* Lenalidomide and dexamethasone with or without clarithromycin in patients with multiple myeloma ineligible for autologous transplant: a randomized trial. *Blood Cancer J.* **11**, 101 (2021).

19. Cavo, M. *et al.* Bortezomib with thalidomide plus dexamethasone compared with

thalidomide plus dexamethasone as induction therapy before, and consolidation therapy after, double autologous stem-cell transplantation in newly diagnosed multiple myeloma: a randomised phase 3. *Lancet* **376**, 2075–2085 (2010).

20. Dimopoulos, M. A. *et al.* Ixazomib as Postinduction Maintenance for Patients With Newly Diagnosed Multiple Myeloma Not Undergoing Autologous Stem Cell Transplantation: The Phase III TOURMALINE-MM4 Trial. *J. Clin. Oncol.* **38**, 4030–4041 (2020).

21. Landgren, O. *et al.* Carfilzomib with immunomodulatory drugs for the treatment of newly diagnosed multiple myeloma. *Leukemia* **33**, 2127–2143 (2019).

22. Falco, P. *et al.* Melphalan and its role in the management of patients with multiple myeloma. *Expert Rev. Anticancer Ther.* **7**, 945–957 (2007).

23. Lenhard, R. E. *et al.* High-dose cyclophosphamide. An effective treatment for advanced refractory multiple myeloma. *Cancer* **53**, 1456–1460 (1984).

24. San-Miguel, J. F. *et al.* Panobinostat plus bortezomib and dexamethasone versus placebo plus bortezomib and dexamethasone in patients with relapsed or relapsed and refractory multiple myeloma: a multicentre, randomised, double-blind phase 3 trial. *Lancet Oncol.* **15**, 1195–1206 (2014).

25. Podar, K., Shah, J., Chari, A., Richardson, P. G. & Jagannath, S. Selinexor for the treatment of multiple myeloma. *Expert Opin. Pharmacother.* **21**, 399–408 (2020).

26. Quach, H. *et al.* Mechanism of action of immunomodulatory drugs (IMiDS) in multiple myeloma. *Leukemia* **24**, 22–32 (2010).

27. Luptakova, K. *et al.* Lenalidomide enhances anti-myeloma cellular immunity. *Cancer Immunol. Immunother.* **62**, 39–49 (2013).

28. Palumbo, A. *et al.* Continuous Lenalidomide Treatment for Newly Diagnosed Multiple Myeloma. *N. Engl. J. Med.* **366**, 1759–1769 (2012).

29. Miguel, J. S. *et al.* Pomalidomide plus low-dose dexamethasone versus high-dose dexamethasone alone for patients with relapsed and refractory multiple myeloma (MM-003): a randomised, open-label, phase 3 trial. *Lancet Oncol.* **14**, 1055–1066 (2013).

30. Malavasi, F. *et al.* Evolution and Function of the ADP Ribosyl Cyclase/CD38 Gene Family in Physiology and Pathology. *Physiol. Rev.* **88**, 841–886 (2008).

31. Morandi, F. *et al.* CD38: A Target for Immunotherapeutic Approaches in Multiple Myeloma. *Front. Immunol.* **9**, (2018).

32. Sanchez, L., Wang, Y., Siegel, D. S. & Wang, M. L. Daratumumab: a first-in-class CD38 monoclonal antibody for the treatment of multiple myeloma. *J. Hematol. Oncol.* **9**, 51 (2016).

33. Attal, M. *et al.* Isatuximab plus pomalidomide and low-dose dexamethasone versus pomalidomide and low-dose dexamethasone in patients with relapsed and refractory multiple myeloma (ICARIA-MM): a randomised, multicentre, open-label, phase 3 study. *Lancet* **394**, 2096–2107 (2019).

34. Krishnan, A. Y. *et al.* Preliminary Results from a Phase 1b Study of TAK-079, an Investigational Anti-CD38 Monoclonal Antibody (mAb) in Patients with Relapsed/ Refractory Multiple Myeloma (RRMM). *Blood* **134**, 140–140 (2019).

35. Kassem, S. *et al.* SAR442085, a novel anti-CD38 antibody with enhanced antitumor

activity against multiple myeloma. *Blood* **139**, 1160–1176 (2022).

36. Sun, J. *et al.* Targeting CD47 as a Novel Immunotherapy for Multiple Myeloma. *Cancers (Basel).* **12**, 305 (2020).

37. Puro, R. J. *et al.* Development of AO-176, a Next-Generation Humanized Anti-CD47 Antibody with Novel Anticancer Properties and Negligible Red Blood Cell Binding. *Mol. Cancer Ther.* **19**, 835–846 (2020).

38. Dizman, N. & Buchbinder, E. I. Cancer Therapy Targeting CD47/SIRPα. *Cancers (Basel).* **13**, 6229 (2021).

39. Fouquet, G. *et al.* Signaling lymphocytic activation molecules Slam and cancers: friends or foes? *Oncotarget* **9**, 16248–16262 (2018).

40. Dimopoulos, M. A. *et al.* Elotuzumab, lenalidomide, and dexamethasone in RRMM: final overall survival results from the phase 3 randomized ELOQUENT-2 study. *Blood Cancer J.* **10**, 91 (2020).

41. Minnie, S. A. *et al.* Myeloma escape after stem cell transplantation is a consequence of T-cell exhaustion and is prevented by TIGIT blockade. *Blood* **132**, 1675–1688 (2018).

42. Hansen, K. *et al.* COM902, a novel therapeutic antibody targeting TIGIT augments anti-tumor T cell function in combination with PVRIG or PD-1 pathway blockade. *Cancer Immunol. Immunother.* **70**, 3525–3540 (2021).

43. A Study to Evaluate the Safety, Tolerability, Pharmacokinetics (PK), Pharmacodynamics (PD), and Preliminary Activity of Tiragolumab in Participants With Relapsed or Refractory Multiple Myeloma or With Relapsed or Refractory B-cell Non-Hodgkin Lymphoma. Available at: https://clinicaltrials.gov/ct2/show/study/NCT04045028.

44. First in Human (FIH) Study of REGN5458 in Patients With Relapsed or Refractory Multiple Myeloma. Available at: https://clinicaltrials.gov/ct2/show/NCT03761108.

45. Rodriguez, C. *et al.* Initial Results of a Phase I Study of TNB-383B, a BCMA x CD3 Bispecific T-Cell Redirecting Antibody, in Relapsed/Refractory Multiple Myeloma. *Blood* **136**, 43–44 (2020).

46. Lesokhin, A. M. *et al.* Preliminary Safety, Efficacy, Pharmacokinetics, and Pharmacodynamics of Subcutaneously (SC) Administered PF-06863135, a B-Cell Maturation Antigen (BCMA)-CD3 Bispecific Antibody, in Patients with Relapsed/Refractory Multiple Myeloma (RRMM). *Blood* **136**, 8–9 (2020).

47. Harrison, S. J. *et al.* A Phase 1 First in Human (FIH) Study of AMG 701, an Anti-B-Cell Maturation Antigen (BCMA) Half-Life Extended (HLE) BiTE® (bispecific T-cell engager) Molecule, in Relapsed/Refractory (RR) Multiple Myeloma (MM). *Blood* **136**, 28–29 (2020).

48. Costa, L. J. *et al.* First Clinical Study of the B-Cell Maturation Antigen (BCMA) 2+1 T Cell Engager (TCE) CC-93269 in Patients (Pts) with Relapsed/Refractory Multiple Myeloma (RRMM): Interim Results of a Phase 1 Multicenter Trial. *Blood* **134**, 143–143 (2019).

49. First In Human (FIH) Study of REGN5459 in Adult Patients With Relapsed or Refractory Multiple Myeloma (MM). Available at: https://clinicaltrials.gov/ct2/show/NCT04083534.

50. Garfall, A. L. *et al.* Updated Phase 1 Results of Teclistamab, a B-Cell Maturation

Antigen (BCMA) x CD3 Bispecific Antibody, in Relapsed and/or Refractory Multiple Myeloma (RRMM). *Blood* **136**, 27–27 (2020).

51. Cohen, A. D. *et al.* Initial Clinical Activity and Safety of BFCR4350A, a FcRH5/CD3 T-Cell-Engaging Bispecific Antibody, in Relapsed/Refractory Multiple Myeloma. *Blood* **136**, 42–43 (2020).

52. Chari, A. *et al.* A Phase 1, First-in-Human Study of Talquetamab, a G Protein-Coupled Receptor Family C Group 5 Member D (GPRC5D) x CD3 Bispecific Antibody, in Patients with Relapsed and/or Refractory Multiple Myeloma (RRMM). *Blood* **136**, 40–41 (2020).

53. Seckinger, A. *et al.* Target Expression, Generation, Preclinical Activity, and Pharmacokinetics of the BCMA-T Cell Bispecific Antibody EM801 for Multiple Myeloma Treatment. *Cancer Cell* **31**, 396–410 (2017).

54. Krishnan, A. Y. *et al.* Updated Phase 1 Results from MonumenTAL-1: First-in-Human Study of Talquetamab, a G Protein-Coupled Receptor Family C Group 5 Member D x CD3 Bispecific Antibody, in Patients with Relapsed/Refractory Multiple Myeloma. *Blood* **138**, 158–158 (2021).

55. Law, C.-L. *et al.* Preclinical and Nonclinical Characterization of HPN217: A Tri-Specific T Cell Activating Construct (TriTAC) Targeting B Cell Maturation Antigen (BCMA) for the Treatment of Multiple Myeloma. *Blood* **132**, 3225–3225 (2018).

56. First-in-human Single Agent Study of SAR442257 in RRMM and RR-NHL. Available at: https://clinicaltrials.gov/ct2/show/NCT04401020.

57. Madry, C. *et al.* The characterization of murine BCMA gene defines it as a new member of the tumor necrosis factor receptor superfamily. *Int. Immunol.* **10**, 1693–1702 (1998).

58. Lonial, S. *et al.* Belantamab mafodotin for relapsed or refractory multiple myeloma (DREAMM-2): a two-arm, randomised, open-label, phase 2 study. *Lancet Oncol.* **21**, 207–221 (2020).

59. Lee, H. C. *et al.* Phase 1 study of the anti-BCMA antibody-drug conjugate AMG 224 in patients with relapsed/refractory multiple myeloma. *Leukemia* **35**, 255–258 (2021).

60. Xing, L. *et al.* A novel BCMA PBD-ADC with ATM/ATR/WEE1 inhibitors or bortezomib induce synergistic lethality in multiple myeloma. *Leukemia* **34**, 2150–2162 (2020).

61. Bruins, W. S. C. *et al.* TAK-169, a Novel Recombinant Immunotoxin Specific for CD38, Induces Powerful Preclinical Activity Against Patient-Derived Multiple Myeloma Cells. *Blood* **136**, 11–12 (2020).

62. A Study to Investigate the Safety, Tolerability, Efficacy, Pharmacokinetics, and Immunogenicity of TAK-573 in Participants With Refractory Multiple Myeloma (MM). Available at: https://clinicaltrials.gov/ct2/show/NCT03215030.

63. Abrahams, C. L. *et al.* Targeting CD74 in multiple myeloma with the novel, site-specific antibody-drug conjugate STRO-001. *Oncotarget* **9**, 37700–37714 (2018).

64. Munshi, N. C. *et al.* Idecabtagene Vicleucel in Relapsed and Refractory Multiple Myeloma. *N. Engl. J. Med.* **384**, 705–716 (2021).

65. Neri, P., Bahlis, N. J. & Lonial, S. New Strategies in Multiple Myeloma: Immunotherapy as a Novel Approach to Treat Patients with Multiple Myeloma. *Clin.*

Cancer Res. **22**, 5959–5965 (2016).

66. Zhou, X., Einsele, H. & Danhof, S. Bispecific Antibodies: A New Era of Treatment for Multiple Myeloma. *J. Clin. Med.* **9**, 2166 (2020).

67. Pratz, K. W. Blinatumomab Induced Response of Multiply Refractory Multiple Myeloma in the Context of Secondary Pre-B Cell Acute Lymphoblastic Leukemia. *Ann. Hematol. Oncol.* **4**, (2017).

68. Leivas, A. *et al.* NKG2D-CAR-transduced natural killer cells efficiently target multiple myeloma. *Blood Cancer J.* **11**, 146 (2021).

69. Garfall, A. L. & Stadtmauer, E. A. Cellular and vaccine immunotherapy for multiple myeloma. *Hematology* **2016**, 521–527 (2016).

70. Rosenblatt, J. *et al.* Vaccination with Dendritic Cell/Tumor Fusions following Autologous Stem Cell Transplant Induces Immunologic and Clinical Responses in Multiple Myeloma Patients. *Clin. Cancer Res.* **19**, 3640–3648 (2013).

71. Biavati, L. *et al.* An Allogeneic Multiple Myeloma GM-CSF–Secreting Vaccine with Lenalidomide Induces Long-term Immunity and Durable Clinical Responses in Patients in Near Complete Remission. *Clin. Cancer Res.* **27**, 6696–6708 (2021).

72. Rapoport, A. P. *et al.* Combination Immunotherapy after ASCT for Multiple Myeloma Using MAGE-A3/Poly-ICLC Immunizations Followed by Adoptive Transfer of Vaccine-Primed and Costimulated Autologous T Cells. *Clin. Cancer Res.* **20**, 1355–1365 (2014).

73. Morgan, G. J., Walker, B. A. & Davies, F. E. The genetic architecture of multiple myeloma. *Nat. Rev. Cancer* **12**, 335–348 (2012).

74. Bustoros, M. *et al.* Genomic profiling of smoldering multiple myeloma identifies patients at a high risk of disease progression. *J. Clin. Oncol.* **38**, 2380–2389 (2020).

75. Boyle, E. M. *et al.* The molecular make up of smoldering myeloma highlights the evolutionary pathways leading to multiple myeloma. *Nat. Commun.* **12**, 293 (2021).

76. Walker, B. A. *et al.* Mutational Spectrum, Copy Number Changes, and Outcome: Results of a Sequencing Study of Patients With Newly Diagnosed Myeloma. *J. Clin. Oncol.* **33**, 3911–3920 (2015).

77. Walker, B. A. *et al.* A high-risk, Double-Hit, group of newly diagnosed myeloma identified by genomic analysis. *Leukemia* **33**, 159–170 (2019).

78. Kawano, Y., Roccaro, A., Azzi, J. & Ghobrial, I. Multiple Myeloma and the immune microenvironment. *Curr. Cancer Drug Targets* **17**, 1–1 (2017).

79. Lomas, O. C., Tahri, S. & Ghobrial, I. M. The microenvironment in myeloma. *Curr. Opin. Oncol.* **32**, 170–175 (2020).

80. Andersen, M. H. The targeting of immunosuppressive mechanisms in hematological malignancies. *Leukemia* **28**, 1784–1792 (2014).

81. Vinay, D. S. *et al.* Immune evasion in cancer: Mechanistic basis and therapeutic strategies. *Semin. Cancer Biol.* **35**, S185–S198 (2015).

82. Rodríguez-Otero, P., Paiva, B., Engelhardt, M., Prósper, F. & San Miguel, J. F. Is immunotherapy here to stay in multiple myeloma? *Haematologica* **102**, 423–432 (2017).

83. Brimnes, M. K. *et al.* Increased Level of both CD4+FOXP3+ Regulatory T Cells and

CD14+HLA-DR−/low Myeloid-Derived Suppressor Cells and Decreased Level of Dendritic Cells in Patients with Multiple Myeloma. *Scand. J. Immunol.* **72**, 540–547 (2010).

84. Beyer, M. *et al.* In vivo peripheral expansion of naive CD4+CD25highFoxP3+ regulatory T cells in patients with multiple myeloma. *Blood* **107**, 3940–3949 (2006).

85. Feyler, S. *et al.* CD4+CD25+FoxP3+ regulatory T cells are increased whilst CD3+CD4-CD8 -αβTCR+ Double Negative T cells are decreased in the peripheral blood of patients with multiple myeloma which correlates with disease burden. *Br. J. Haematol.* **144**, 686–695 (2009).

86. Muthu Raja, K. R. *et al.* Increased T Regulatory Cells Are Associated with Adverse Clinical Features and Predict Progression in Multiple Myeloma. *PLoS One* **7**, e47077 (2012).

87. Giannopoulos, K., Kaminska, W., Hus, I. & Dmoszynska, A. The frequency of T regulatory cells modulates the survival of multiple myeloma patients: Detailed characterisation of immune status in multiple myeloma. *Br. J. Cancer* **106**, 546–552 (2012).

88. Galustian, C. *et al.* The anti-cancer agents lenalidomide and pomalidomide inhibit the proliferation and function of T regulatory cells. *Cancer Immunol. Immunother.* **58**, 1033–1045 (2009).

89. Almand, B. *et al.* Increased Production of Immature Myeloid Cells in Cancer Patients: A Mechanism of Immunosuppression in Cancer. *J. Immunol.* **166**, 678–689 (2001).

90. Gabrilovich, D. I., Ostrand-Rosenberg, S. & Bronte, V. Coordinated regulation of myeloid cells by tumours. *Nat. Rev. Immunol.* **12**, 253–268 (2012).

91. Botta, C., GullÃ, A., Correale, P., Tagliaferri, P. & Tassone, P. Myeloid-Derived Suppressor Cells in Multiple Myeloma: Pre-Clinical Research and Translational Opportunities. *Front. Oncol.* **4**, (2014).

92. Gabrilovich, D. I. & Nagaraj, S. Myeloid-derived suppressor cells as regulators of the immune system. *Nat. Rev. Immunol.* **9**, 162–174 (2009).

93. Solito, S. *et al.* A human promyelocytic-like population is responsible for the immune suppression mediated by myeloid-derived suppressor cells. *Blood* **118**, 2254–2265 (2011).

94. Favaloro, J. *et al.* Myeloid derived suppressor cells are numerically, functionally and phenotypically different in patients with multiple myeloma. *Leuk. Lymphoma* **55**, 2893–2900 (2014).

95. Görgün, G. T. *et al.* Tumor-promoting immune-suppressive myeloid-derived suppressor cells in the multiple myeloma microenvironment in humans. *Blood* **121**, 2975–2988 (2013).

96. Giese, M. A., Hind, L. E. & Huttenlocher, A. Neutrophil plasticity in the tumor microenvironment. *Blood* **133**, 2159–2167 (2019).

97. Bronte, V. *et al.* Recommendations for myeloid-derived suppressor cell nomenclature and characterization standards. *Nat. Commun.* **7**, 12150 (2016).

98. van der Leun, A. M., Thommen, D. S. & Schumacher, T. N. CD8+ T cell states in human cancer: insights from single-cell analysis. *Nat. Rev. Cancer* **20**, 218–232 (2020).

99. Zheng, L. *et al.* Pan-cancer single-cell landscape of tumor-infiltrating T cells. *Science (80-.).* **374**, (2021).

100. Liu, Z. *et al.* Detecting Tumor Antigen-Specific T Cells via Interaction-Dependent Fucosyl-Biotinylation. *Cell* **183**, 1117-1133.e19 (2020).

101. Schumacher, T. N. & Schreiber, R. D. Neoantigens in cancer immunotherapy. *Science (80-.).* **348**, 69–74 (2015).

102. Simoni, Y. *et al.* Bystander CD8+ T cells are abundant and phenotypically distinct in human tumour infiltrates. *Nature* **557**, 575–579 (2018).

103. Scheper, W. *et al.* Low and variable tumor reactivity of the intratumoral TCR repertoire in human cancers. *Nat. Med.* **25**, 89–94 (2019).

104. Rasche, L., Hudecek, M. & Einsele, H. What is the future of immunotherapy in multiple myeloma? *Blood* **136**, 2491–2497 (2020).

105. Zavidij, O. *et al.* Single-cell RNA sequencing reveals compromised immune microenvironment in precursor stages of multiple myeloma. *Nat. Cancer* **1**, 493–506 (2020).

106. Jhunjhunwala, S., Hammer, C. & Delamarre, L. Antigen presentation in cancer: insights into tumour immunogenicity and immune evasion. *Nat. Rev. Cancer* **21**, 298–312 (2021).

107. Karlsson, J. *et al.* Comparative Study of Immune Status to Infectious Agents in Elderly Patients with Multiple Myeloma, Waldenstrom's Macroglobulinemia, and Monoclonal Gammopathy of Undetermined Significance. *Clin. Vaccine Immunol.* **18**, 969–977 (2011).

108. Dhodapkar, M. V. MGUS to myeloma: a mysterious gammopathy of underexplored significance. *Blood* **128**, 2599–2606 (2016).

109. Mateos, M.-V. *et al.* Lenalidomide plus Dexamethasone for High-Risk Smoldering Multiple Myeloma. *N. Engl. J. Med.* **369**, 438–447 (2013).

110. Lonial, S. *et al.* Randomized Trial of Lenalidomide Versus Observation in Smoldering Multiple Myeloma. *J. Clin. Oncol.* **38**, 1126–1137 (2020).

111. Paiva, B. *et al.* Immune status of high-risk smoldering multiple myeloma patients and its therapeutic modulation under LenDex: a longitudinal analysis. *Blood* **127**, 1151–1162 (2016).

112. Saeys, Y., Van Gassen, S. & Lambrecht, B. N. Computational flow cytometry: helping to make sense of high-dimensional immunology data. *Nat. Rev. Immunol.* **16**, 449–462 (2016).

113. Keyes, T. J., Domizi, P., Lo, Y., Nolan, G. P. & Davis, K. L. A Cancer Biologist's Primer on Machine Learning Applications in High-Dimensional Cytometry. *Cytom. Part A* **97**, 782–799 (2020).

114. McKinnon, K. M. Multiparameter Conventional Flow Cytometry. in 139–150 (2018). doi:10.1007/978-1-4939-7346-0_8

115. Garcés, J.-J. *et al.* Circulating tumor cells for comprehensive and multiregional non-invasive genetic characterization of multiple myeloma. *Leukemia* **34**, 3007–3018 (2020).

116. Paiva, B., Merino, J. & San Miguel, J. F. Utility of flow cytometry studies in the management of patients with multiple myeloma. *Curr. Opin. Oncol.* **28**, 511–517

(2016).

117. Jelinek, T. *et al.* Current applications of multiparameter flow cytometry in plasma cell disorders. *Blood Cancer J.* **7**, e617–e617 (2017).

118. Botta, C. *et al.* FlowCT for the analysis of large immunophenotypic datasets and biomarker discovery in cancer immunology. *Blood Adv.* (2021). doi:10.1182/bloodadvances.2021005198

119. Paiva, B. *et al.* Minimal residual disease monitoring and immune profiling in multiple myeloma in elderly patients. *Blood* **127**, 3165–3174 (2016).

120. Ward, M. D. & Kaduchak, G. Fundamentals of Acoustic Cytometry. *Curr. Protoc. Cytom.* **84**, (2018).

121. Bonilla, D. L., Reinin, G. & Chua, E. Full Spectrum Flow Cytometry as a Powerful Technology for Cancer Immunotherapy Research. *Front. Mol. Biosci.* **7**, (2021).

122. Nolan, J. P. & Condello, D. Spectral Flow Cytometry. *Curr. Protoc. Cytom.* **63**, (2013).

123. Bendall, S. C. *et al.* Single-Cell Mass Cytometry of Differential Immune and Drug Responses Across a Human Hematopoietic Continuum. *Science (80-.).* **332**, 687–696 (2011).

124. Smets, T., Stevenaert, F., Adams, H. & Vanhoof, G. Deep Profiling of the Immune System of Multiple Myeloma Patients Using Cytometry by Time-of-Flight (CyTOF). in 47–54 (2018). doi:10.1007/978-1-4939-7865-6_4

125. Baughn, L. B. *et al.* Phenotypic and Functional Characterization of Multiple Myeloma By Single Cell Mass Cytometry (CyTOF). *Blood* **136**, 40–41 (2020).

126. Palit, S., Heuser, C., de Almeida, G. P., Theis, F. J. & Zielinski, C. E. Meeting the Challenges of High-Dimensional Single-Cell Data Analysis in Immunology. *Front. Immunol.* **10**, (2019).

127. Abe, K., Minoura, K., Maeda, Y., Nishikawa, H. & Shimamura, T. Model-based clustering for flow and mass cytometry data with clinical information. *BMC Bioinformatics* **21**, 393 (2020).

128. Van Gassen, S. *et al.* FlowSOM: Using self-organizing maps for visualization and interpretation of cytometry data. *Cytom. Part A* **87**, 636–645 (2015).

129. Nowicka, M. *et al.* CyTOF workflow: differential discovery in high-throughput high-dimensional cytometry datasets. *F1000Research* **6**, 748 (2019).

130. Ferrer-Font, L. *et al.* High-Dimensional Data Analysis Algorithms Yield Comparable Results for Mass Cytometry and Spectral Flow Cytometry Data. *Cytom. Part A* **97**, 824–831 (2020).

131. Stassen, S. V *et al.* PARC: ultrafast and accurate clustering of phenotypic data of millions of single cells. *Bioinformatics* **36**, 2778–2786 (2020).

132. Kratochvíl, M., Bednárek, D., Sieger, T., Fišer, K. & Vondrášek, J. ShinySOM: graphical SOM-based analysis of single-cell cytometry data. *Bioinformatics* **36**, 3288–3289 (2020).

133. Monaco, G. *et al.* flowAI: automatic and interactive anomaly discerning tools for flow cytometry data. *Bioinformatics* **32**, 2473–2480 (2016).

134. Finak, G. *et al.* OpenCyto: An Open Source Infrastructure for Scalable, Robust,

Reproducible, and Automated, End-to-End Flow Cytometry Data Analysis. *PLoS Comput. Biol.* **10**, e1003806 (2014).

135. Saliba, A.-E., Westermann, A. J., Gorski, S. A. & Vogel, J. Single-cell RNA-seq: advances and future challenges. *Nucleic Acids Res.* **42**, 8845–8860 (2014).

136. Lim, B., Lin, Y. & Navin, N. Advancing Cancer Research and Medicine with Single-Cell Genomics. *Cancer Cell* **37**, 456–470 (2020).

137. Haque, A., Engel, J., Teichmann, S. A. & Lönnberg, T. A practical guide to single-cell RNA-sequencing for biomedical research and clinical applications. *Genome Med.* **9**, 75 (2017).

138. Trapnell, C. Defining cell types and states with single-cell genomics. *Genome Res.* **25**, 1491–1498 (2015).

139. Liu, R. *et al.* Co-evolution of tumor and immune cells during progression of multiple myeloma. *Nat. Commun.* **12**, 2559 (2021).

140. Cohen, Y. C. *et al.* Identification of resistance pathways and therapeutic targets in relapsed multiple myeloma patients through single-cell sequencing. *Nat. Med.* **27**, 491–503 (2021).

141. Jang, J. S. *et al.* Molecular signatures of multiple myeloma progression through single cell RNA-Seq. *Blood Cancer J.* **9**, (2019).

142. Waldschmidt, J. M. *et al.* Single-Cell Profiling Reveals Metabolic Reprogramming as a Resistance Mechanism in BRAF -Mutated Multiple Myeloma. *Clin. Cancer Res.* **27**, 6432–6444 (2021).

143. Ledergor, G. *et al.* Single cell dissection of plasma cell heterogeneity in symptomatic and asymptomatic myeloma. *Nat. Med.* **24**, 1867–1876 (2018).

144. Carter, J. A. *et al.* Single T Cell Sequencing Demonstrates the Functional Role of αβ TCR Pairing in Cell Lineage and Antigen Specificity. *Front. Immunol.* **10**, (2019).

145. Tu, A. A. *et al.* TCR sequencing paired with massively parallel 3′ RNA-seq reveals clonotypic T cell signatures. *Nat. Immunol.* **20**, 1692–1699 (2019).

146. Chiffelle, J. *et al.* T-cell repertoire analysis and metrics of diversity and clonality. *Curr. Opin. Biotechnol.* **65**, 284–295 (2020).

147. Pai, J. A. & Satpathy, A. T. High-throughput and single-cell T cell receptor sequencing technologies. *Nat. Methods* **18**, 881–892 (2021).

148. Bradley, P. & Thomas, P. G. Using T Cell Receptor Repertoires to Understand the Principles of Adaptive Immune Recognition. *Annu. Rev. Immunol.* **37**, 547–570 (2019).

149. Riaz, N. *et al.* Tumor and Microenvironment Evolution during Immunotherapy with Nivolumab. *Cell* **171**, 934-949.e16 (2017).

150. Yost, K. E. *et al.* Clonal replacement of tumor-specific T cells following PD-1 blockade. *Nat. Med.* **25**, 1251–1259 (2019).

151. Rodríguez, S. *et al.* Discordances between Immunofixation (IFx) and Minimal Residual Disease (MRD) Assessment with Next-Generation Flow (NGF) and Sequencing (NGS) in Patients (Pts) with Multiple Myeloma (MM): Clinical and Pathogenic Significance. *Blood* **136**, 5–6 (2020).

152. Neri, P. *et al.* Identification of Specificity Groups in Myeloma Patients T Cell

Receptor (TCR) Repertoire through Single Cell TCR Sequencing. *Blood* **132**, 4459–4459 (2018).

153. Evrony, G. D., Hinch, A. G. & Luo, C. Applications of Single-Cell DNA Sequencing. *Annu. Rev. Genomics Hum. Genet.* **22**, 171–197 (2021).

154. Pellegrino, M. *et al.* High-throughput single-cell DNA sequencing of acute myeloid leukemia tumors with droplet microfluidics. *Genome Res.* **28**, 1345–1352 (2018).

155. Samur, M. K. *et al.* 16p Deletion Involving BCMA Locus Is Frequent and Predominantly Observed with del17p. *Blood* **138**, 1590–1590 (2021).

156. Stoeckius, M. *et al.* Simultaneous epitope and transcriptome measurement in single cells. *Nat. Methods* **14**, 865–868 (2017).

157. Leblay, N. *et al.* Cite-Seq Profiling of T Cells in Multiple Myeloma Patients Undergoing BCMA Targeting CAR-T or Bites Immunotherapy. *Blood* **136**, 11–12 (2020).

158. Buenrostro, J. D., Wu, B., Chang, H. Y. & Greenleaf, W. J. ATAC-seq: A Method for Assaying Chromatin Accessibility Genome-Wide. *Curr. Protoc. Mol. Biol.* **109**, (2015).

159. Zong, D. *et al.* Chromatin accessibility landscapes of immune cells in rheumatoid arthritis nominate monocytes in disease pathogenesis. *BMC Biol.* **19**, 79 (2021).

160. Barwick, B. G. *et al.* Chromatin Accessibility Identifies Regulatory Elements Predictive of Gene Expression and Disease Outcome in Multiple Myeloma. *Clin. Cancer Res.* **27**, 3178–3189 (2021).

161. Rusk, N. Spatial transcriptomics. *Nat. Methods* **13**, 710–710 (2016).

162. Ståhl, P. L. *et al.* Visualization and analysis of gene expression in tissue sections by spatial transcriptomics. *Science (80-.).* **353**, 78–82 (2016).

163. Paiva, B. *et al.* Measurable Residual Disease by Next-Generation Flow Cytometry in Multiple Myeloma. *J. Clin. Oncol.* **38**, 784–792 (2020).

164. Greten, T. F., Manns, M. P. & Korangy, F. Myeloid derived suppressor cells in human diseases. *Int. Immunopharmacol.* **11**, 802–807 (2011).

165. De Veirman, K. *et al.* Myeloid-derived suppressor cells as therapeutic target in hematological malignancies. *Front. Oncol.* **4**, 1–11 (2014).

166. Malek, E. *et al.* Myeloid-derived suppressor cells: The green light for myeloma immune escape. *Blood Rev.* **30**, 341–348 (2016).

167. Rachamandran, I. *et al.* Myeloid derived suppressor cells regulate growth of multiple myeloma by inhibiting T cells in bone marrow. *J. Immunol.* **190**, 3815–3823 (2013).

168. De Veirman, K. *et al.* Myeloid-derived suppressor cells induce multiple myeloma cell survival by activating the AMPK pathway. *Cancer Lett.* **442**, 233–241 (2019).

169. Chesney, J. A., Mitchell, R. A. & Yaddanapudi, K. Myeloid-derived suppressor cells—a new therapeutic target to overcome resistance to cancer immunotherapy. *J. Leukoc. Biol.* **102**, 727–740 (2017).

170. Alameda, D. *et al.* Characterization of freshly isolated mesenchymal stromal cells from healthy and multiple myeloma bone marrow: transcriptional modulation of the microenvironment. *Haematologica* haematol.2019.235135 (2020). doi:10.3324/haematol.2019.235135

171. Jaitin, D. *et al.* Massively Parallel Single-Cell RNA-Seq for marker-free decomposition of tissues into cell types. *Science (80-.).* **343**, 776–779 (2014).

172. José-Enériz, E. S. *et al.* Discovery of first-in-class reversible dual small molecule inhibitors against G9a and DNMTs in hematological malignancies. *Nat. Commun.* **8**, (2017).

173. Korsunsky, I. *et al.* Fast, sensitive and accurate integration of single-cell data with Harmony. *Nat. Methods* **16**, 1289–1296 (2019).

174. Qiu, X. *et al.* Reversed graph embedding resolves complex single-cell trajectories. *Nat. Methods* **14**, 979–982 (2017).

175. Borcherding, N., Bormann, N. L. & Kraus, G. scRepertoire: An R-based toolkit for single-cell immune receptor analysis. *F1000Research* **9**, 47 (2020).

176. Szolek, A. *et al.* OptiType: Precision HLA typing from next-generation sequencing data. *Bioinformatics* **30**, 3310–3316 (2014).

177. Springer, I., Besser, H., Tickotsky-Moskovitz, N., Dvorkin, S. & Louzoun, Y. Prediction of Specific TCR-Peptide Binding From Large Dictionaries of TCR-Peptide Pairs. *Front. Immunol.* **11**, (2020).

178. Bagaev, D. V *et al.* VDJdb in 2019: database extension, new analysis infrastructure and a T-cell receptor motif compendium. *Nucleic Acids Res.* **48**, D1057–D1062 (2020).

179. Singh, A. K. *et al.* TBI with lung dose reduction does not improve hematopoietic cell homing to BM during allogeneic transplantation. *Bone Marrow Transplant.* **45**, 25–30 (2010).

180. Strasser, A. *et al.* Enforced BCL2 expression in B-lymphoid cells prolongs antibody responses and elicits autoimmune disease. *Proc. Natl. Acad. Sci.* **88**, 8661–8665 (1991).

181. Marino, S., Vooijs, M., van Der Gulden, H., Jonkers, J. & Berns, A. Induction of medulloblastomas in p53-null mutant mice by somatic inactivation of Rb in the external granular layer cells of the cerebellum. *Genes Dev.* **14**, 994–1004 (2000).

182. Casola, S. *et al.* Tracking germinal center B cells expressing germ-line immunoglobulin 1 transcripts by conditional gene targeting. *Proc. Natl. Acad. Sci.* **103**, 7396–7401 (2006).

183. Srinivas, S. *et al.* Cre reporter strains produced by targeted insertion of EYFP and ECFP into the ROSA26 locus. *BMC Dev. Biol.* **1**, 1–8 (2001).

184. Krejcik, J. *et al.* Daratumumab depletes CD38+immune regulatory cells, promotes T-cell expansion, and skews T-cell repertoire in multiple myeloma. *Blood* (2016). doi:10.1182/blood-2015-12-687749

185. Frassanito, M. A. *et al.* Halting pro-survival autophagy by TGFβ inhibition in bone marrow fibroblasts overcomes bortezomib resistance in multiple myeloma patients. *Leukemia* **30**, 640–648 (2016).

186. Lu, A. *et al.* Inhibition of transforming growth factor-β activation diminishes tumor progression and osteolytic bone disease in mouse models of multiple myeloma. *Am. J. Pathol.* **186**, 678–690 (2016).

187. Chao, A. & Lee, S. M. Estimating the number of classes via sample coverage. *J. Am. Stat. Assoc.* **87**, 210–217 (1992).

188. Chao, Anne. Nonparametric Estimation of the Number of Classes in a Population. *Scand. J. Stat.* **11**, 265–270 (1984).

189. van Dongen, J. J. M. *et al.* EuroFlow antibody panels for standardized n-dimensional flow cytometric immunophenotyping of normal, reactive and malignant leukocytes. *Leukemia* **26**, 1908–1975 (2012).

190. Facon, T. *et al.* Daratumumab plus lenalidomide and dexamethasone for untreated Myeloma. *N. Engl. J. Med.* **380**, 2104–2115 (2019).

191. Raje, N. *et al.* Anti-BCMA CAR T-Cell Therapy bb2121 in Relapsed or Refractory Multiple Myeloma. *N. Engl. J. Med.* **380**, 1726–1737 (2019).

192. Gabrilovich, D. I. *et al.* The terminology issue for myeloid-derived suppressor cells [1]. *Cancer Res.* **67**, 425 (2007).

193. Sagiv, J. Y. *et al.* Phenotypic diversity and plasticity in circulating neutrophil subpopulations in cancer. *Cell Rep.* **10**, 562–573 (2015).

194. Pillay, J., Tak, T., Kamp, V. M. & Koenderman, L. Immune suppression by neutrophils and granulocytic myeloid-derived suppressor cells: Similarities and differences. *Cell. Mol. Life Sci.* **70**, 3813–3827 (2013).

195. Damasceno, D. *et al.* Expression profile of novel cell surface molecules on different subsets of human peripheral blood antigen-presenting cells. *Clin. Transl. Immunol.* **5**, e100 (2016).

196. Condamine, T., Mastio, J. & Gabrilovich, D. I. Transcriptional regulation of myeloid-derived suppressor cells. *J. Leukoc. Biol.* **98**, 913–922 (2015).

197. Fan, C., Stendahl, U., Stjernberg, N. & Beckman, L. Association between Orosomucoid Types and Cancer. *Oncology* **52**, 498–500 (1995).

198. Yuan, M. *et al.* Tumor-Derived CXCL1 Promotes Lung Cancer Growth via Recruitment of Tumor-Associated Neutrophils. *J. Immunol. Res.* **2016**, 1–11 (2016).

199. Ng, L. G., Ostuni, R. & Hidalgo, A. Heterogeneity of neutrophils. *Nat. Rev. Immunol.* **19**, 255–265 (2019).

200. Andzinski, L. *et al.* Type i IFNs induce anti-tumor polarization of tumor associated neutrophils in mice and human. *Int. J. Cancer* **138**, 1982–1993 (2016).

201. Pylaeva, E., Lang, S. & Jablonska, J. The essential role of type I interferons in differentiation and activation of tumor-associated neutrophils. *Front. Immunol.* **7**, 1–13 (2016).

202. Wu, T. D. *et al.* Peripheral T cell expansion predicts tumour infiltration and clinical response. *Nature* **579**, 274–278 (2020).

203. Joshua, D. E. *et al.* Treg and Oligoclonal Expansion of Terminal Effector CD8+ T Cell as Key Players in Multiple Myeloma. *Front. Immunol.* **12**, 6–12 (2021).

204. Suen, H. *et al.* Multiple myeloma causes clonal T-cell immunosenescence: identification of potential novel targets for promoting tumour immunity and implications for checkpoint blockade. *Leukemia* **30**, 1716–1724 (2016).

205. Mateos, M.-V. *et al.* Pembrolizumab plus pomalidomide and dexamethasone for patients with relapsed or refractory multiple myeloma (KEYNOTE-183): a randomised, open-label, phase 3 trial. *Lancet Haematol.* **6**, e459–e469 (2019).

206. Usmani, S. Z. *et al.* Pembrolizumab plus lenalidomide and dexamethasone for

patients with treatment-naive multiple myeloma (KEYNOTE-185): a randomised, open-label, phase 3 trial. *Lancet Haematol.* **6**, e448–e458 (2019).

207. Cohen, R. *et al.* Immune Checkpoint Inhibition in Colorectal Cancer: Microsatellite Instability and Beyond. *Target. Oncol.* **15**, 11–24 (2020).

208. de Almeida, D. V. P., Fong, L., Rettig, M. B. & Autio, K. A. Immune Checkpoint Blockade for Prostate Cancer: Niche Role or Next Breakthrough? *Am. Soc. Clin. Oncol. Educ. B.* e89–e106 (2020). doi:10.1200/EDBK_278853

209. Michel, L. L. *et al.* Immune Checkpoint Blockade in Patients with Triple-Negative Breast Cancer. *Target. Oncol.* **15**, 415–428 (2020).

210. Zhou, F., Qiao, M. & Zhou, C. The cutting-edge progress of immune-checkpoint blockade in lung cancer. *Cell. Mol. Immunol.* **18**, 279–293 (2021).

211. Manasanch, E. E. *et al.* A pilot study of pembrolizumab in smoldering myeloma: report of the clinical, immune, and genomic analysis. *Blood Adv.* **3**, 2400–2408 (2019).

212. Guillerey, C. *et al.* TIGIT immune checkpoint blockade restores CD81 T-cell immunity against multiple myeloma. *Blood* **132**, 1689–1694 (2018).

213. Bae, J. *et al.* Targeting LAG3/GAL-3 to overcome immunosuppression and enhance anti-tumor immune responses in multiple myeloma. *Leukemia* **36**, 138–154 (2022).

214. Kumar, S. K. *et al.* Multiple Myeloma, Version 3.2021, NCCN Clinical Practice Guidelines in Oncology. *J. Natl. Compr. Cancer Netw.* **18**, 1685–1717 (2020).

215. Zhu, Y. X. *et al.* Identification of cereblon-binding proteins and relationship with response and survival after IMiDs in multiple myeloma. *Blood* **124**, 536–545 (2014).

216. Zhu, Y. X. *et al.* Identification of lenalidomide resistance pathways in myeloma and targeted resensitization using cereblon replacement, inhibition of STAT3 or targeting of IRF4. *Blood Cancer J.* **9**, 19 (2019).

217. Haertle, L. *et al.* Cereblon enhancer methylation and IMiD resistance in multiple myeloma. *Blood* **138**, 1721–1726 (2021).

218. Jones, J. R. *et al.* Mutations in CRBN and other cereblon pathway genes are infrequently associated with acquired resistance to immunomodulatory drugs. *Leukemia* **35**, 3017–3020 (2021).

219. Flores-Montero, J. *et al.* Next Generation Flow for highly sensitive and standardized detection of minimal residual disease in multiple myeloma. *Leukemia* **31**, 2094–2103 (2017).

220. Schreiber, R. D., Old, L. J. & Smyth, M. J. Cancer Immunoediting: Integrating Immunity's Roles in Cancer Suppression and Promotion. *Science (80-.).* **331**, 1565–1570 (2011).

9. Annexes

List of investigators in the GEM (Grupo Español de Mieloma)/PETHEMA (Programa para el Estudio de la Terapéutica en Hemopatías Malignas) cooperative study group.

Hospital	Investigator
Complejo Hospitalario Costa del Sol	Dra. María Casanova Espinosa
H. Especialidades de Jerez de la Frontera	Dr. José Luís Guzman Zamudio
H. Nuestra Señora de Valme	Dr. Eduardo Ríos Herranz
H. Universitario Virgen de las Nieves	Dr. Rafael Rios Tamayo
Complejo Hospitalario Regional Virgen del Rocío	Dr. Jesús Martín Sánchez
H. Clínico Universitario Lozano Blesa	Dr. Luís Palomera Bernal
H. Universitario Central de Asturias	Dra. Ana Pilar González Rodríguez
H. Cabueñes	Dra. María Esther González García
Complejo Asistencial Son Espases	Dra. Antonia Sampol Mayol
H. Son Llátzer	Dr. Joan Bargay Lleonart
H. de Gran Canaria Dr. Negrín	Dra. Alexia Suárez
H. Universitario de Canarias	Dr. Miguel Teodoro Hernández García
H. Universitario Marqués de Valdecilla	Dra. Carmen Montes Gaisán
H. General de Ciudad Real	Dra. Belén Hernández Ruiz
Complejo Hospitalario de Toledo	Dr. Felipe Casado Montero
H. Universitario de Guadalajara	Dra. Dunia de Miguel Llorente
H. Nuestra Señora del Prado (Talavera)	Dr. Fernando Solano Ramos
H. General de Albacete	Dra. Ángela Ibañez Garcia
H. Clínico de Salamanca	Dra. Mariví Mateos Manteca
Complejo Hospitalario H. General de Segovia	Dr. José Mariano Hernández Martín
H. de León	Dr. Fernando Escalante Barrigón
H. Universitario Rio Hortega	Dr. Javier García Frade
H. Clínico Universitario de Valladolid	Dr. Alfonso García de Coca
H. Santa Bárbara	Dr. Carlos Aguilar Franco
Hospital Universitario de Burgos	Dr. Jorge Labrador Gómez:
H. Althaia, Xarxa Asistencial de Manresa (Sant Joan de Deu)	Dra. Elena Cabezudo Pérez

H CLINIC	Dr. Joan Bladé Creixentí
H. Durán i Reynals - ICO L´Hospitalet	Dra. Ana Mª Sureda Balari
ICO Girona, H. Universitario de Girona Dr. Josep Trueta	Dra. Yolanda González Montes
H. UNIVERSITARI JOAN XXII DE TARRAGONA	Dra. Lourdes Escoda Teigell
Hospital Universitari Arnau de Vilanova de Lleida	Dr. Antonio García Guiñón
H. del Mar	Dra. Eugenia Abella Monreal
H. de Sabadell (Parc Taulí)	Dr. Juan Alfonso Soler Campos
Hospital Universitario Mútua de Terrassa	Dr. Josep Mª Martí Tutusaus
H. Germans Trias i Pujol	Dr. Albert Oriol Rocafiguera
H. de la Santa Creu i Sant Pau	Dr. Miquel Granell Gorrochategui
H. Vall d´Hebrón	Dra. Mercedes Gironella Mesa
H. San Pedro de Alcántara (Complejo Hospitalario de Cáceres)	Dra. Carmen Cabrera Silva
Complejo Hospitalario Universitario de Santiago	Dra. Marta Sonia González Pérez
Complejo Hospitalario de Pontevedra	Dra. Ana Dios Loureiro
Complejo Hospitalario de Ourense	Dr. José Angel Méndez Sánchez
H. San Pedro	Dra. María Josefa Nájera Irazu
H. Universitario Fundación de Alcorcón	Dr. Francisco Javier Peñalver Párraga
H. Universitario 12 de Octubre	Dr. Juan José Lahuerta Palacios
H. de Fuenlabrada	Dra. Pilar Bravo Barahona
H. General Universitario Gregorio Marañón	Dra. Cristina Encinas Rodríguez
H. Infanta Leonor	Dr. José Ángel Hernández Rivas
H. Universitario Madrid - Sanchinarro	Dr. Jaime Pérez de Oteyza
Centro Oncológico MD Anderson	Dra. Rebeca Iglesias del Barrio
H. Universitario La Paz	Dra. Ana López de la Guia
H. Universitario de la Princesa	Dr. Adrián Alegre Amor
Fundación Jiménez Díaz-UTE	Dra. Elena Prieto Pareja
Hospital Universitario Puerta de Hierro - Majadahonda	Dra. Isabel Krsnik Castelló
H. Ramón y Cajal	Dra. Mª Jesús Blanchard Rodríguez
H. Universitario de San Carlos	Dr. Rafael Martínez Martínez

H. Severo Ochoa	Dra. Rosalía Riaza Grau
H. INFANTA SOFÍA	Dr. Eugenio Giménez Mesa
HOSPITAL DEL TAJO	Dra. Elena Ruiz Sainz
H. Morales Meseguer	Dr. Felipe de Arriba
H. Universitario Virgen de la Arrixaca	Dr. Jose María Moraleda Jiménez
H. General Universitario Santa Lucia	Dra. Marta Romera
Clínica Universidad de Navarra	Dr. Felipe Prósper Cardoso
Complejo Hospitalario de Navarra	Dr. José Mª Arguiñano Pérez
H. de Cruces	Dra. María Puente Pomposo
H. de Txagorritxu	Dr. Ernesto Pérez Persona
H. Clínico Universitario de Valencia	Dra. Ana Isabel Teruel Casasús
H. Universitario Dr. Peset	Dra. Paz Ribas García
H. Universitario La Fe	Dr. Isidro Jarque Ramos
H. General Universitario de Alicante	Dra. María Blanca Villarrubia Lor
H. TORREVIEJA SALUD UTE	Dr. Pedro Luis Fernández García
H. del Vinalopo	Dr. Pedro Luis Fernández García
H. Quirón	Dra. Carmen Martínez Chamorro

Supplemental Figure 1. Semi-automated pipeline that performs batch-analyses of flow cytometry data to avoid variability intrinsic to manual analysis, and unveils full cellular diversity based on unbiased clustering. This strategy allowed the systematic identification and quantification of a variable number of cell clusters, which grouped according to the similarity of antigen expression profiles by using the bioinformatic algorithm FlowSOM.

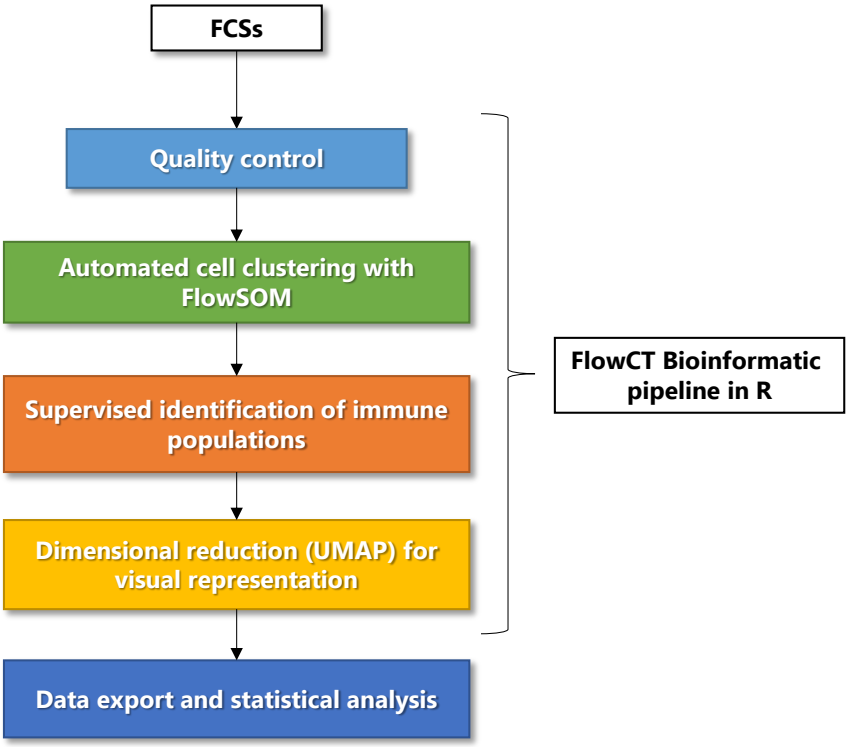

Supplemental Figure 2. Characterization of G-MDSCs based on conventional criteria. Flow cytometry analysis using the conventional gating strategy for G-MDSCs based on the expression of CD11b, CD14, CD15, CD33 and HLADR antigens. $CD11b^{+}CD14^{-}CD15^{+}CD33^{+}HLADR^{-}$ cells included a mixture of immature and mature neutrophil subsets plus eosinophils.

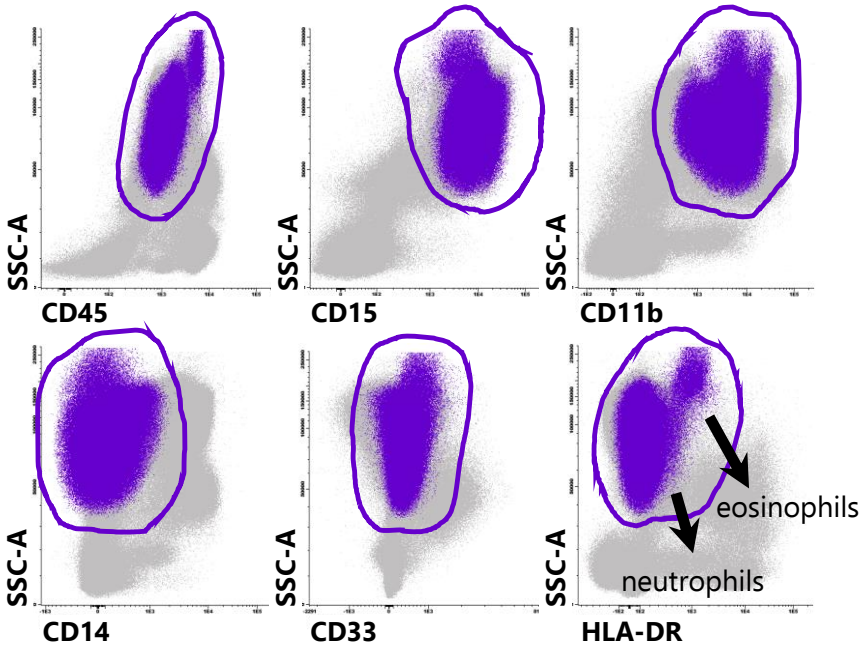

Supplemental Figure 3. Phenotypic and transcriptional profile of mature neutrophils present in matched BM and PB samples from MM patients. (A) Flow cytometry analysis of neutrophils from paired samples of BM and PB (N = 5) show no differences in the immunophenotype of BM and PB neutrophils. Boxes represent the mean and lines the standard deviation (from five independent experiments. **(B)** Principal component analysis of BM and PB neutrophils show that circulating mature neutrophils overlap with BM mature neutrophils. Lines represent the standard deviation and dots the median values. **(C)** Transcriptomic signature of mature BM and PB neutrophils show that circulating neutrophils from MM patients cluster with patient-matched BM neutrophils rather than with mature neutrophils from HA.

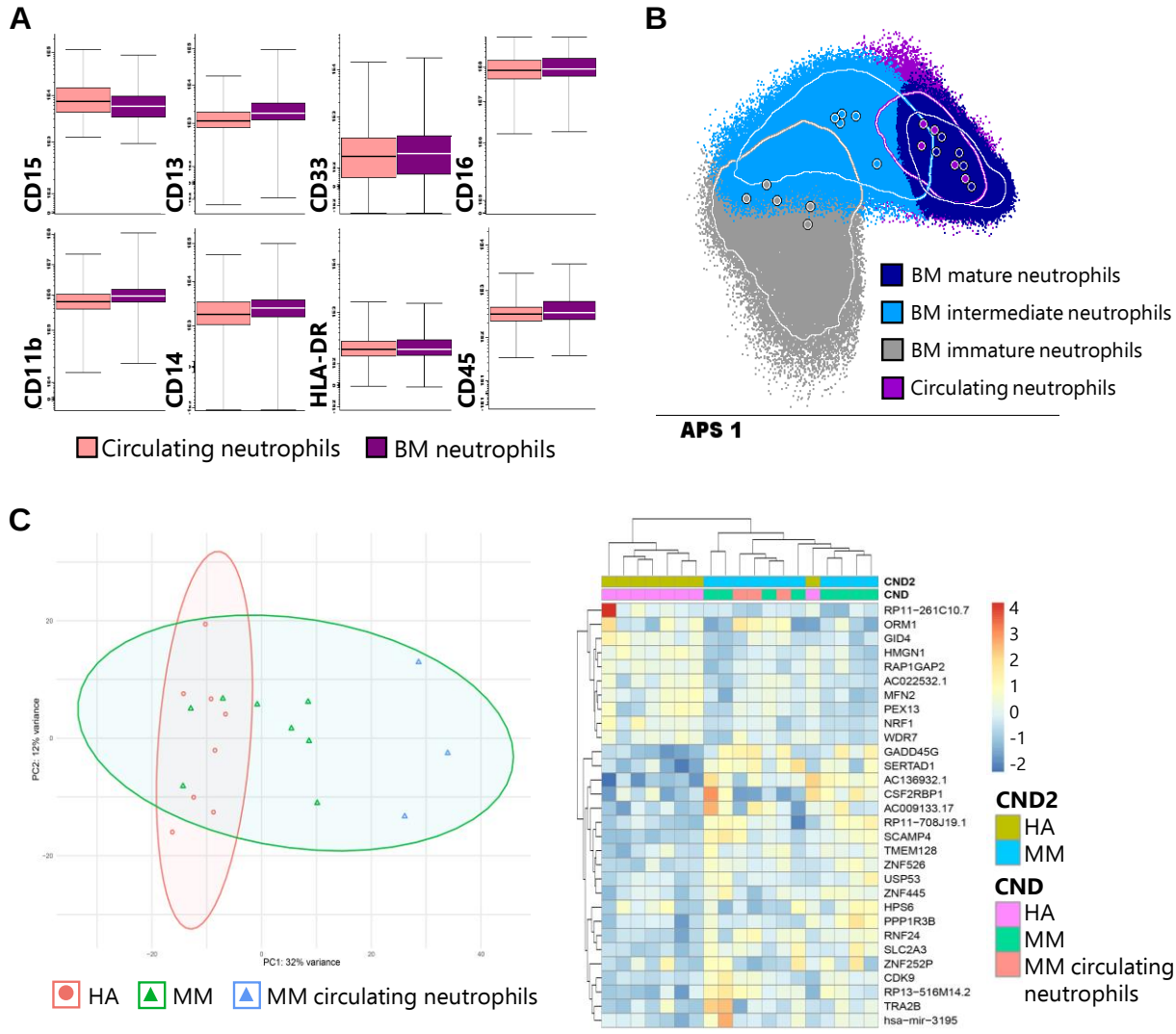

Supplemental Figure 4. Daratumumab has no long-term *in vitro* effect on BM granulocytes from MM patients. (A) BM samples from MM patients (N = 3) were cultured in a 3-dimensional organoid model to enable long-term treatment. **(B)** After 10-day treatment, daratumumab induced a significant depletion of tumor plasma cells. **(C)** No significant differences in the percentage of $CD11b^{+}CD14^{-}CD15^{+}CD33^{+}HLADR^{-}$ cells. Bar graphs represent the mean and lines the standard deviation. The statistical significance was evaluated using the t-Student test. **(D)** or any other granulocytic subsets before and after treatment. **(E)** Flow cytometry analysis of BM samples from MM patients (N = 36) before and after treatment with daratumumab show no significant differences in each granulocytic subset.

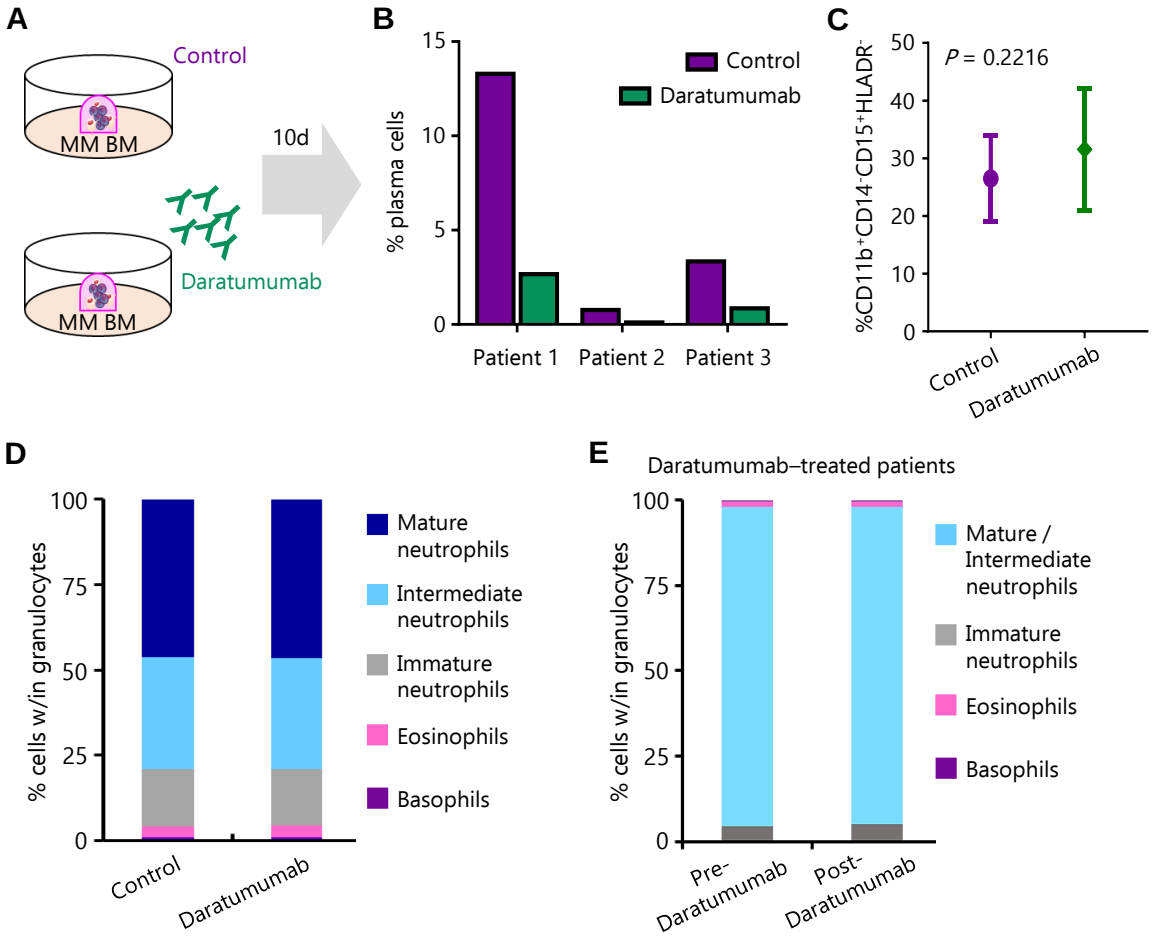

Supplemental Figure 5. (A) Correlations between granulocytic subsets and other BM populations (nucleated red blood cells –NRBCs-, T cells and tumor cells) with clinical parameters. **(B)** Progression-free survival according to high vs low abundance of intermediate and immature neutrophils, eosinophils and basophils). Boxes represent the mean and lines the standard deviation.

A

	Basophils	Eosinophils	Mature neutrophils	Intermediate neutrophils	Immature neutrophils	NRBCs	T cells	Tumor cells
ISS (I vs II vs III)	0.734	0.433	0.449	0.250	0.868	0.232	**0.020**	**0.010**
cytogenetic (high vs standard risk)	0.975	0.337	0.597	0.808	0.150	**0.011**	0.624	0.869
LDH (normal vs ULN)	0.193	0.315	0.246	0.824	0.632	0.541	**0.046**	0.345

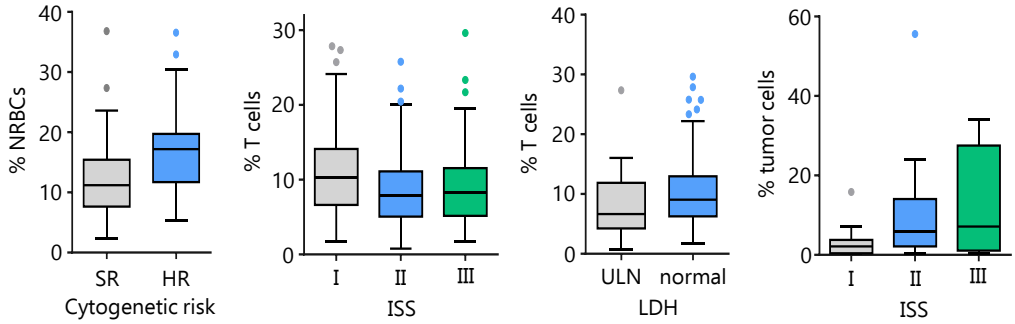

B

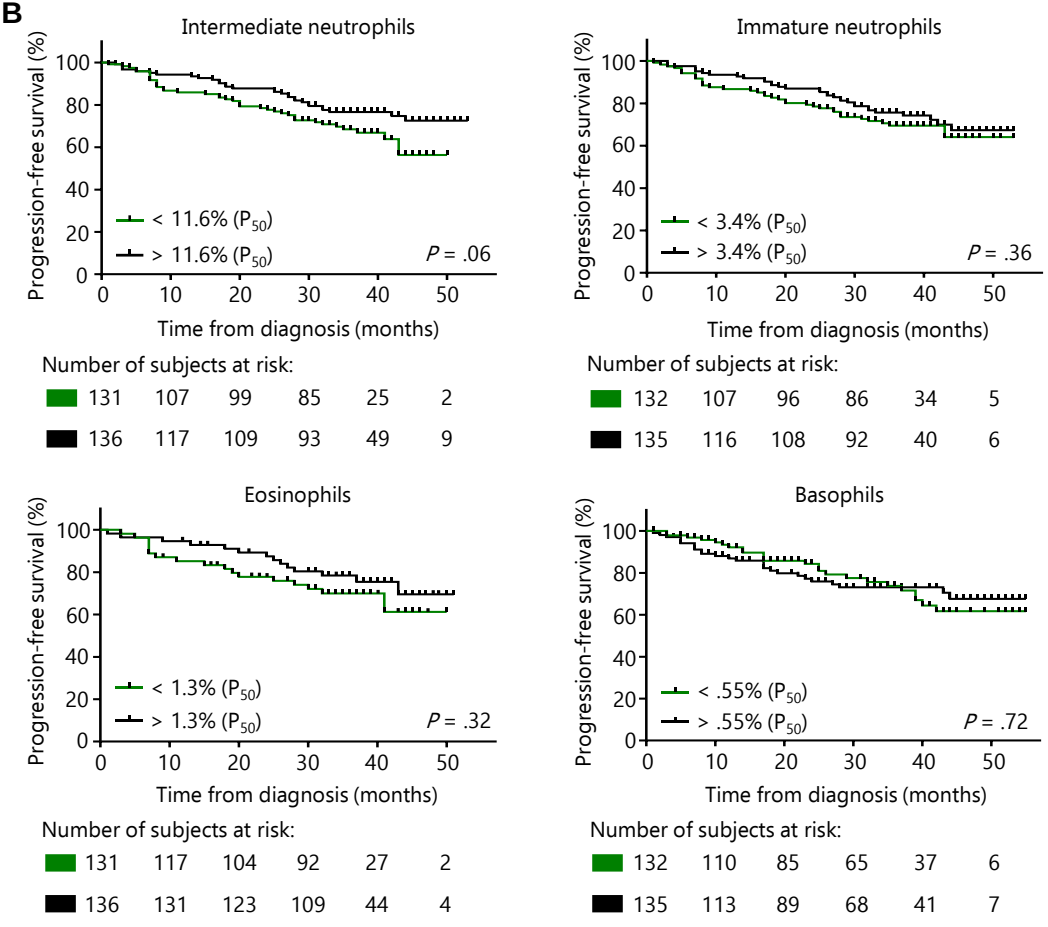

Supplemental Figure 6. (A and B) Graphical representation of 21 genes from the KEGG cytokine-cytokine receptor interaction pathway list, which displayed significantly different expression levels in immature, intermediate and mature neutrophils from HA (N = 8) and MM patients (N = 8). Patterns of gene expression were similar in HA and MM patients with the exception of a significant and progressive upregulation of VEGFA and TGFB1 and a lack of increase of CXCL1 in MM neutrophils. **(C)** All genes with significant differences in expression levels found in mature neutrophils from HA and MM patients.

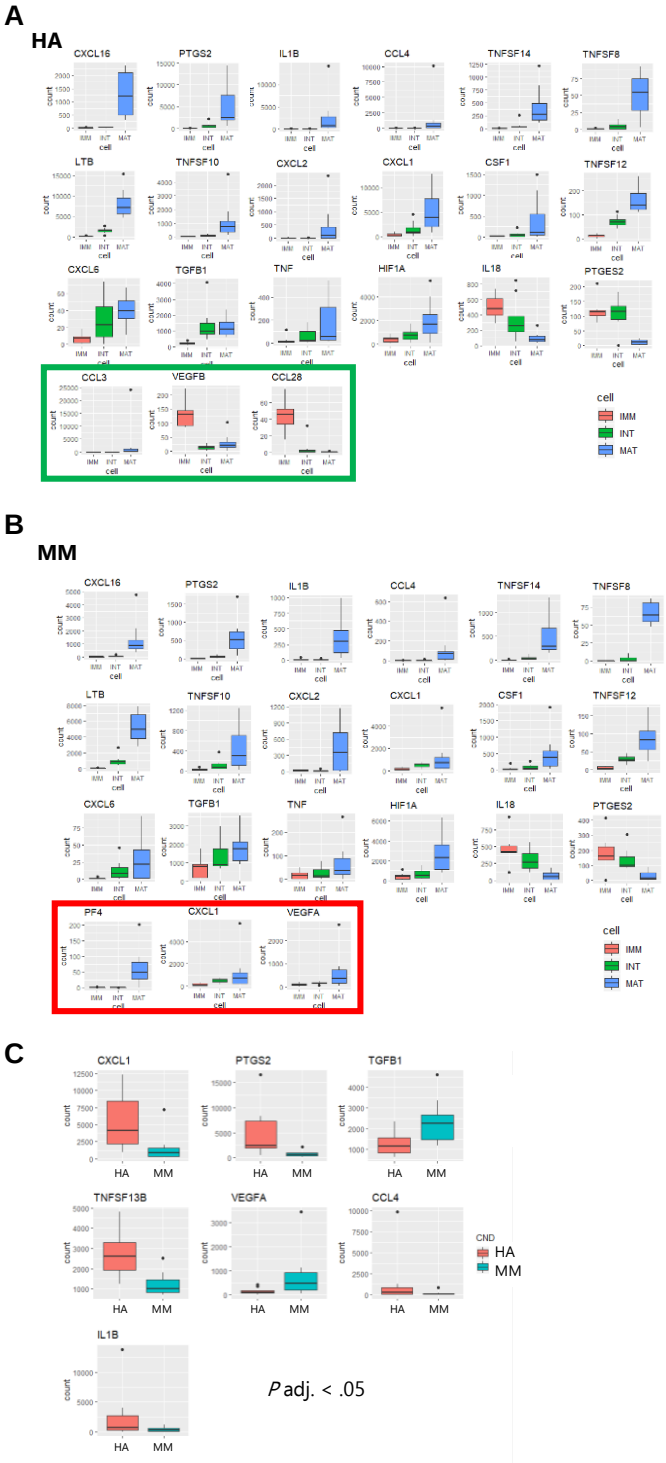

Supplemental Figure 7. Molecular characterization of neutrophil differentiation in the BM of HA and MM patients. Unsupervised clustering of RNAseq data showed incomplete segregation between HA and MM regarding the transcriptional profile of immature and intermediate neutrophils.

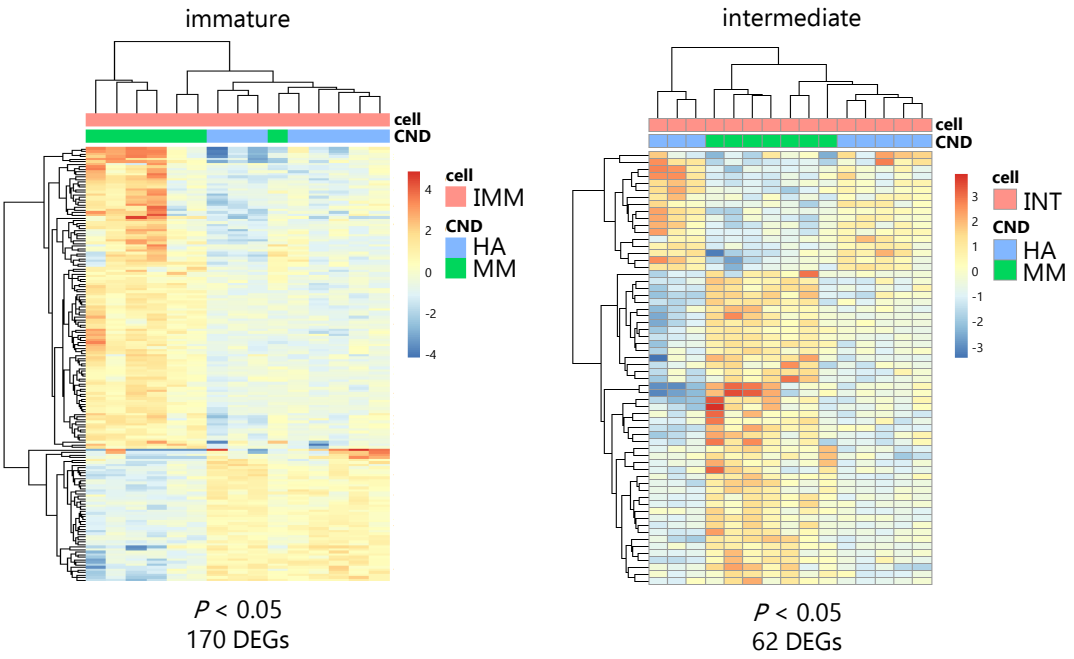

Supplemental Figure 8. Genes coding for cytokines/chemokines with significantly different expression in mesenchymal stromal cells from BM aspirates of HA (N = 8) and MM patients (N = 56). No differences were noted in TGF-β expression.

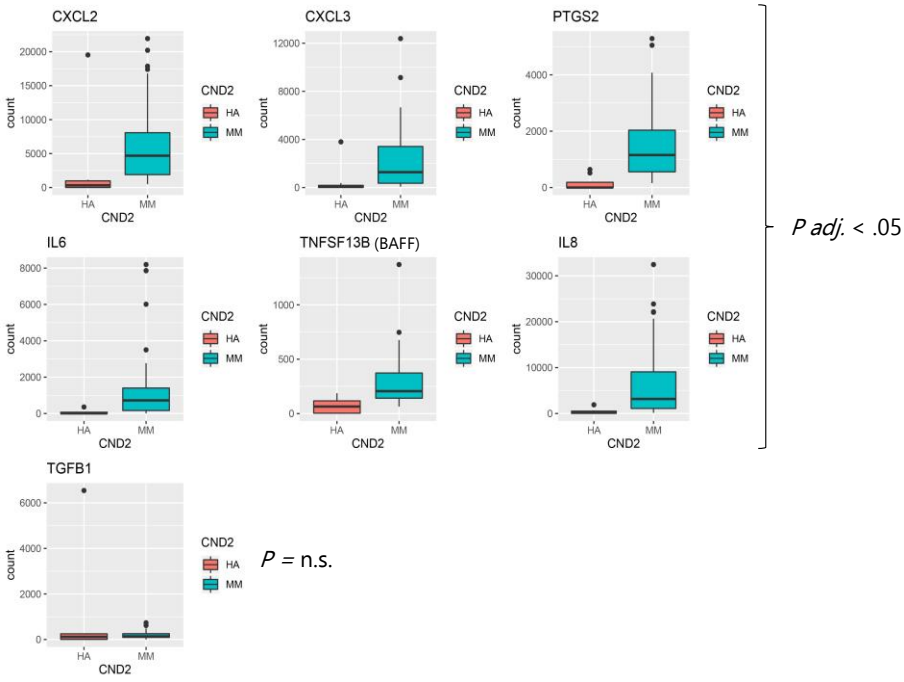

Supplemental Figure 9. The transcriptional network of mature neutrophils is epigenetically deregulated in MM. (A) Differential open chromatin sites (peaks) were annotated to the nearest gene based on their distance to transcription start sites (TSS). 50% of these peaks were in potential promoter regions within 3 kb of a TSS, suggesting that these gains/losses in accessibility could exert regulatory activity. **(B)** Significant correlation between gains or losses of chromatin accessibility near TSS and gene expression for each normal and tumor derived neutrophil samples based on paired ATAC-seq and RNA-seq data. **(C)** CD83 showed significantly higher mRNA expression in MM vs HA as well as concordant transcriptional and chromatin accessibility data. Flow cytometry data show increased protein expression in MM in accordance to molecular data. Boxes represent the mean and lines the standard deviation (from three independent experiments).

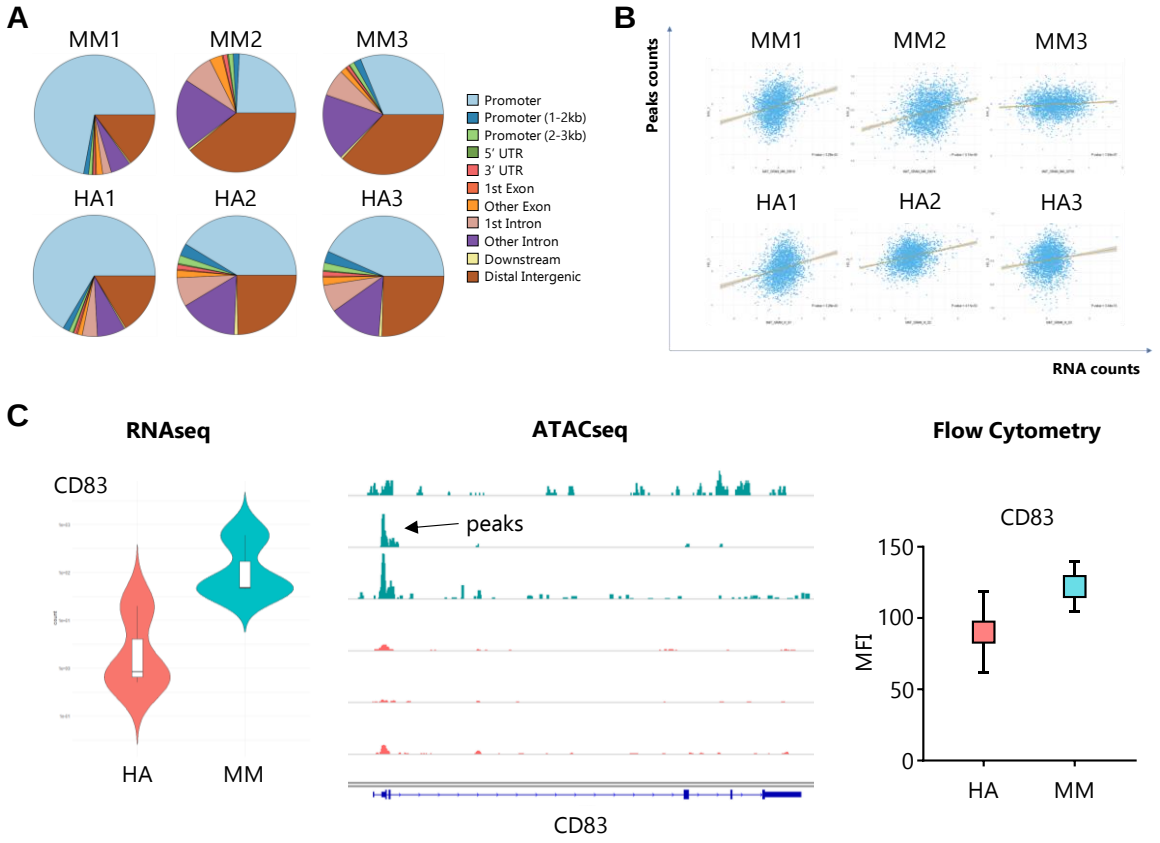

Supplemental Figure 10. Mode of action of CM-272 was confirmed by validating the induced expression of several type I IFN related genes described below.

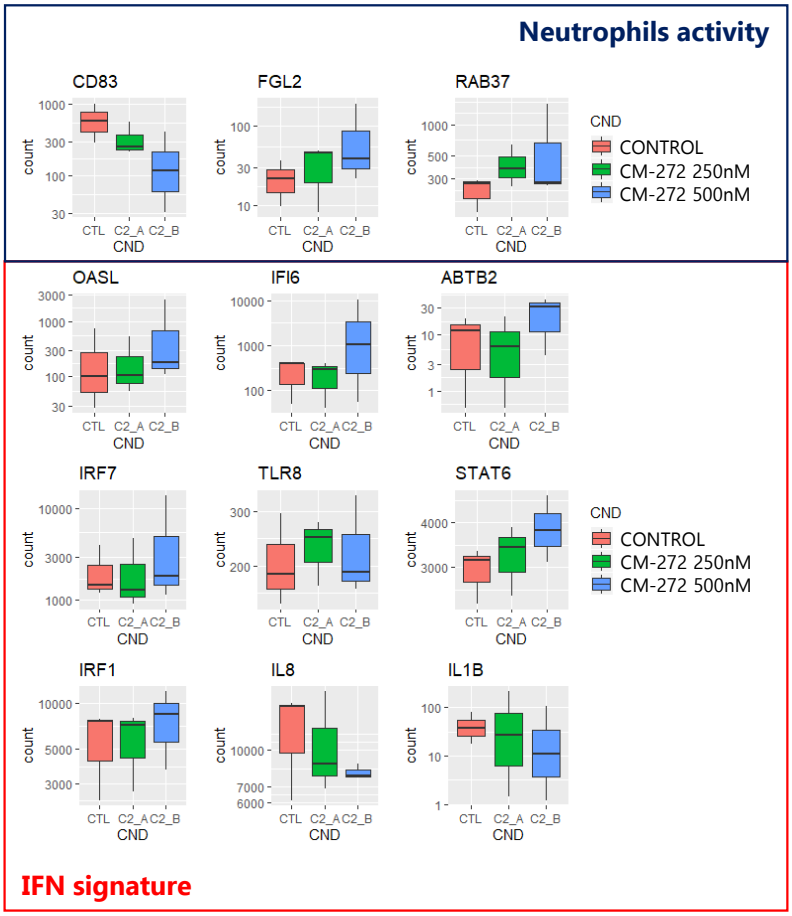

Supplemental Figure 11. Combination of CM-272 and a BCMAxCD3 bispecific antibody show that CM-272 is able to abrogate the immunosuppressive activity exerted by mature neutrophils. The combination significantly increased the activity of T cells against H929 MM cells when compared to single-agent BCMAxCD3 bispecific antibody ($P \leq .01$). Bar graphs represent the mean and lines the standard deviation (from five independent experiments).

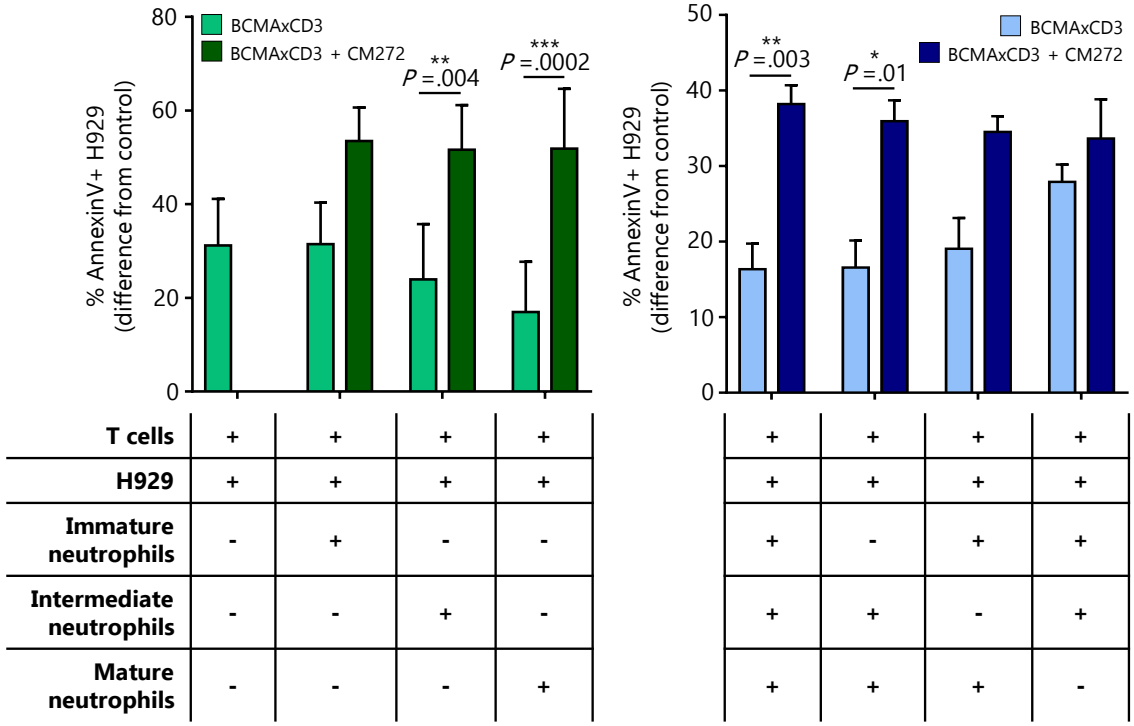

Supplemental Figure 12. (A) Heatmap representing the transcriptional profile of 17 different T cell clusters detectable in BM aspirates from HA (N = 3), MGUS/SMM (N = 5) and MM (N = 9) patients. Genes were color-coded according to the log-transformed fold-change expression, with dark blue and yellow representing the lowest and highest expression values. **(B)** UMAP showing the distribution and modulation of clonotypic T cells within the different T cell clusters according to disease evolution stage. **(C and D)** Density UMAP showing the expression of markers of exhaustion/activation (TOX, TIGIT, LAMP1) **(C)** as well as cytolysis (GZMK, GZMB and PRF1) **(D)** along MM evolution

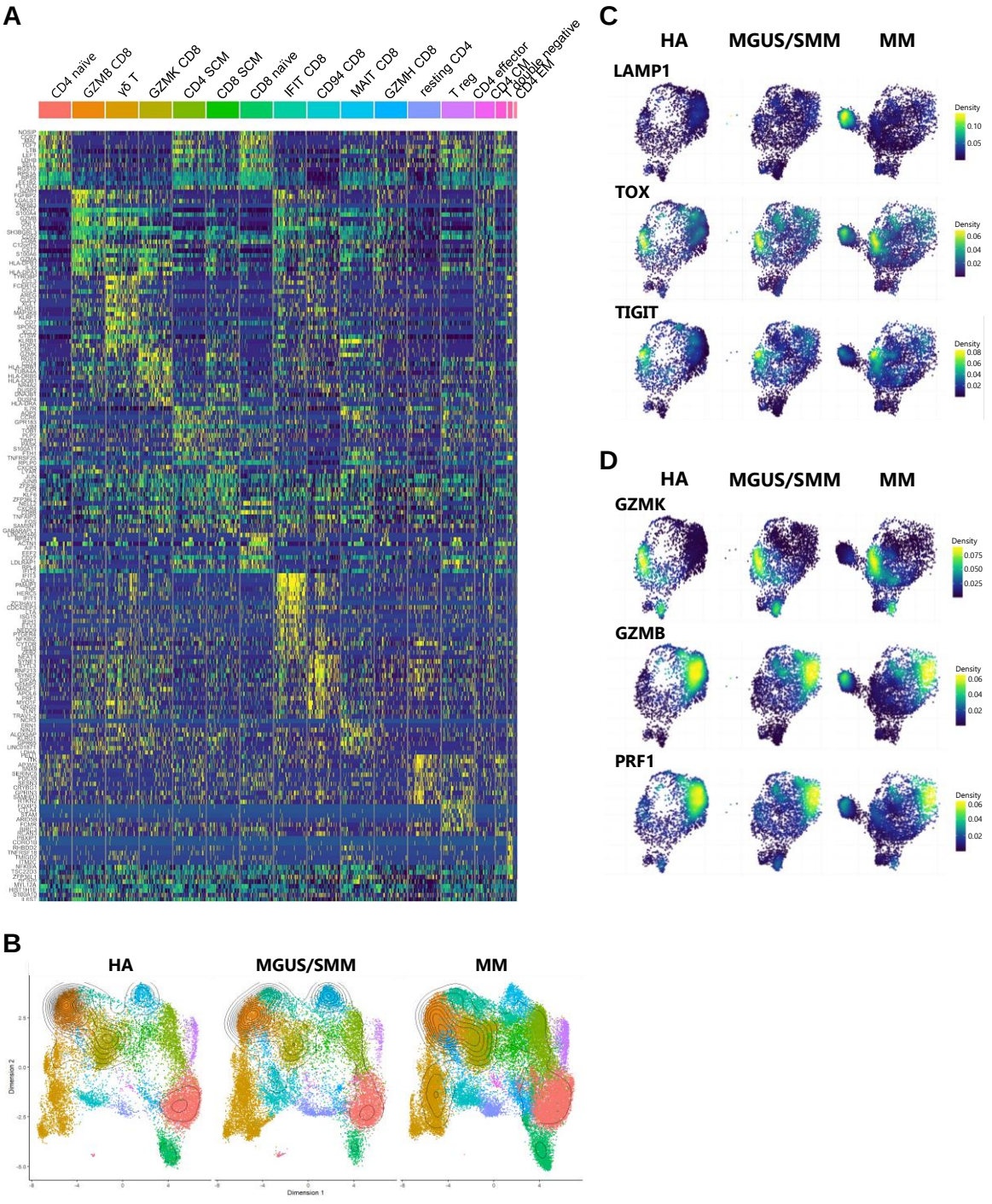

Supplemental Figure 13. **(A)** Schematic representation of the transgenic mouse lines that develop MM. $BI_{cγ1}$ mice were generated by crossing mice with expression of heterozygous BCL2 and $IKK2^{NF\text{-}κB}$ alleles to cγ1-cre mice, leading to transgene activation from germinal center B cells. $PBI_{cγ1}$ mice were generated by crossing $BI_{cγ1}$ mice. As controls, $YFP_{cγ1}$ mice, which were generated by crossing yellow fluorescence protein (YFP) reporter mice with cγ1-cre mice, were used. Following immunization with red blood sheep cells, $BI_{cγ1}$ and $PBI_{cγ1}$ mice developed fully penetrant tumors in the BM that fulfilled the biological features of MM, and shortened median overall survival (OS) with respect to control mice, as shown in the Kaplan-Meier overall survival curves. **(B)** Flow cytometry analysis in a representative BM sample from a $BI_{cγ1}$ mouse at 6 month of age (MGUS stage) and at the time of death (11 months, MM stage), which shows a progressive increase in the number of $CD138^{+}B220^{-}$ plasma cells (PCs), most of which express GFP and are negative for surface IgM expression (sIgM−). Controls correspond to $YFP_{cγ1}$ mice. On the right, quantification of the number of transgenic $GFP^{+}CD138^{+}B220^{-}$ PCs in the BM of $BI_{cγ1}$ mice at MGUS and MM stages is shown. **(C)** Electrophoresis analysis of Ig secretion in serum samples from $BI_{cγ1}$ mice at MGUS and MM stages with respect to $YFP_{cγ1}$ control mice; the M spikes correspond to the γ fraction (left). Quantification of Ig isotypes in serum samples by ELISA in $BI_{cγ1}$ and $YFP_{cγ1}$ mice (middle). A representative example of the clonal of IgG1 secretion in a $BI_{cγ1}$ mouse with MM is shown (right). **(D)** Distribution of lymphoid cell subpopulations measured by flow cytometry analysis in the BM of $BI_{cγ1}$ mice at MGUS and MM stages in comparison to control age-matched $YFP_{cγ1}$ mice, including $CD4^{+}$ and $CD8^{+}$ T lymphocytes, $CD4^{+}CD25^{+}Foxp3^{+}$ regulatory T (Treg) cells, and $Nk1.1^{+}$ NK cells. The percentage of BM $CD4^{+}$ and $CD8^{+}$ T cells with surface expression of *Lag3*, *Pd1*, and *Tigit* at MGUS and MM stages, measured by flow cytometry, is shown (bottom). **P* < 0.05; ***P* < 0.01; ****P* < 0.001; n.s., non-significant values.

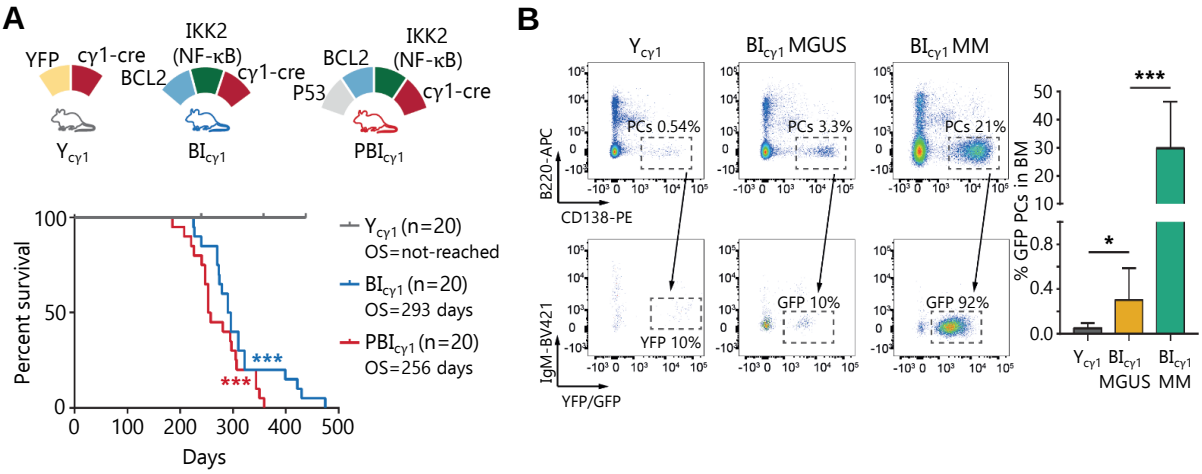

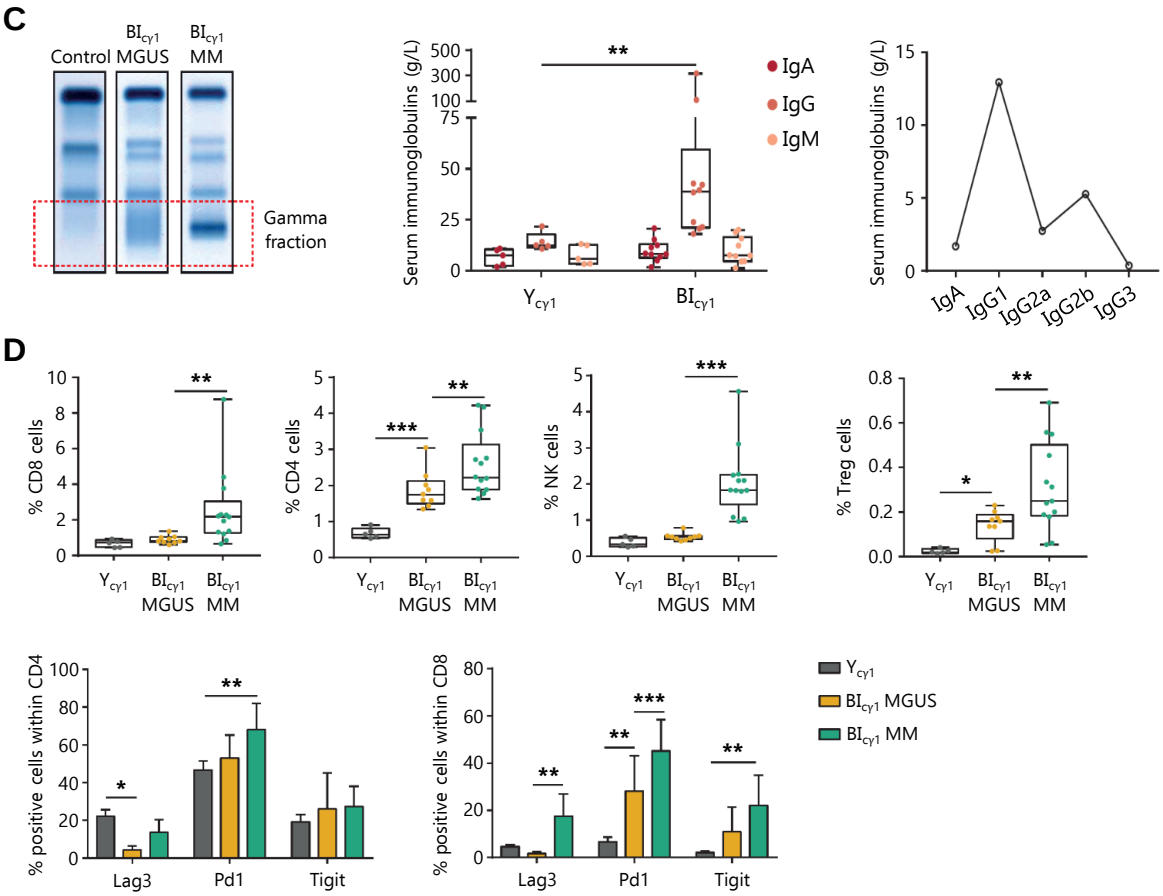
C
Control
BIcγ1 MGUS
BIcγ1 MM
Gamma fraction
Serum immunoglobulins (g/L)
IgA
IgG
IgM
Ycγ1
BIcγ1
IgA
IgG1
IgG2a
IgG2b
IgG3
D
% CD8 cells
% CD4 cells
% NK cells
% Treg cells
Ycγ1
BIcγ1 MGUS
BIcγ1 MM
% positive cells within CD4
% positive cells within CD8
Lag3
Pd1
Tigit

Supplemental Figure 14. (**A)** Expression of the immune checkpoints *Lag3*, *Pd1* and *Tigit* in healthy (N = 2), MGUS (N = 3) and MM (N = 3) bearing mice, measured by scRNA-seq and MFC. Error bars represent mean ± SEM, **P* < .05. (**B)** Heatmaps of genes belonging to the immune checkpoint group which are significantly differentially expressed among clonotypic and non-clonotypic cells in humans and mice according to disease stages. Shared genes are reported in the boxes between the heatmaps.

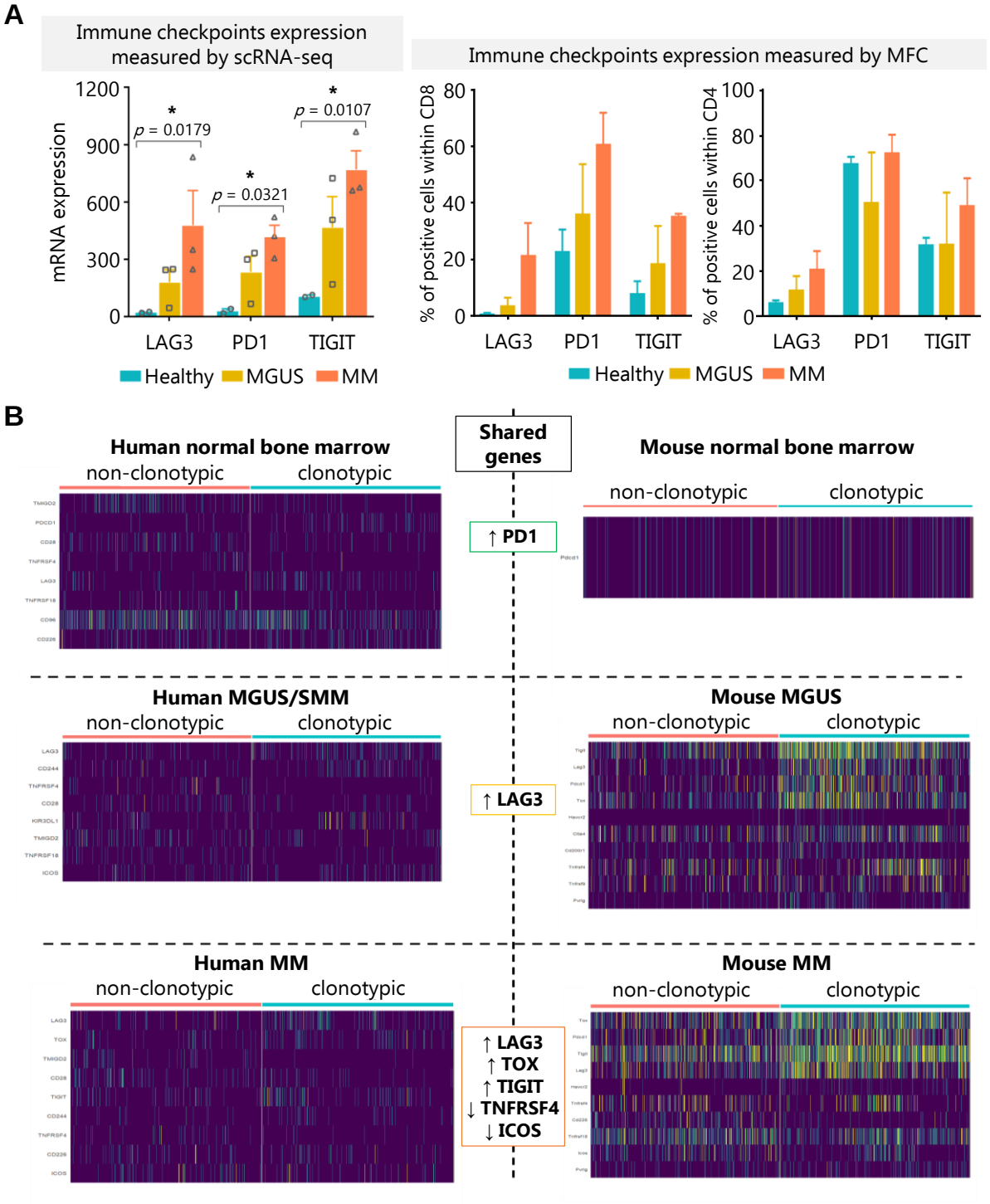

Supplemental Figure 15. C57B6 immunocompetent mice were injected with the 5080 murine MM cell line, which was established from P53-$BI_{cγ1}$ mice. Percentage of plasma cells, $CD8^+$ and $CD4^+$ T cells, and NK cells in the BM of healthy vs MM5080 mice (top) and the expression of immune checkpoints in $CD8^+$ and $CD4^+$ T cells. Error bars represent mean ± SEM, **P* < .05, ***P* < .01 and ****P* < .001.

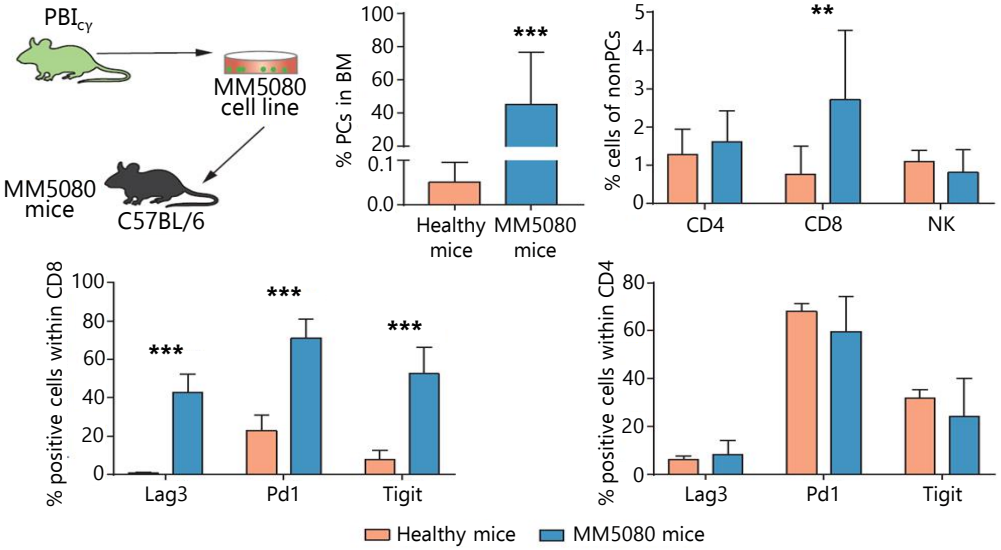

Supplemental Figure 16. (A) Manual analysis of the flow cytometry tube used for the FlowCT computational analysis. **(B)** Heatmap showing the expression of all markers used for flow cytometry analysis in the 19 cell populations found in the BM of HA, MGUS, SMM, NDMM and RRMM patients. **(C)** Dotplot showing the median fluorescence of each marker used for flow cytometry analysis in the 19 cell populations.

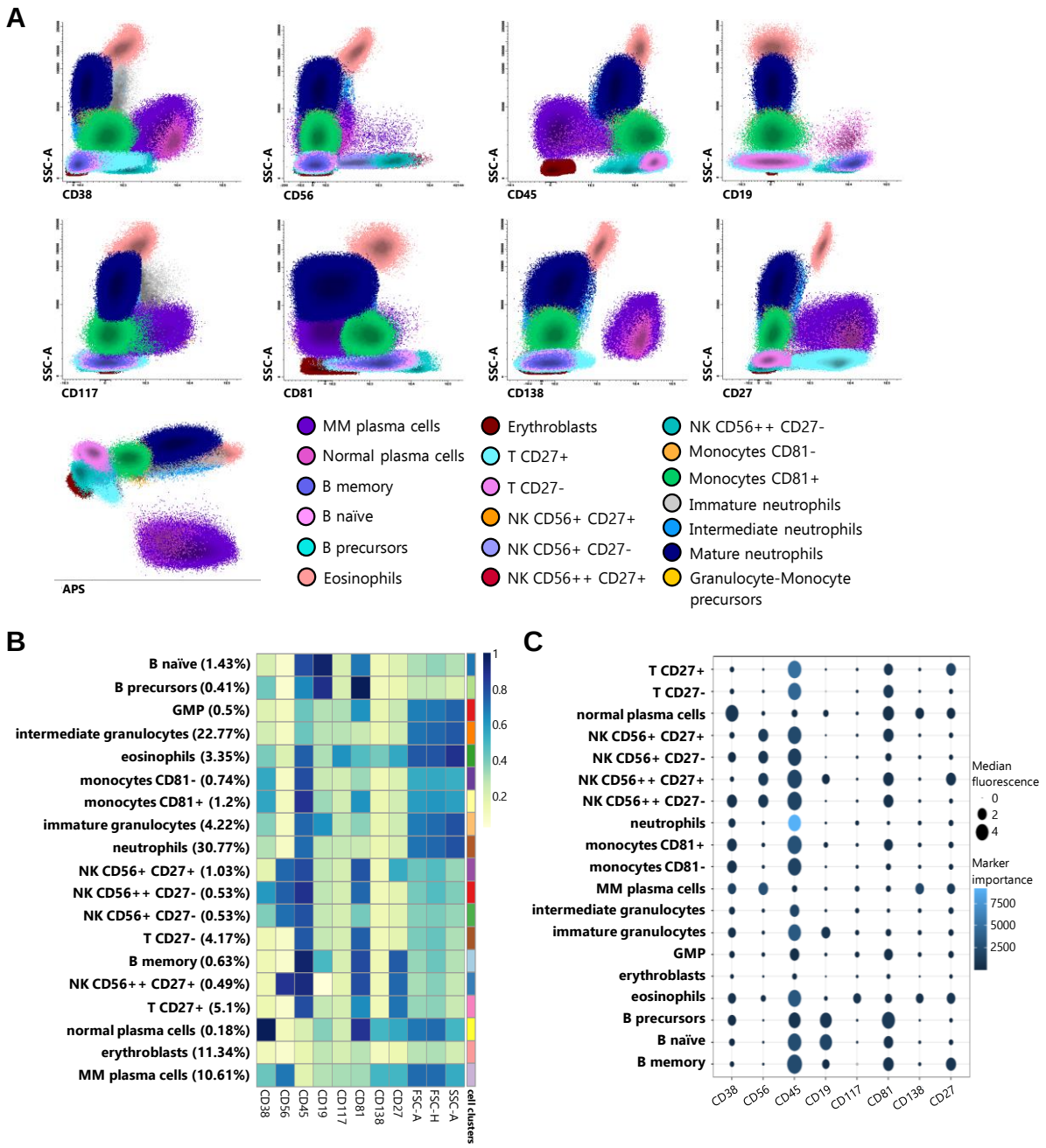

Supplemental Figure 17. Overall survival of transplant-eligible MM patients, stratified according to the median value of the CD27 ratio between negative and positive BM T cells (0.3).

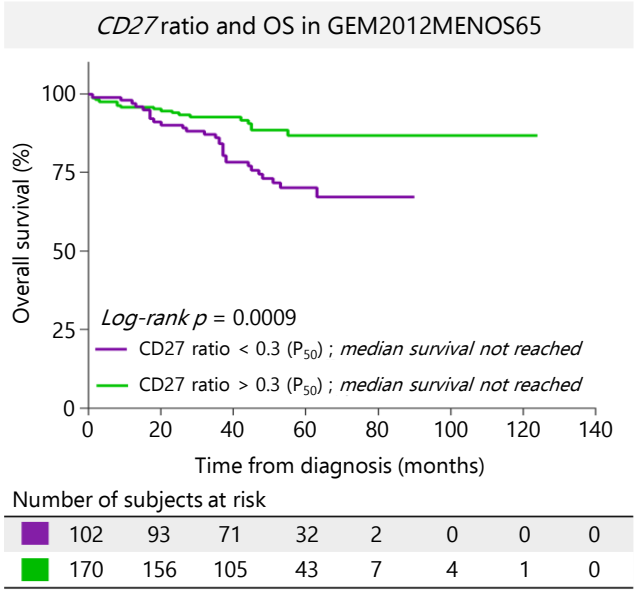

Supplemental Figure 18. (A) Bar chart and heatmap showing the number of different mutations present in tumor plasma cells from 23 MM patients, stratified according to the median value of the CD27 ratio between negative and positive BM T cells (0.3). The median number of somatic mutations was 35 and 23 in the groups of patients with a median value of the CD27 ratio lower and equal or greater than 0.3, respectively. **(B)** Volcano plot representing the transcriptional profile of tumor plasma cells from MM patients, stratified according to the median value of the CD27 ratio (0.3). There were 57 differentially expressed genes between the two groups as measured by log2 fold-change.

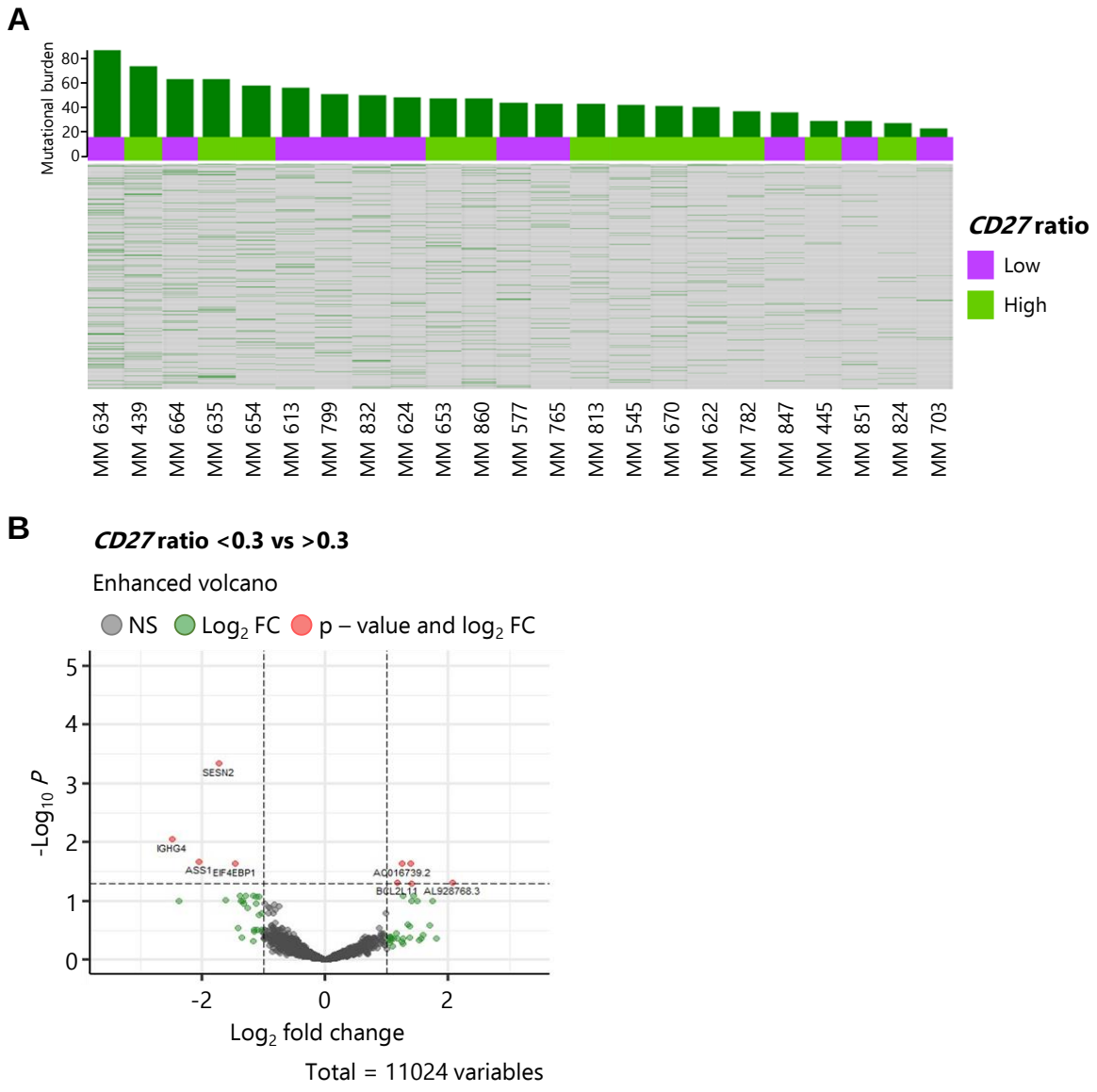

Supplemental Figure 19. (A) UMAP representations of PB T cells from 54 MM patients enrolled in the PETHEMA/GEM-CLARIDEX clinical trial. Samples were divided by condition (diagnosis or cycle 3 of treatment). All samples were stained with the same eight-color monoclonal antibody combination described in the panel, and processed using standardized protocols. **(B)** Significant differences in the distribution of T cells subsets within the T cell compartment of paired PB samples from MM patients at diagnosis and after three induction courses, according to the GEM-CLARIDEX protocol. Error bars represent mean ± SEM, **P* < .05, ****P* < .001.

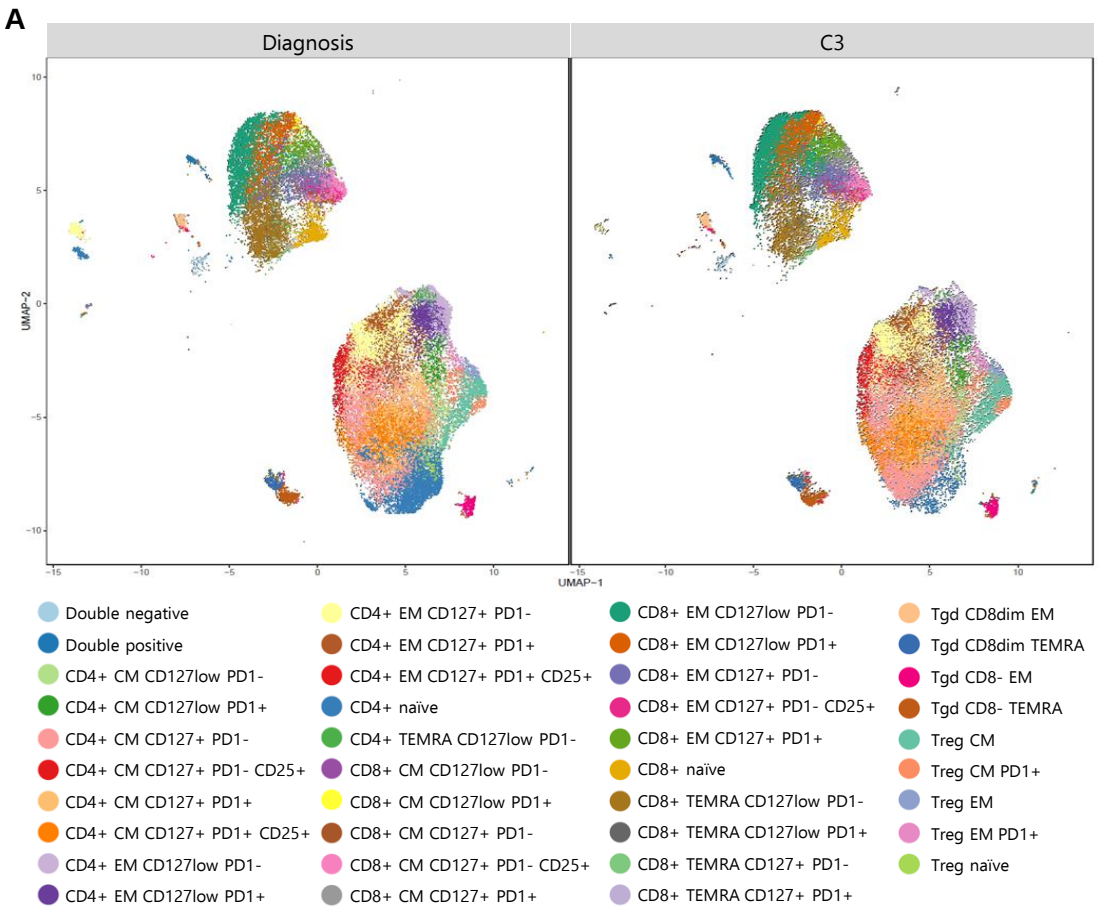

Supplemental Table 1. KEGG cytokine-cytokine receptor interaction pathway list.

AC005840.1	CCR6	EPO	IL12RB1	IL7R	TNFRSF11B
ACVR1	CCR7	EPOR	IL12RB2	IL8	TNFRSF12A
ACVR1B	CCR8	FAS	IL13	IL9	TNFRSF13B
ACVR2A	CCR9	FASLG	IL13RA1	IL9R	TNFRSF13C
ACVR2B	CD27	FLT1	IL15	INHBA	TNFRSF14
ACVRL1	CD40	FLT3	IL15RA	INHBB	TNFRSF17
AMH	CD40LG	FLT3LG	IL17A	INHBC	TNFRSF18
AMHR2	CD70	FLT4	IL17B	INHBE	TNFRSF19
BMP2	CLCF1	GDF5	IL17RA	KDR	TNFRSF1A
BMP7	CNTF	GH1	IL17RB	KIT	TNFRSF1B
BMPR1A	CNTFR	GH2	IL18	KITLG	TNFRSF21
BMPR1B	CRLF2	GHR	IL18R1	LEP	TNFRSF25
BMPR2	CSF1	HGF	IL18RAP	LEPR	TNFRSF4
CCL1	CSF1R	IFNA1	IL19	LIF	TNFRSF6B
CCL11	CSF2	IFNA10	IL1A	LIFR	TNFRSF8
CCL13	CSF2RA	IFNA13	IL1B	LTA	TNFRSF9
CCL14	CSF2RB	IFNA14	IL1R1	LTB	TNFSF10
CCL15	CSF3	IFNA16	IL1R2	MET	TNFSF11
CCL16	CSF3R	IFNA17	IL1RAP	MPL	TNFSF12
CCL17	CTF1	IFNA2	IL2	NGFR	TNFSF13
CCL18	CX3CL1	IFNA21	IL20	OSM	TNFSF13B
CCL19	CX3CR1	IFNA4	IL20RA	OSMR	TNFSF14
CCL2	CXCL1	IFNA5	IL20RB	PDGFA	TNFSF15
CCL20	CXCL10	IFNA6	IL21	PDGFB	TNFSF18
CCL21	CXCL11	IFNA7	IL21R	PDGFC	TNFSF4
CCL22	CXCL12	IFNA8	IL22	PDGFRA	TNFSF8
CCL23	CXCL13	IFNAR1	IL22RA1	PDGFRB	TNFSF9
CCL24	CXCL14	IFNAR2	IL22RA2	PF4	TPO
CCL25	CXCL16	IFNB1	IL23A	PF4V1	TSLP
CCL26	CXCL2	IFNE	IL23R	PLEKHO2	VEGFA
CCL27	CXCL3	IFNG	IL24	PPBP	VEGFB
CCL28	CXCL5	IFNGR1	IL25	PPBPP1	VEGFC

CCL3	CXCL6	IFNGR2	IL26	PRL	VEGFD
CCL3L1	CXCL8	IFNK	IL2RA	PRLR	XCL1
CCL3L3	CXCL9	IFNL1	IL2RB	RELT	XCL2
CCL4	CXCR1	IFNL2	IL2RG	TGFB1	XCR1
CCL4L2	CXCR2	IFNL3	IL3	TGFB2	HIF1A
CCL5	CXCR3	IFNLR1	IL3RA	TGFB3	CEBPB
CCL7	CXCR4	IFNW1	IL4	TGFBR1	STAT1
CCL8	CXCR5	IL10	IL4R	TGFBR2	STAT3
CCR1	CXCR6	IL10RA	IL5	TNF	NOS2
CCR10	EDA	IL10RB	IL5RA	TNFRSF10A	ARG1
CCR2	EDA2R	IL11	IL6	TNFRSF10B	PTGS2
CCR3	EDAR	IL11RA	IL6R	TNFRSF10C	PTGES2
CCR4	EGF	IL12A	IL6ST	TNFRSF10D	S100A8
CCR5	EGFR	IL12B	IL7	TNFRSF11A	S100A9

Supplemental Table 2. Demographics and disease characteristics of the 17 individuals studied by scRNA-seq and scTCR-seq.

Patient	Health condition	Age (years)	Sex	Cytogenetic abnormalities						Cytogenetic risk
				del17p	del1p	gain1q	amp1q	IGH_FGFR3	IGH_MAF	
HA1	HA	72	female	N/A	N/A	N/A	N/A	N/A	N/A	N/A
HA2	HA	52	N/A	N/A	N/A	N/A	N/A	N/A	N/A	N/A
HA3	HA	90	N/A	N/A	N/A	N/A	N/A	N/A	N/A	N/A
34661	MGUS	68	male	N/A	N/A	N/A	N/A	N/A	N/A	N/A
35162	MGUS	87	male	negative	negative	negative	positive	negative	negative	high risk
36784	MGUS	55	male	negative	negative	positive	negative	negative	negative	standard risk
34800	SMM	35	male	N/A	N/A	N/A	N/A	N/A	N/A	N/A
36142	SMM	51	female	N/A	N/A	N/A	N/A	N/A	N/A	N/A
573	NDMM	55	female	negative	negative	negative	negative	negative	negative	standard risk
611	NDMM	54	female	negative	negative	negative	negative	negative	negative	standard risk
693	NDMM	50	female	negative	negative	negative	negative	negative	negative	standard risk
824	NDMM	58	female	negative	negative	negative	negative	negative	negative	standard risk
860	NDMM	64	female	negative	negative	negative	negative	negative	negative	standard risk
20547	NDMM	51	male	positive	negative	negative	negative	negative	negative	high risk
22165	NDMM	71	male	negative	negative	negative	negative	negative	negative	standard risk
22577	NDMM	73	female	negative	negative	negative	negative	negative	negative	standard risk
MM9	NDMM	N/A	N/A	N/A	N/A	N/A	N/A	N/A	N/A	N/A

Supplemental Table 3. Clonotype ID and CDR3 of α- or β-chains.

	clonotype_id	cdr3s_aa
HA1_TGTATTCAGCGTAATA	HA1_clonotype1	TRA:CATLRGDKLIF; TRB:CSASDLAGDEQYF
HA1_AGGCCGTCAGTGACAG	HA1_clonotype10	TRA:CALVNSGGYQKVTF; TRB:CASSLGSSPHQPQHF
HA1_GGCCGATGTAGCACGA	HA1_clonotype11	TRA:CAVRDSNYQLIW; TRB:CASSLTRDSDYEQYF
HA1_CTACATTCAGTGGAGT	HA1_clonotype12	TRA:CAMREYNTDKLIF; TRB:CASSPGLAGGFDNEQFF
HA1_CGGACACCAACGATCT	HA1_clonotype13	TRA:CALSPLKTSYDKVIF; TRB:CASSLGESTYYGYTF
HA1_CATATGGGTTTGCATG	HA1_clonotype13	TRB:CASSLGESTYYGYTF
HA1_CTGATCCAGTCCATAC	HA1_clonotype14	TRA:CAASVVNDMRF; TRB:CASSHRGGAKNIQYF
HA1_CGTTAGAAGTACGTTC	HA1_clonotype15	TRA:CAVDPSGNDYKLSF; TRB:CASSFGGMNTEAFF
HA1_AAGGAGCAGACGACGT	HA1_clonotype18	TRB:CASSLTAGGPHEQFF
HA1_ACATCAGAGAGACTAT	HA1_clonotype18	TRA:CAVKSNTGKLIF; TRB:CASSLTAGGPHEQFF
HA1_AAGGTTCCAAGCGATG	HA1_clonotype2	TRA:CAGKSGATNKLIF; TRB:CASSYQGATEAFF
HA1_GAGTCCGAGCAAATCA	HA1_clonotype2	TRB:CASSYQGATEAFF
HA1_CGCTTCAAGATGTTAG	HA1_clonotype21	TRA:CAVGPYSGGGADGLTF; TRB:CASRAQAASSYNEQFF
HA1_GTTTCTAAGCTGTTCA	HA1_clonotype21	TRA:CILRDVDISNTGKLIF; TRB:CATSPTAGETQYF
HA1_CTAGCCTAGAGCCCAA	HA1_clonotype22	TRA:CAVRDGDYKLSF; TRB:CASLETAAGANEQYF
HA1_GTACTTTAGAAACGAG	HA1_clonotype22	TRA:CAASIGNFGNEKLTF; TRB:CASSPQRNTEAFF
HA1_TGGTTAGAGTGCTGCC	HA1_clonotype23	TRB:CASSLTRDSDYEQYF
HA1_GGAATAAGTGCAGGTA	HA1_clonotype23	TRA:CAGAPGTYKYIF; TRB:CASSLSISGSYEQYF
HA1_TCAGATGCAAGAGGCT	HA1_clonotype24	TRA:CAAILWGWELPTHF; TRB:CASSYQGATEAFF
HA1_CGGAGTCCACCAGGTC	HA1_clonotype24	TRA:CAASIRGSTLGRLYF; TRB:CASSVETGGKTEAFF
HA1_TCATTTGCAGCCTATA	HA1_clonotype25	TRB:CSASDLAGDEQYF
HA1_ACCTTTATCAGTGTTG	HA1_clonotype25	TRB:CASRAQAASSYNEQFF
HA1_CTCAGAAAGCGATATA	HA1_clonotype26	TRA:CATEIRMDSSYKLIF; TRB:CASSYRDYGDNEQFF
HA1_ACGCCAGGTCTTTCAT	HA1_clonotype26	TRA:CAAGLNSGYSTLTF; TRB:CASSGTGGANEKLFF
HA1_TTTGGTTTCTGTCTAT	HA1_clonotype27	TRA:CILRDVDISNTGKLIF; TRA:CATENDFGNEKLTF; TRB:CATSPTAGETQYF
HA1_TGTATTCTCATGTCTT	HA1_clonotype27	TRA:CAVNALGRGSTLGRLYF
HA1_GAAGCAGTCAGCTTAG	HA1_clonotype28	TRA:CATERNFGNEKLTF; TRB:CATSRTGGETQYF
HA1_TCGCGTTGTCAACTGT	HA1_clonotype28	TRA:CAGVDSNYQLIW; TRB:CASSDVAGGSTGELFF
HA1_TCTTTCCCATACAGCT	HA1_clonotype29	TRB:CASSRRSGSRNEQYF
…		
…		

Table continues in “Supplemental Table 3” in the shared folder

Supplemental Table 4. Comparison of the positive predictions between TCR α- and β-chains of clonal T cells and peptide-MHC cognates found with VDJBD 10X database and ERGO database.

Patient 1

TCR alpha	TCR beta	predicted peptide	VDJ_10	ERGO(VDJ)
CAAEPTSLGGKLIF	CASNLQGSTEAFF	DLSRVPIAK	0.04927	0.93297
CAGRGSNTGKLIF	CASNLQGSTEAFF	DLSRVPIAK	0.04385	0.93297
CAAEPTSLGGKLIF	CASNLQGSTEAFF	AVREIYEELGR	0.00047	0.00000
CAGRGSNTGKLIF	CASNLQGSTEAFF	AVREIYEELGR	0.00004	0.00000
CAAEPTSLGGKLIF	CASNLQGSTEAFF	ILYFRAPV	0.00534	0.00000
CAGRGSNTGKLIF	CASNLQGSTEAFF	ILYFRAPV	0.02030	0.00000
CAAEPTSLGGKLIF	CASNLQGSTEAFF	AQSPIPNLYL	0.00012	0.00000
CAGRGSNTGKLIF	CASNLQGSTEAFF	AQSPIPNLYL	0.00001	0.00000
CAAEPTSLGGKLIF	CASNLQGSTEAFF	APGPGDSNIFWGL	0.00000	0.98204
CAGRGSNTGKLIF	CASNLQGSTEAFF	APGPGDSNIFWGL	0.00000	0.98204
CAAEPTSLGGKLIF	CASNLQGSTEAFF	VPIAKILLENV	0.00017	0.00158
CAGRGSNTGKLIF	CASNLQGSTEAFF	VPIAKILLENV	0.00005	0.00158
CAAEPTSLGGKLIF	CASNLQGSTEAFF	ILAVREIYEELG	0.00263	0.00000
CAGRGSNTGKLIF	CASNLQGSTEAFF	ILAVREIYEELG	0.00158	0.00000
CILRDGASSGSARQLT	CASSFGRGSSYEQYF	DLSRVPIAK	0.01909	0.00415
CILRDGASSGSARQLT	CASSFGRGSSYEQYF	AVREIYEELGR	0.00008	0.00000
CILRDGASSGSARQLT	CASSFGRGSSYEQYF	ILYFRAPV	0.00243	0.00000
CILRDGASSGSARQLT	CASSFGRGSSYEQYF	AQSPIPNLYL	0.00001	0.00000
CILRDGASSGSARQLT	CASSFGRGSSYEQYF	APGPGDSNIFWGL	0.00000	0.00351
CILRDGASSGSARQLT	CASSFGRGSSYEQYF	VPIAKILLENV	0.00001	0.00228
CILRDGASSGSARQLT	CASSFGRGSSYEQYF	ILAVREIYEELG	0.00061	0.00000
CAVSDRSGGGADGLTF	CASSLGLHYEQYF	DLSRVPIAK	0.12880	0.00570
CAVSDRSGGGADGLTF	CASSLGLHYEQYF	AVREIYEELGR	0.00411	0.00001
CAVSDRSGGGADGLTF	CASSLGLHYEQYF	ILYFRAPV	0.02064	0.00030
CAVSDRSGGGADGLTF	CASSLGLHYEQYF	AQSPIPNLYL	0.00219	0.00089
CAVSDRSGGGADGLTF	CASSLGLHYEQYF	APGPGDSNIFWGL	0.00000	0.25852
CAVSDRSGGGADGLTF	CASSLGLHYEQYF	VPIAKILLENV	0.00153	0.01779
CAVSDRSGGGADGLTF	CASSLGLHYEQYF	ILAVREIYEELG	0.01634	0.00034
CAVINTGTASKLTF	CASSLPGSGRSTDTQYF	DLSRVPIAK	0.00000	0.41171
CAVINTGTASKLTF	CASSLPGSGRSTDTQYF	AVREIYEELGR	0.00000	0.00000
CAVINTGTASKLTF	CASSLPGSGRSTDTQYF	ILYFRAPV	0.00000	0.00000
CAVINTGTASKLTF	CASSLPGSGRSTDTQYF	AQSPIPNLYL	0.00000	0.00000
CAVINTGTASKLTF	CASSLPGSGRSTDTQYF	APGPGDSNIFWGL	0.00000	0.71362
CAVINTGTASKLTF	CASSLPGSGRSTDTQYF	VPIAKILLENV	0.00000	0.03101
CAVINTGTASKLTF	CASSLPGSGRSTDTQYF	ILAVREIYEELG	0.00000	0.00000
CAGRSSNTGKLIF	CASSYQGSVGYTF	DLSRVPIAK	0.00020	0.02571
CAGRSSNTGKLIF	CASSYQGSVGYTF	AVREIYEELGR	0.00000	0.00000
CAGRSSNTGKLIF	CASSYQGSVGYTF	ILYFRAPV	0.00000	0.00000
CAGRSSNTGKLIF	CASSYQGSVGYTF	AQSPIPNLYL	0.00000	0.00000
CAGRSSNTGKLIF	CASSYQGSVGYTF	APGPGDSNIFWGL	0.00000	0.00000
CAGRSSNTGKLIF	CASSYQGSVGYTF	VPIAKILLENV	0.00000	0.00003
CAGRSSNTGKLIF	CASSYQGSVGYTF	ILAVREIYEELG	0.00000	0.00000

Patient 2

TCR alpha	TCR beta	predicted peptide	VDJ_10	ERGO(VDJ)
CAVKILWNNDMRF	CASNSGTGTSGANVLTF	VMVHRQDAYRALQK	0.51167	0.75302
CAVKILWNNDMRF	CASNSGTGTSGANVLTF	QNRRKSERF	0.03287	0.09947
CAVKILWNNDMRF	CASNSGTGTSGANVLTF	QIPPIHEQFAILEK	0.00599	0.14480
CAVKILWNNDMRF	CASNSGTGTSGANVLTF	VMVHRQDA	0.00236	0.00021
CAVKILWNNDMRF	CASNSGTGTSGANVLTF	QIPPIHEQF	0.00000	0.12986
CAVKILWNNDMRF	CASNSGTGTSGANVLTF	GAISCPICR	0.00000	0.17641
CAYGPNARLMF	CASRSTDTQYF	VMVHRQDAYRALQK	0.00249	0.60222
CAYGPNARLMF	CASRSTDTQYF	QNRRKSERF	0.00115	0.38540
CAYGPNARLMF	CASRSTDTQYF	VMVHRQDA	0.00000	0.00000
CAYGPNARLMF	CASRSTDTQYF	QIPPIHEQFAILEK	0.00000	0.35296
CAYGPNARLMF	CASRSTDTQYF	GAISCPICR	0.00000	0.15383
CAYGPNARLMF	CASRSTDTQYF	QIPPIHEQF	0.00000	0.00004
CVVNSGNEKLTF	CASSHGAPYGYTF	VMVHRQDAYRALQK	0.00121	0.00000
CVVNSGNEKLTF	CASSHGAPYGYTF	QNRRKSERF	0.00004	0.16440
CVVNSGNEKLTF	CASSHGAPYGYTF	VMVHRQDA	0.00000	0.37206
CVVNSGNEKLTF	CASSHGAPYGYTF	QIPPIHEQFAILEK	0.00000	0.00000
CVVNSGNEKLTF	CASSHGAPYGYTF	GAISCPICR	0.00000	0.00000
CVVNSGNEKLTF	CASSHGAPYGYTF	QIPPIHEQF	0.00000	0.00011
CATDGFSSNSGYALNF	CASSLDSTGSNIQYF	VMVHRQDAYRALQK	0.24327	0.76828
CATDGFSSNSGYALNF	CASSLDSTGSNIQYF	QNRRKSERF	0.02114	0.81040
CATDGFSSNSGYALNF	CASSLDSTGSNIQYF	VMVHRQDA	0.01169	0.00150
CATDGFSSNSGYALNF	CASSLDSTGSNIQYF	QIPPIHEQFAILEK	0.00099	0.15568
CATDGFSSNSGYALNF	CASSLDSTGSNIQYF	QIPPIHEQF	0.00008	0.00702
CATDGFSSNSGYALNF	CASSLDSTGSNIQYF	GAISCPICR	0.00007	0.80670
CVVSADPRGSTLGRLYF	CASSLRFRGGEKLFF	VMVHRQDAYRALQK	0.32878	0.95635
CVVSADPRGSTLGRLYF	CASSLRFRGGEKLFF	QNRRKSERF	0.01781	0.06817
CVVSADPRGSTLGRLYF	CASSLRFRGGEKLFF	VMVHRQDA	0.00255	0.00001
CVVSADPRGSTLGRLYF	CASSLRFRGGEKLFF	QIPPIHEQFAILEK	0.00056	0.94737
CVVSADPRGSTLGRLYF	CASSLRFRGGEKLFF	GAISCPICR	0.00000	0.05056
CVVSADPRGSTLGRLYF	CASSLRFRGGEKLFF	QIPPIHEQF	0.00000	0.04509
CAVILFTGGGNKLTF	CASSLTSGQETQYF	QNRRKSERF	0.05111	0.93108
CAVILFTGGGNKLTF	CASSLTSGQETQYF	VMVHRQDAYRALQK	0.03875	0.50874
CAVILFTGGGNKLTF	CASSLTSGQETQYF	VMVHRQDA	0.00017	0.00155
CAVILFTGGGNKLTF	CASSLTSGQETQYF	QIPPIHEQFAILEK	0.00001	0.00261
CAVILFTGGGNKLTF	CASSLTSGQETQYF	GAISCPICR	0.00000	0.04548
CAVILFTGGGNKLTF	CASSLTSGQETQYF	QIPPIHEQF	0.00000	0.06276
CAPEDTGRRALTF	CASSNGEQPQHF	VMVHRQDAYRALQK	0.76505	0.70706
CAPEDTGRRALTF	CASSNGEQPQHF	QNRRKSERF	0.33040	0.00000
CAPEDTGRRALTF	CASSNGEQPQHF	VMVHRQDA	0.01405	0.00001
CAPEDTGRRALTF	CASSNGEQPQHF	QIPPIHEQFAILEK	0.00040	0.00999
CAPEDTGRRALTF	CASSNGEQPQHF	GAISCPICR	0.00009	0.02148
CAPEDTGRRALTF	CASSNGEQPQHF	QIPPIHEQF	0.00002	0.00222
CVVNSGNEKLTF	CASSPQVSGQGYETQYF	VMVHRQDAYRALQK	0.21773	0.00512
CVVNSGNEKLTF	CASSPQVSGQGYETQYF	QNRRKSERF	0.03666	0.00235
CVVNSGNEKLTF	CASSPQVSGQGYETQYF	VMVHRQDA	0.00101	0.02991
CVVNSGNEKLTF	CASSPQVSGQGYETQYF	QIPPIHEQFAILEK	0.00019	0.00004

CVVNSGNEKLTF	CASSPQVSGQGYETQYF	GAISCPICR	0.00000	0.00004
CVVNSGNEKLTF	CASSPQVSGQGYETQYF	QIPPIHEQF	0.00000	0.25090
CGVRVGGSYIPTF	CASSSLGGTLNTEAFF	VMVHRQDAYRALQK	0.10256	0.85282
CGVRVGGSYIPTF	CASSSLGGTLNTEAFF	QNRRKSERF	0.00375	0.89488
CGVRVGGSYIPTF	CASSSLGGTLNTEAFF	VMVHRQDA	0.00024	0.00000
CGVRVGGSYIPTF	CASSSLGGTLNTEAFF	QIPPIHEQFAILEK	0.00005	0.00000
CGVRVGGSYIPTF	CASSSLGGTLNTEAFF	QIPPIHEQF	0.00001	0.00000
CGVRVGGSYIPTF	CASSSLGGTLNTEAFF	GAISCPICR	0.00000	0.00011
CALSVDTGGFKTIF	CASTDGRARGHQPQHF	VMVHRQDAYRALQK	0.46930	0.01650
CALSVDTGGFKTIF	CASTDGRARGHQPQHF	QNRRKSERF	0.19137	0.99961
CAVANNARLMF	CASTDGRARGHQPQHF	QNRRKSERF	0.08025	0.99961
CAVANNARLMF	CASTDGRARGHQPQHF	VMVHRQDAYRALQK	0.07401	0.01650
CALSVDTGGFKTIF	CASTDGRARGHQPQHF	VMVHRQDA	0.01553	0.00000
CALSVDTGGFKTIF	CASTDGRARGHQPQHF	QIPPIHEQFAILEK	0.00130	0.00000
CAVANNARLMF	CASTDGRARGHQPQHF	VMVHRQDA	0.00110	0.00000
CALSVDTGGFKTIF	CASTDGRARGHQPQHF	GAISCPICR	0.00012	0.00000
CALSVDTGGFKTIF	CASTDGRARGHQPQHF	QIPPIHEQF	0.00009	0.00001
CAVANNARLMF	CASTDGRARGHQPQHF	QIPPIHEQFAILEK	0.00005	0.00000
CAVANNARLMF	CASTDGRARGHQPQHF	GAISCPICR	0.00000	0.00000
CAVANNARLMF	CASTDGRARGHQPQHF	QIPPIHEQF	0.00000	0.00001
CAVIPEDYQLIW	CASTKNAESGEQYF	QNRRKSERF	0.42681	0.00516
CAVIPEDYQLIW	CASTKNAESGEQYF	VMVHRQDAYRALQK	0.20272	0.00000
CAVIPEDYQLIW	CASTKNAESGEQYF	VMVHRQDA	0.05630	0.09721
CAVIPEDYQLIW	CASTKNAESGEQYF	QIPPIHEQFAILEK	0.00737	0.00000
CAVIPEDYQLIW	CASTKNAESGEQYF	QIPPIHEQF	0.00004	0.00029
CAVIPEDYQLIW	CASTKNAESGEQYF	GAISCPICR	0.00004	0.00000
CAMREYQTGANNLFF	CSAREGQGVNTEAFF	QNRRKSERF	0.08730	0.00002
CAMREYQTGANNLFF	CSAREGQGVNTEAFF	VMVHRQDAYRALQK	0.06671	0.00000
CAMREYQTGANNLFF	CSAREGQGVNTEAFF	VMVHRQDA	0.01321	0.00000
CAMREYQTGANNLFF	CSAREGQGVNTEAFF	GAISCPICR	0.00262	0.00000
CAMREYQTGANNLFF	CSAREGQGVNTEAFF	QIPPIHEQFAILEK	0.00021	0.00000
CAMREYQTGANNLFF	CSAREGQGVNTEAFF	QIPPIHEQF	0.00012	0.00020
CAMREWQTGANNLFF	CSARSGSTDTQYF	VMVHRQDAYRALQK	0.27962	0.66614
CAMREWQTGANNLFF	CSARSGSTDTQYF	QNRRKSERF	0.18777	0.55277
CAMREWQTGANNLFF	CSARSGSTDTQYF	VMVHRQDA	0.06458	0.00261
CAMREWQTGANNLFF	CSARSGSTDTQYF	QIPPIHEQFAILEK	0.01108	0.00644
CAMREWQTGANNLFF	CSARSGSTDTQYF	GAISCPICR	0.00163	0.00781
CAMREWQTGANNLFF	CSARSGSTDTQYF	QIPPIHEQF	0.00009	0.00013
CLVGEMDSSYKLIF	CSVDMDTEAFF	QNRRKSERF	0.24624	0.01226
CLVGEMDSSYKLIF	CSVDMDTEAFF	VMVHRQDAYRALQK	0.06130	0.00080
CLVGEMDSSYKLIF	CSVDMDTEAFF	VMVHRQDA	0.02937	0.00000
CLVGEMDSSYKLIF	CSVDMDTEAFF	QIPPIHEQFAILEK	0.00095	0.00026
CLVGEMDSSYKLIF	CSVDMDTEAFF	QIPPIHEQF	0.00002	0.00001
CLVGEMDSSYKLIF	CSVDMDTEAFF	GAISCPICR	0.00000	0.00027

Supplemental Table 5. Gene signatures used for the identification of T cell clusters in BM aspirates of HA (N = 3), MGUS/SMM (N = 5) and MM (N = 9) patients.

	p_val	avg_log2FC	pct.1	pct.2	p_val_adj	cluster	gene
CCR7	0	1.163111989	0.47	0.128	0	CD4_Naive	CCR7
TCF7	0	1.004000959	0.492	0.197	0	CD4_Naive	TCF7
LTB	0	0.988792206	0.812	0.43	0	CD4_Naive	LTB
LEF1	0	0.960959328	0.402	0.119	0	CD4_Naive	LEF1
SELL	0	0.922113787	0.52	0.218	0	CD4_Naive	SELL
FLT3LG	0	0.715611821	0.536	0.303	0	CD4_Naive	FLT3LG
IL7R	0	0.631779499	0.799	0.5	0	CD4_Naive	IL7R
AIF1	0	0.61060583	0.25	0.086	0	CD4_Naive	AIF1
TMEM123	0	0.595834875	0.538	0.34	0	CD4_Naive	TMEM123
IL6ST	0	0.570520347	0.369	0.184	0	CD4_Naive	IL6ST
RPS6	0	0.552669202	0.997	0.967	0	CD4_Naive	RPS6
CD27	0	0.520487967	0.322	0.155	0	CD4_Naive	CD27
FOXP1	0	0.50549611	0.528	0.346	0	CD4_Naive	FOXP1
PIK3IP1	0	0.448935328	0.618	0.455	0	CD4_Naive	PIK3IP1
…							
GZMH	0	2.240182461	0.857	0.219	0	GZMB_CD8	GZMH
LGALS1	0	1.513256298	0.624	0.236	0	GZMB_CD8	LGALS1
ZNF683	0	1.490194002	0.337	0.036	0	GZMB_CD8	ZNF683
NKG7	0	1.416254726	0.992	0.567	0	GZMB_CD8	NKG7
GZMB	0	1.225258703	0.674	0.211	0	GZMB_CD8	GZMB
GNLY	0	1.195071548	0.79	0.411	0	GZMB_CD8	GNLY
CCL5	0	1.154609679	0.993	0.588	0	GZMB_CD8	CCL5
CD52	0	1.072774505	0.906	0.689	0	GZMB_CD8	CD52
CD8A	0	1.043828391	0.581	0.29	0	GZMB_CD8	CD8A
CST7	0	0.948560553	0.894	0.483	0	GZMB_CD8	CST7
CD99	0	0.89715556	0.892	0.641	0	GZMB_CD8	CD99
GZMA	0	0.877811791	0.706	0.358	0	GZMB_CD8	GZMA
…							
TYROBP	0	2.376707211	0.78	0.172	0	gd_T	TYROBP
GNLY1	0	2.360805083	0.818	0.385	0	gd_T	GNLY
CCL3	0	2.277105082	0.43	0.095	0	gd_T	CCL3
FCER1G	0	2.143134151	0.495	0.065	0	gd_T	FCER1G
CCL4	0	2.140519102	0.669	0.295	0	gd_T	CCL4
GZMB1	0	1.704100125	0.636	0.192	0	gd_T	GZMB
XCL1	0	1.669971983	0.398	0.098	0	gd_T	XCL1
KLRD11	0	1.644767302	0.758	0.223	0	gd_T	KLRD1
NKG71	0	1.611606439	0.985	0.544	0	gd_T	NKG7
KLRF1	0	1.608777777	0.479	0.057	0	gd_T	KLRF1
…							
…							

Table continues in “Supplemental Table 5” in the shared folder

Supplemental Table 6. Distribution of T cell subsets in BM aspirates of HA (N = 3), MGUS/SMM (N = 5) and MM (N = 9) patients.

	HA 1	HA 2	HA 3	MGUS 34661	MGUS 35162	MGUS 36784	SMM 34800	SMM 36142	MM 611	MM 693	MM 22165	MM 20547	MM 9	MM 573	MM 824	MM 860	MM 22577
CD4 naïve	12.4	33.0	7.5	5.0	22.1	5.9	27.1	17.4	8.2	8.0	10.7	11.5	37.6	15.4	22.1	14.4	14.4
GZMB CD8	13.5	3.7	25.7	13.0	12.6	18.7	8.7	5.7	16.4	16.7	10.3	10.1	8.9	5.5	14.2	21.5	16.1
gd T	14.5	17.5	18.3	36.7	17.0	19.0	17.8	24.0	21.9	21.0	15.5	15.1	9.1	6.6	10.5	10.2	19.0
GZMK CD8	21.5	5.6	18.3	12.5	13.2	6.7	10.1	7.3	12.1	12.5	22.9	22.1	11.0	10.1	9.6	18.0	15.2
CD4 SCM	10.3	12.5	6.1	6.0	4.5	5.5	6.3	14.8	7.6	9.4	11.4	11.1	10.3	10.1	9.4	6.7	8.0
CD8 SCM	7.9	3.3	5.8	3.9	4.1	1.9	4.2	5.5	4.8	4.5	7.0	6.7	4.2	4.5	6.2	9.1	6.5
CD8 naive	3.8	10.6	1.5	1.2	1.8	1.1	6.1	4.1	1.5	1.6	2.3	2.9	3.9	32.1	2.1	1.8	2.6
IFIT CD8	1.9	0.5	2.7	9.1	1.4	9.0	4.0	0.9	10.4	10.1	3.9	3.1	1.0	0.9	2.7	2.8	1.8
CD94 CD8	1.8	2.7	4.8	2.1	5.1	13.9	2.4	2.2	4.7	4.2	3.7	3.2	2.7	1.7	4.6	3.6	4.1
MAIT CD8	7.5	3.8	2.0	5.4	8.3	1.2	6.5	12.6	2.1	2.5	2.1	2.7	2.6	3.4	2.6	2.1	3.3
CD8	2.1	1.7	3.2	2.0	3.1	4.3	3.7	1.5	5.7	5.3	5.4	5.5	3.6	1.8	5.1	3.8	5.1
resting CD4	1.0	0.7	2.0	0.9	4.0	8.4	0.9	1.2	1.6	1.6	1.6	2.1	1.8	1.5	7.8	4.0	1.2
T regs	1.4	3.8	1.8	0.9	1.2	1.1	1.6	1.8	2.5	2.2	2.9	3.0	2.1	5.4	2.8	1.4	2.3
CD4 effector	0.2	0.3	0.3	0.5	1.6	0.3	0.3	0.3	0.5	0.4	0.5	0.2	0.5	0.3	0.3	0.2	0.5
CD4 CM	0.0	0.0	0.0	0.0	0.0	2.5	0.0	0.0	0.0	0.0	0.0	0.0	0.0	0.0	0.0	0.0	0.0
T_double negative	0.2	0.0	0.0	1.0	0.0	0.5	0.3	0.0	0.0	0.0	0.0	0.0	0.0	0.0	0.0	0.0	0.0
CD4 EM	0.1	0.2	0.0	0.0	0.0	0.0	0.0	0.6	0.0	0.0	0.0	0.9	0.6	0.5	0.0	0.1	0.0

Supplemental Table 7. Distribution of T cell subsets within non-clonotypic and clonotypic T cells, in BM aspirates of HA (N = 3), MGUS/SMM (N = 5) and MM (N = 9) patients.

	% non-clonotypic T cells within total T cells																
	HA 1	HA 2	HA 3	MGUS 34661	MGUS 35162	MGUS 36784	SMM 34800	SMM 36142	MM 611	MM 693	MM 22165	MM 20547	MM 9	MM 573	MM 824	MM 860	MM 22577
CD4 naïve	20.88	36.48	15.70	6.11	30.82	10.54	36.64	20.84	15.69	16.90	51.82	19.71	13.29	9.97	23.71	14.64	31.15
CD4 SCM	14.03	11.63	9.95	9.08	5.29	6.69	7.25	14.70	9.91	14.59	11.10	10.57	11.38	8.36	8.44	12.16	10.89
MAIT CD8	4.35	4.13	8.68	10.53	10.01	3.77	5.29	8.36	8.06	5.48	4.56	1.42	4.06	1.39	11.81	10.34	2.17
CD8	6.28	10.98	2.89	1.45	1.97	0.96	8.12	5.69	2.46	3.50	4.56	19.26	2.29	1.61	3.91	1.89	6.74
resting CD4	7.30	3.94	6.91	3.94	2.31	3.42	3.49	4.93	5.72	7.33	3.25	6.15	5.21	10.63	6.48	3.57	4.05
CD8 GZMK	20.39	6.43	14.00	15.19	18.11	10.73	13.98	19.06	11.75	18.42	8.58	8.23	18.36	21.63	12.52	8.81	9.75
CD8 CD94	6.32	2.38	3.84	16.40	6.69	6.09	3.85	6.77	5.78	3.70	2.71	0.96	2.26	6.01	4.71	10.85	4.19
CD8 GZMB	5.87	3.23	10.75	11.17	8.10	22.98	7.09	5.58	14.40	9.83	4.08	3.49	9.20	11.44	9.41	12.09	9.66
T reg	1.97	4.22	3.58	1.61	1.24	1.29	1.70	2.11	4.12	4.36	1.98	6.02	3.58	2.35	3.20	2.26	5.98
CD8 SCM	1.56	2.76	8.14	2.41	4.27	8.22	1.28	1.98	3.20	3.23	1.55	0.72	3.58	4.18	4.62	4.44	2.26
CD8 IFIT	4.47	6.21	8.14	11.25	1.74	8.60	5.55	5.95	10.65	6.73	3.01	4.04	5.55	4.33	6.66	15.44	4.95
CD8 naïve	4.22	4.08	3.94	7.32	2.76	3.34	2.93	2.67	6.89	4.36	0.82	0.73	1.53	2.64	2.49	2.11	5.51
CD4 CM	1.80	3.00	3.26	1.21	5.23	1.77	2.16	1.09	0.86	1.32	1.64	16.84	1.42	2.13	1.87	1.24	2.40
CD4 effector	0.00	0.00	0.00	0.00	0.00	0.00	0.00	0.00	0.00	0.00	0.00	0.00	11.49	9.31	0.00	0.00	0.00
CD4 EM	0.00	0.00	0.00	0.00	0.00	4.11	0.00	0.00	0.00	0.00	0.00	0.00	0.00	0.00	0.00	0.00	0.05
gd T	0.08	0.00	0.00	0.00	0.00	0.00	0.00	0.00	0.00	0.00	0.00	1.54	0.03	0.00	0.00	0.00	0.00
T double negative	0.49	0.55	0.22	2.33	1.46	7.50	0.67	0.30	0.49	0.26	0.33	0.32	6.77	4.03	0.18	0.15	0.24

	% clonotypic T cells within total T cells																
	HA 1	HA 2	HA 3	MGUS 34661	MGUS 35162	MGUS 36784	SMM 34800	SMM 36142	MM 611	MM 693	MM 22165	MM 20547	MM 9	MM 573	MM 824	MM 860	MM 22577
CD4 naïve	0.00	0.00	0.00	0.00	0.00	0.00	0.00	0.00	0.00	0.00	0.00	0.00	0.00	0.00	0.00	0.00	0.00
CD4 SCM	0.00	0.00	0.00	0.00	0.00	0.00	0.00	0.00	0.00	0.00	0.00	0.00	0.00	0.00	0.00	0.00	0.00
MAIT CD8	0.00	0.00	0.00	0.00	0.00	0.00	0.00	0.00	0.00	0.00	0.00	0.00	0.00	0.00	0.00	0.00	0.00
CD8	0.54	0.76	22.21	1.09	0.14	0.17	0.00	0.00	0.09	0.00	0.00	0.17	2.20	0.00	0.00	0.00	0.22
resting CD4	0.00	0.00	0.00	0.00	0.00	0.00	0.00	0.00	0.00	0.00	0.00	0.00	0.00	0.00	0.00	0.00	0.00
CD8 GZMK	24.56	26.39	6.22	26.47	12.68	18.51	25.96	35.38	23.06	57.43	46.49	41.33	30.84	62.66	47.42	20.64	34.95
CD8 CD94	26.46	5.43	6.19	10.23	14.99	6.61	12.29	10.58	6.73	15.37	5.83	16.41	5.09	8.62	7.32	4.45	8.35
CD8 GZMB	33.61	46.21	20.88	29.47	45.53	43.55	41.32	41.50	35.06	7.56	30.32	22.14	42.91	15.72	22.30	19.16	38.02
T reg	0.00	0.00	0.00	0.00	0.00	0.00	0.00	0.00	0.00	0.00	0.00	0.00	0.00	0.00	0.00	0.00	0.00
CD8 SCM	0.48	0.13	0.10	8.19	0.14	5.35	1.84	1.11	7.29	4.41	0.48	1.01	3.89	2.73	0.50	17.90	2.86
CD8 IFIT	2.72	4.92	0.50	13.78	1.01	22.08	10.14	4.74	12.27	7.68	2.97	4.97	8.78	4.26	5.16	29.65	7.91
CD8 naïve	6.12	9.22	2.99	8.19	18.30	2.91	5.68	5.71	13.65	6.68	12.13	9.09	3.29	4.69	16.81	6.84	5.71
CD4 CM	0.00	0.00	0.00	0.00	0.00	0.00	0.00	0.00	0.00	0.00	0.00	0.00	0.00	0.00	0.00	0.00	0.00
CD4 effector	1.22	2.40	13.50	0.82	0.86	0.35	1.23	0.56	0.18	0.25	0.95	2.10	1.50	1.09	0.17	0.34	0.44
CD4 EM	0.00	0.00	0.00	0.00	0.00	0.00	0.00	0.00	0.00	0.00	0.00	0.00	0.00	0.00	0.00	0.00	0.00
gd T	0.20	0.76	9.41	0.41	0.14	0.00	0.00	0.00	0.00	0.00	0.00	0.25	0.10	0.00	0.00	0.00	0.00
T double negative	4.08	3.79	17.99	1.36	6.20	0.48	1.54	0.42	1.66	0.63	0.83	2.53	1.40	0.22	0.33	1.03	1.54

Supplemental Table 8. Gene signatures used for the identification of clusters within clonotypic T cells in BM aspirates of HA (N = 3), MGUS/SMM (N = 5) and MM (N = 9) patients.

	p_val	avg_log2FC	pct.1	pct.2	p_val_adj	cluster	gene
S100A4	0	-0.916963938	0.83	0.915	0	CD8 GZMK	S100A4
HOPX	1.33E-231	-0.573303541	0.161	0.432	2.29E-227	CD8 GZMK	HOPX
IFITM2	6.96E-229	-0.663842121	0.614	0.792	1.20E-224	CD8 GZMK	IFITM2
PFN1	2.44E-215	-0.574542099	0.924	0.962	4.21E-211	CD8 GZMK	PFN1
CD52	3.63E-206	-0.735817087	0.718	0.802	6.25E-202	CD8 GZMK	CD52
GZMB	2.72E-199	-0.675528489	0.233	0.48	4.68E-195	CD8 GZMK	GZMB
S100A6	1.12E-194	-0.517993341	0.808	0.897	1.93E-190	CD8 GZMK	S100A6
SARAF	4.85E-183	0.396530456	0.953	0.863	8.34E-179	CD8 GZMK	SARAF
NKG7	2.75E-182	-0.519200144	0.98	0.965	4.72E-178	CD8 GZMK	NKG7
B2M	7.16E-177	-0.26463916	1	1	1.23E-172	CD8 GZMK	B2M
SH3BGRL3	7.33E-173	-0.521439535	0.943	0.952	1.26E-168	CD8 GZMK	SH3BGRL3
CFL1	3.92E-172	-0.470534876	0.843	0.916	6.74E-168	CD8 GZMK	CFL1
LGALS1	3.71E-169	-0.658985779	0.269	0.488	6.38E-165	CD8 GZMK	LGALS1
GZMH	3.15E-165	-0.726671448	0.541	0.672	5.41E-161	CD8 GZMK	GZMH
IL32	3.29E-165	-0.582048985	0.74	0.872	5.67E-161	CD8 GZMK	IL32
GNLY	6.19E-163	-1.225668306	0.54	0.666	1.07E-158	CD8 GZMK	GNLY
EIF1	1.65E-162	0.295701336	1	0.998	2.84E-158	CD8 GZMK	EIF1
TYROBP	3.56E-152	-0.669282669	0.104	0.303	6.12E-148	CD8 GZMK	TYROBP
MYL12A	4.40E-151	-0.486570797	0.771	0.856	7.58E-147	CD8 GZMK	MYL12A
TMSB10	1.24E-140	-0.320159982	0.999	0.999	2.13E-136	CD8 GZMK	TMSB10
FGFBP2	2.85E-139	-0.589390704	0.284	0.484	4.91E-135	CD8 GZMK	FGFBP2
CYBA	4.60E-130	-0.446390959	0.47	0.651	7.91E-126	CD8 GZMK	CYBA
FTH1	4.67E-129	0.353131565	0.998	0.992	8.04E-125	CD8 GZMK	FTH1
CXCR4	3.93E-128	0.355530895	0.856	0.698	6.75E-124	CD8 GZMK	CXCR4
LEPROTL1	1.84E-122	0.344150003	0.69	0.518	3.17E-118	CD8 GZMK	LEPROTL1
UCP2	4.10E-120	-0.361608474	0.179	0.366	7.06E-116	CD8 GZMK	UCP2
RAC2	3.33E-117	-0.427471631	0.435	0.616	5.74E-113	CD8 GZMK	RAC2
IFITM1	7.47E-117	-0.303282213	0.934	0.97	1.29E-112	CD8 GZMK	IFITM1
PRF1	4.14E-116	-0.425921595	0.25	0.434	7.12E-112	CD8 GZMK	PRF1
CD8A	6.79E-115	0.324511787	0.73	0.515	1.17E-110	CD8 GZMK	CD8A
GZMK	9.05E-114	0.495830299	0.52	0.342	1.56E-109	CD8 GZMK	GZMK
RGS1	1.11E-112	0.364661101	0.48	0.295	1.91E-108	CD8 GZMK	RGS1
MTRNR2L12	1.52E-111	0.519750335	0.967	0.899	2.61E-107	CD8 GZMK	MTRNR2L12
CLIC1	8.60E-109	-0.428517606	0.472	0.625	1.48E-104	CD8 GZMK	CLIC1
SERF2	7.35E-108	-0.305859065	0.82	0.901	1.27E-103	CD8 GZMK	SERF2
ACTB	1.73E-99	-0.5079252	0.996	0.998	2.97E-95	CD8 GZMK	ACTB
…							
…							

Table continues in “Supplemental Table 8” in the shared folder

Supplemental Table 9. Distribution of clusters within clonotypic T cells in BM aspirates of HA (N = 3), MGUS/SMM (N = 5) and MM (N = 9) patients.

	HA 1	HA 2	HA 3	MGUS 34661	MGUS 35162	MGUS 36784	SMM 34800	SMM 36142	MM 611	MM 693	MM 22165	MM 20547	MM 9	MM 573	MM 824	MM 860	MM 22577
CD8 GZMK	18.78	15.15	4.66	15.01	10.66	11.78	15.05	21.03	11.90	36.27	26.28	29.29	17.07	47.60	34.61	13.00	17.36
CD8 GZMK PD1	5.78	11.24	1.56	11.46	2.02	6.74	10.91	14.35	11.16	21.16	20.21	12.04	13.77	15.07	12.81	7.64	17.58
CD8 GZMB	33.33	45.96	20.69	29.06	45.24	36.72	41.32	41.36	35.06	7.43	29.96	21.72	42.71	15.72	22.30	19.16	38.02
CD8 CD94	26.46	5.43	6.19	10.23	14.99	6.61	12.29	10.58	6.73	15.37	5.83	16.41	5.09	8.62	7.32	4.45	8.35
CD8 IFIT	2.72	4.92	0.50	13.78	1.01	22.08	10.14	4.74	12.27	7.68	2.97	4.97	8.78	4.26	5.16	29.65	7.91
CD8 SCM	0.48	0.13	0.10	8.19	0.14	5.35	1.84	1.11	7.29	4.41	0.48	1.01	3.89	2.73	0.50	17.90	2.86
CD8 naïve	6.12	9.22	2.99	8.19	18.30	2.91	5.68	5.71	13.65	6.68	12.13	9.09	3.29	4.69	16.81	6.84	5.71
CD8 CD107a	0.54	0.76	22.21	1.09	0.14	0.17	0.00	0.00	0.09	0.00	0.00	0.17	2.20	0.00	0.00	0.00	0.22
T double negative	4.08	3.79	17.99	1.36	6.20	0.48	1.54	0.42	1.66	0.63	0.83	2.53	1.40	0.22	0.33	1.03	1.54
gd T	0.20	0.76	9.41	0.41	0.14	0.00	0.00	0.00	0.00	0.00	0.00	0.25	0.10	0.00	0.00	0.00	0.00
CD4 effector	0.68	1.39	8.45	0.14	0.43	0.04	0.00	0.14	0.00	0.00	0.24	0.59	0.10	0.11	0.17	0.00	0.00
CD4 effector PD1	0.54	1.01	5.05	0.68	0.43	0.30	1.23	0.42	0.18	0.25	0.71	1.52	1.40	0.98	0.00	0.34	0.44
CD8 GZMB TIGIT	0.27	0.25	0.20	0.41	0.29	6.82	0.00	0.14	0.00	0.13	0.36	0.42	0.20	0.00	0.00	0.00	0.00

Supplemental Table 10. Differentially expressed genes between non-clonotypic and clonotypic T cells in MGUS/SMM (N = 5) and MM (N = 9) patients.

	p_val	avg_log2FC	pct.1	pct.2	p_val_adj
RPL22	0	-0.414278143	0.974	0.945	0
RPL11	0	-0.267057627	0.999	0.989	0
SH3BGRL3	0	0.950589808	0.954	0.813	0
CD52	0	0.841387503	0.851	0.69	0
ZNF683	0	1.199430084	0.26	0.037	0
RPS8	0	-0.330156439	0.999	0.988	0
CD2	0	0.606324082	0.56	0.371	0
S100A10	0	0.557335757	0.798	0.63	0
S100A6	0	0.803444223	0.908	0.74	0
S100A4	0	1.207416405	0.923	0.721	0
FCRL6	0	0.622577826	0.259	0.074	0
SELL	0	-0.827801626	0.129	0.295	0
C1orf21	0	0.413409387	0.219	0.085	0
LINC01871	0	0.697235271	0.288	0.106	0
PLEK	0	0.614661207	0.319	0.127	0
GNLY	0	0.447934564	0.639	0.423	0
CD8A	0	1.117529792	0.601	0.273	0
CD8B	0	0.853486886	0.489	0.199	0
CYTOR	0	0.510345002	0.316	0.136	0
MAL	0	-0.805871369	0.028	0.209	0
MIR4435-2HG	0	0.370403324	0.165	0.06	0
ZEB2	0	0.345892796	0.386	0.202	0
ARPC2	0	0.378436755	0.824	0.688	0
RPL32	0	-0.330964609	0.999	0.988	0
LYAR	0	0.490696623	0.454	0.246	0
FGFBP2	0	1.132551531	0.527	0.19	0
RPL9	0	-0.345268876	0.983	0.962	0
HOPX	0	0.682869842	0.466	0.21	0
LEF1	0	-0.7121235	0.038	0.191	0
RPL34	0	-0.278724423	0.999	0.99	0
ANXA5	0	0.49694401	0.318	0.16	0
RPS3A	0	-0.354565053	0.997	0.986	0
RPL37	0	-0.231821651	0.997	0.983	0
GZMA	0	1.060837704	0.749	0.335	0
TCF7	0	-0.763647699	0.106	0.273	0
ADRB2	0	0.404143763	0.183	0.067	0
CD74	0	0.482548829	0.858	0.715	0
HLA-A	0	0.283954705	0.989	0.957	0
…					
…					

Table continues in “Supplemental Table 10” in the shared folder

Supplemental Table 11. Differentially expressed genes between non-clonotypic and clonotypic T cells in MGUS/SMM (N = 5) and MM (N = 9) patients, which coded for cell surface proteins**.**

	p_val	avg_log2FC	pct.1	pct.2	p_val_adj
CD52	0	0.841387503	0.851	0.69	0
CD2	0	0.606324082	0.56	0.371	0
SELL	0	-0.827801626	0.129	0.295	0
CD8A	0	1.117529792	0.601	0.273	0
CD8B	0	0.853486886	0.489	0.199	0
CD74	0	0.482548829	0.858	0.715	0
CD99	0	0.804730617	0.876	0.633	0
CD3E	0	0.541249236	0.929	0.76	0
CD3D	0	0.705343504	0.78	0.519	0
CD3G	0	0.730859754	0.643	0.385	0
ITGB1	0	0.616756331	0.398	0.212	0
CCR7	0	-0.94245222	0.024	0.216	0
CD320	0	0.607453678	0.25	0.104	0
LILRB1	0	0.262694	0.083	0.018	0
ITGB2	0	0.584901784	0.685	0.484	0
LAG3	1.62E-265	0.309587485	0.144	0.055	4.25E-261
KLRD1	2.79E-260	0.228612897	0.472	0.282	7.29E-256
CD63	1.14E-232	0.349337965	0.328	0.192	2.98E-228
CD27	1.70E-219	-0.486108986	0.079	0.203	4.45E-215
BSG	1.37E-201	0.343971616	0.393	0.26	3.59E-197
CD7	1.03E-196	-0.608676149	0.556	0.652	2.70E-192
IL7R	4.92E-191	-0.585589151	0.456	0.568	1.29E-186
SPN	1.48E-188	0.346659071	0.268	0.159	3.88E-184
ITGAL	1.03E-184	0.30767806	0.28	0.166	2.69E-180
CD55	3.09E-183	-0.559347913	0.168	0.291	8.10E-179
CD53	5.11E-144	0.335488969	0.453	0.338	1.34E-139
CD300A	2.92E-127	0.247044785	0.155	0.084	7.66E-123
CD28	2.02E-121	-0.352593183	0.044	0.115	5.30E-117
IL6ST	2.66E-117	-0.491183499	0.14	0.23	6.96E-113
SLAMF7	1.63E-111	0.164995789	0.111	0.055	4.27E-107
TNFSF8	3.37E-111	-0.338912891	0.052	0.123	8.82E-107
IL2RG	8.39E-110	0.342753837	0.205	0.13	2.20E-105
CXCR3	1.55E-106	0.198917153	0.207	0.128	4.05E-102
ITGA4	2.51E-105	0.223110903	0.354	0.254	6.57E-101
CD58	2.43E-101	0.183832099	0.12	0.064	6.37E-97
IFITM1	5.08E-99	0.126798054	0.959	0.906	1.33E-94
ICAM3	9.95E-96	0.230626512	0.485	0.384	2.60E-91
LAIR2	7.36E-95	0.180860444	0.058	0.023	1.93E-90
TNFRSF4	1.11E-83	-0.27541763	0.015	0.057	2.91E-79
CD244	2.29E-82	0.135453766	0.082	0.041	6.00E-78
CD69	3.96E-78	-0.360161452	0.658	0.713	1.04E-73

SELPLG	3.08E-74	0.238119255	0.278	0.207	8.06E-70
CD84	2.32E-71	0.161835763	0.09	0.049	6.07E-67
ITGA6	6.24E-69	-0.194436978	0.021	0.061	1.63E-64
CRTAM	1.06E-65	0.180913477	0.106	0.062	2.77E-61
CD81	1.69E-61	0.10926242	0.078	0.043	4.43E-57
ITGAM	2.29E-61	0.105580123	0.086	0.048	6.00E-57
TNFRSF1B	3.81E-60	0.130042202	0.241	0.173	9.98E-56
SLAMF6	2.21E-56	0.153849637	0.09	0.053	5.79E-52
CD151	1.53E-53	0.126481718	0.085	0.05	4.01E-49
NCR3	2.02E-53	0.231315329	0.175	0.123	5.30E-49
CD226	9.88E-52	0.123450256	0.109	0.069	2.59E-47
CD37	2.15E-48	0.133124258	0.805	0.725	5.64E-44
TNFRSF1A	6.07E-45	0.126598139	0.083	0.051	1.59E-40
SIRPG	4.73E-44	-0.139086249	0.05	0.09	1.24E-39
KLRB1	8.06E-40	-0.143952541	0.255	0.314	2.11E-35
TNFRSF18	2.20E-39	-0.182055436	0.023	0.051	5.77E-35
BST2	2.67E-39	0.130854393	0.317	0.259	6.99E-35
LY9	4.06E-39	0.151769826	0.188	0.144	1.06E-34
IL12RB1	3.60E-37	0.115670672	0.115	0.079	9.44E-33
IL4R	1.61E-32	-0.206501104	0.071	0.107	4.22E-28
TNFRSF14	9.66E-31	0.12112461	0.323	0.273	2.53E-26
ICOS	1.30E-30	-0.218317189	0.06	0.092	3.42E-26
CCR6	3.96E-30	-0.156950682	0.037	0.064	1.04E-25
CD38	3.13E-23	-0.18927015	0.038	0.061	8.20E-19
CD44	1.76E-21	-0.230981519	0.534	0.549	4.60E-17
TNFRSF10A	2.86E-20	-0.103737555	0.038	0.06	7.49E-16
ADGRE5	2.59E-14	-0.135069598	0.443	0.387	6.78E-10
S1PR1	2.21E-11	-0.1533672	0.164	0.188	5.79E-07
ICAM1	2.59E-10	-0.177001299	0.041	0.055	6.77E-06
NCR1	3.39E-10	-0.12235212	0.041	0.054	8.88E-06

Supplemental Table 12. Demographics and disease characteristics of the 90 SMM patients with multidimensional flow cytometry characterization of BM T cells.

Patient	Age	Sex	TTP	Progression to active MM	% PCs morphology	Serum M component (g/dL)	sFLCr	B2m (mg/L)	2/20/20 model risk
61516	60	F	24	yes	12	2.9	0.14	2.4	Intermediate
62187	64	F	32	no	15	2.1	23.41	2.41	High
63473	73	F	4	yes	16.8	2.28	0.19	3.03	Intermediate
63569	77	F	0	yes	12	2.1	0.05	1.94	High
63743	52	F	16	yes	25	0.94	36.68	2.23	High
64246	75	F	6	yes	24.8	1.17	0.02	2.21	High
64376	74	F	26	no	4.4	1.78	29.1	3.76	Intermediate
64627	76	F	7	yes	4.8	0.73	0.01	2.16	Intermediate
65085	79	M	25	no	3.2	2.25	0.27	4.9	Intermediate
65581	55	M	16	yes	6.8	1.44	96.49	1.62	Intermediate
65726	70	M	24	no	8.8	0.8	18.68	N/A	Low
65901	67	F	15	no	15	1.5	1.61	3.02	Intermediate
66135	82	F	6	no	12	2.12	34.93	6.3	High
66491	36	F	20	no	2.8	1.45	5.52	1.77	Low
66979	43	F	10	no	12	1.26	2.1	1.18	Low
67019	73	F	8	yes	30	1.85	0.01	2.2	High
67124	50	F	26	no	3	2.5	0.27	1.7	Low
67162	59	F	21	no	24.5	1.98	1.69	1.8	Intermediate
67574	78	M	16	yes	15	2.73	0.8	2.29	Intermediate
67575	63	M	23	no	8	2.49	8.27	3.02	Intermediate
67622	70	M	18	no	18	3.22	0.17	3.01	Intermediate
67823	53	M	11	yes	10	2.69	1.75	2.1	Intermediate
67881	67	F	1	yes	15	2.9	15.19	7.8	Intermediate
67883	73	F	24	no	13	2.1	0.31	18.5	Intermediate
68016	77	F	25	no	12	0.92	7.59	2.48	Low
68074	63	M	14	yes	15	2.5	11.1	2.33	Intermediate
68402	76	F	21	no	25	1.85	1.5	2.34	Intermediate
68469	68	F	20	no	13	0.74	9.52	1.32	Low
68575	73	F	23	no	23	1.64	116.62	3	High
68645	82	M	23	no	12	2.28	3.06	2.44	Intermediate
68647	62	M	16	no	35	1.17	2.66	2.33	Intermediate

68855	79	F	0	yes	20	N/A	0.11	N/A	Low
69105	75	M	24	no	6	0.9	1.51	N/A	Low
69135	79	M	5	yes	9	2.37	2.67	16.6	Intermediate
69610	51	M	18	no	10	0.48	1	1.28	Low
69728	86	F	2	yes	20	1.67	6.31	1.44	High
69768	75	F	18	no	1	0.34	2.12	2.07	Low
69914	46	F	23	no	12	1.73	0.26	1.6	Low
70041	60	F	22	no	10	3.26	0.71	3.92	High
70239	68	F	20	yes	5.6	0.34	12.01	N/A	Intermediate
70243	76	F	12	no	15	3	23.33	3.73	High
70503	56	M	22	no	21	3.2	0.04	N/A	High
70952	72	M	26	no	11	1.56	0.04	1.59	Intermediate
71014	67	M	20	no	12	2.4	9.46	2.19	Intermediate
71162	71	F	9	yes	26	0.72	0.01	2.7	High
71572	47	M	12	no	3.6	1.41	0.04	N/A	Intermediate
71722	67	F	15	no	18	1.22	0.04	2.8	Intermediate
71962	66	M	0	no	7	N/A	0.01	2.6	Low
72050	64	M	17	yes	27.5	0.14	2.69	2.4	Intermediate
72600	72	F	18	no	18	1.48	0.01	3.56	Low
72922	79	F	19	no	10	1.21	2.35	1.99	Low
72923	79	M	13	no	18	1.56	2.25	2.94	Low
73027	79	M	7	no	10	0.35	12.11	2.27	Low
73196	80	F	24	no	13	1.71	15.08	2.14	Low
73265	51	F	18	no	16	0.8	12.74	1.63	Low
73689	73	F	15	no	15	2.57	4.86	4.26	Intermediate
73730	84	M	7	yes	38	4.1	2	5.4	High
74048	58	F	13	no	16	1.4	0.08	1.9	Low
74083	76	M	8	yes	32	N/A	0.1	2.6	Intermediate
74752	84	M	11	no	25	2.35	0.06	3.23	Intermediate
75218	68	M	14	no	14	2.6	0.08	N/A	Intermediate
76479	66	F	12	no	1.6	2.56	24.76	2.32	High
76922	78	M	9	no	10	1.75	13.36	2.89	Low
76943	62	F	11	no	12	1.67	6.31	1.44	Low
77017	64	M	10	no	27	3.26	0.56	2.94	Intermediate
77073	77	M	11	no	10	4.1	5.35	3.24	Intermediate
77151	75	M	5	no	14	0.34	2.12	2.07	Low

78144	N/A	N/A	5	no	N/A	N/A	N/A	N/A	N/A
78624	63	M	6	no	6	1.67	9.31	1.35	Low
79503	83	M	6	no	14	2	28.36	N/A	Intermediate
79651	36	N/A	0	no	9	1.2	16.56	N/A	Low
80444	N/A	N/A	5	no	N/A	N/A	N/A	N/A	N/A
81492	42	F	0	no	N/A	3.48	4.42	2.13	Intermediate
82434	N/A	N/A	0	no	N/A	3	3.56	2.5	N/A
82877	76	M	0	no	N/A	1.82	0.02	N/A	Intermediate
83018	45	F	0	no	N/A	1.61	N/A	1.34	N/A
83309	81	M	0	no	N/A	0.5	5.36	2.75	N/A
83332	76	F	0	no	N/A	N/A	N/A	N/A	N/A
83683	64	M	0	no	N/A	2.5	0.2	3.11	Intermediate
83709	80	M	0	no	N/A	1.59	N/A	N/A	N/A
83923	83	M	0	no	N/A	2.3	8.61	N/A	Low
84607	68	M	0	no	N/A	N/A	N/A	N/A	N/A
84834	57	M	0	no	N/A	3.03	21.28	2.18	High
84918	50	M	0	no	N/A	1.18	0.15	1.52	Low
85064	59	F	0	no	N/A	N/A	N/A	N/A	N/A
85222	77	F	0	no	N/A	N/A	N/A	N/A	N/A
85303	63	F	0	no	N/A	N/A	N/A	N/A	N/A
85399	N/A	N/A	0	no	N/A	N/A	N/A	N/A	N/A
86000	72	M	0	no	29	1.2	20.15	2.9	Intermediate
83003	70	M	0	no	31	2.2	0.07	N/A	High

Supplemental Table 13. Disease characteristics of the eight mice studied by scRNA-seq and scTCR-seq.

Mouse	Health condition	Age (days)	Sex	Genotype
YC101	Healthy	551	male	Yc
YC102	Healthy	551	male	Yc
2751	MGUS	179	female	BIc
2752	MGUS	179	female	BIc
2573	MGUS	207	male	BIc
6917	MM	307	female	BIc
2264	MM	215	female	BIc
1728	MM	322	male	BIc

Supplemental Table 14. Multivariate Cox regression analysis for PFS

	B	SE	Wald	df	Sig.	Hazard Ratio	95.0% CI	
							<	>
ISS	.353	.371	.908	1	.341	1.423	.689	2.942
Cytogenetic risk	.609	.623	.957	1	.328	1.839	.543	6.231
LDH	.620	.769	.650	1	.420	1.859	.412	8.389
CD27 ratio	1.245	.634	3.860	1	.049	3.473	1.003	12.024

Supplemental Table 15. Association between the CD27 ratio and LDH.

		CD27 ratio		Total
		low	high	
LDH	normal	120	108	228
	high	12	32	44
Total		132	140	272
		value	df	Significance (bilateral)
Chi-square Pearson		2.374	1	.123

Supplemental Table 16. Association between the CD27 ratio and cytogenetic abnormalities.

		CD27 ratio		Total
		low	high	
del17p	absence	114	138	252
	presence	12	8	20
Total		126	146	272
		value	df	Significance (bilateral)
Chi-square Pearson		.402	1	.526

		CD27 ratio		Total
		low	high	
del1p	absence	118	138	256
	presence	8	8	16
Total		126	146	272
		value	df	Significance (bilateral)
Chi-square Pearson		.022	1	.881

		CD27 ratio		Total
		low	high	
amp1q	absence	79	95	174
	presence	47	51	98
Total		126	146	272
		value	df	Significance (bilateral)
Chi-square Pearson		.042	1	.839

		CD27 ratio		Total
		low	high	
t(4;14)	absence	102	126	228
	presence	24	20	44
Total		126	146	272
		value	df	Significance (bilateral)
	Chi-square Pearson	.351	1	.553

		CD27 ratio		Total
		low	high	
t(14;16)	absence	118	138	256
	presence	8	8	16
Total		126	146	272
		value	df	Significance (bilateral)
	Chi-square Pearson	.022	1	.881

Zenit